

## **Synchronous states of slowly rotating pendula**

Marcin Kapitaniak<sup>1,2</sup>, Krzysztof Czolczynski<sup>1</sup>, Przemysław Perlikowski<sup>1</sup>,  
Andrzej Stefanski<sup>1</sup>, and Tomasz Kapitaniak<sup>1\*</sup>

<sup>1</sup>*Division of Dynamics, Technical University of Lodz, Stefanowskiego 1/15, 90-924 Lodz,  
Poland*

<sup>2</sup>*Centre for Applied Dynamics Research, School of Engineering, University of Aberdeen  
AB24 3UE, Aberdeen, Scotland*

*PACS:* 45.40.-f, 05.45.-a

*Keywords:* coupled systems, synchronization, rotating pendula.

**Abstract:** Coupled systems that contain rotating elements are typical in physical, biological and engineering applications and for years have been the subject of intensive studies. One problem of scientific interest, which among others occurs in such systems is the phenomenon of synchronization of different rotating parts. Despite different initial conditions, after a sufficiently long transient, the rotating parts move in the same way – complete synchronization, or a permanent constant shift is established between their displacements, i.e., the angles of rotation - phase synchronization. Synchronization occurs due to dependence of the periods of rotating elements motion and the displacement of the base on which these elements are mounted.

We review the studies on the synchronization of rotating pendula and compare them with the results obtained for oscillating pendula. As an example we consider the dynamics of the system consisting of  $n$  pendula mounted on the movable beam. The pendula are excited by the external torques which are inversely proportional to the angular velocities of the pendula. As the result of such excitation each pendulum rotates around its axis of rotation. It has been assumed that all pendula rotate in the same direction or in the opposite directions. We consider the case of slowly rotating pendulums and estimate the influence of the gravity on their motion. We classify the synchronous states of the identical pendula and observe how the parameters mismatch can influence them. We give evidence that synchronous states are robust as they exist in the wide range of system parameters and can be observed in a simple experiments.

\*Corresponding author.

E-mail address: [tomaszka@p.lodz.pl](mailto:tomaszka@p.lodz.pl) (T. Kapitaniak).

## Contents

1. Introduction
2. Synchronous states of rotating pendula
3. Synchronization mechanism
  - 3.1 Equations of motion
  - 3.2 Synchronization conditions
    - 3.2.1 Energy balance of pendula
    - 3.2.2 Energy balance of the beam
    - 3.2.3 Synchronization conditions - linearized model
4. Numerical examples
  - 4.1 Two pendula rotating in the same direction
  - 4.2 Three pendula rotating in the same direction
  - 4.3 Large system of pendula rotating in the same direction
  - 4.4 Two pendula rotating in the opposite directions
  - 4.5 Three pendula rotating in various directions
  - 4.6 Large system of pendula rotating in different directions
  - 4.7 Two pendula with different driving torques, rotating in the same direction
5. Synchronization extends the life time of rotation
6. Discussion and conclusions

## References

## Nomenclature

$\alpha$ [rad/s]	-angular frequency of pendulum rotation;
$\alpha_x$ [rad/s]	-angular frequency of the beam-pendula system oscillations-rotations;
$\beta_i$ [rad],	-phase shift between pendula;
$\Delta$	- logarithmic decrement of damping
$\Phi_i, \Phi$ [rad]	- amplitudes of oscillations of the pendulum;
$\varphi_i, \dot{\varphi}_i, \ddot{\varphi}_i$	- displacement [rad], velocity [rad/s] and acceleration [rad/s <sup>2</sup> ] of the $i$ -th pendulum;
$\varphi_{i0}, \dot{\varphi}_{i0}$	- initial conditions of the $i$ -th pendulum motion;
$\xi$	- scale factor of pendulums;
$\dot{\varphi}_i$ [rad/s]	- velocity of $i$ -th pendulum;
$\dot{\varphi}_{iN}$ [rad/s]	- nominal velocity of $i$ -th pendulum;
$A$ [m]	- amplitude of parametric excitation;
$A_b$ [m/s <sup>2</sup> ]	- amplitude of beam acceleration;
$b$ [rad]	- amplitude of harmonic component of rotation angle;
$c_{\varphi_i}$ [Nsm]	- damping coefficient of the $i$ -th pendulum damper;
$c_x$ [Ns/m]	- damping coefficient of the damper between the beam and the basis;
$T, U$ [Nm]	- kinetic and potential energy;
$F$ [N]	- resulting force with which pendulums act on the beam;
$g$ [m/s <sup>2</sup> ]	- gravitational acceleration;
$k_x$ [N/m]	- stiffness coefficient of the spring between the beam and the basis;
$l, l_i$ [m]	- length of the pendulum;
$m_b$ [kg]	- mass of the beam;
$m, m_i$ [kg]	- mass of the pendulum;
$n$	- number of pendulums in the system;
$N$	- number of periods $T$ of pendula oscillations ( $NT$ - unit of time);

- $p = p_{0i} - \dot{\phi}_i p_{1i}$  [Nm] - driving torque;  
 $s$  [m] - length of the arc of the circle;  
 $t$  [s] - time;  
 $U$  [kg] - global mass of the system (beam plus pendula);  
 $W_{\text{beam}}$  [Nm] - energy dissipated by the beam during one period of motion;  
 $W_i^{\text{DAMP}}$  [Nm] - energy dissipated by the  $i$ -th pendulum during one period of motion;  
 $W_{\text{beam}}^{\text{DRIVE}}$  [Nm] - energy delivered to the beam during one period of motion;  
 $W_i^{\text{DRIVE}}$  [Nm] - energy delivered to the  $i$ -th pendulum during one period of motion;  
 $W_i^{\text{SYN}}$  [Nm] - energy delivered from the  $i$ -th pendulum to the beam during one period of motion;  
 $X$  [m] - amplitude of the beam oscillations;  
 $X_{1i}, X_{3i}$  [m] - amplitudes of first and third harmonic component of the beam oscillations;  
 $x, \dot{x}, \ddot{x}$  - displacement [m], velocity [m/s] and acceleration [m/s<sup>2</sup>] of the beam;  
 $x_0, \dot{x}_0$  - initial values of displacement and velocity of the beam;

\* In this paper all values of the parameters and state variables are given in the above units. For simplicity of the presentation the units are omitted in the text.

## 1. Introduction

A pendulum is an archetype for strongly nonlinear dynamical systems, which naturally has been given a great deal of attention in literature [1,50 and ref. within]. In the last few decades, particularly since the experimental verification of chaotic motion of pendulum [46], there has been an explosion of work in this area.

The plane pendulum is a constrained system: a mass point  $m$  moves on a circle of constant radius  $l$ , as sketched in Figure 1. We denote by  $\varphi(t)$  the angle that measures the deviation of the pendulum from the vertical line and by  $s(t)=l\varphi(t)$  the length of the corresponding arc on the circle. We then have kinematic  $T$  and potential  $U$  energies given respectively as  $T = \frac{1}{2}ml^2\dot{\varphi}^2$  and  $U = -mgl[\cos \varphi - 1]$ , where  $g$  is the acceleration due to the gravity. Let us introduce the constant

$$\varepsilon = \frac{T + U}{2mgl} = \frac{1}{2} \left( \frac{1}{2\omega^2} \dot{\varphi}^2 + 1 - \cos \varphi \right),$$

where  $a^2 = \frac{g}{l}$  [3]. For  $\varepsilon < 1$  the pendulum performs oscillations around the stable equilibrium point  $\varphi=0$ , while for  $\varepsilon > 1$  the pendulum always swings in one direction, i.e., it rotates either clockwise or counterclockwise. The boundary  $\varepsilon=1$  between these qualitatively different domains is a singular value and corresponds to the motion where the pendulum reaches the uppermost position but cannot swing beyond it. This singular trajectory is called the separatrix, it separates the domain of oscillatory and rotational behavior.

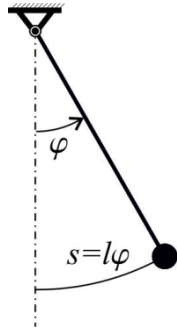


Figure 1. The planar pendulum.

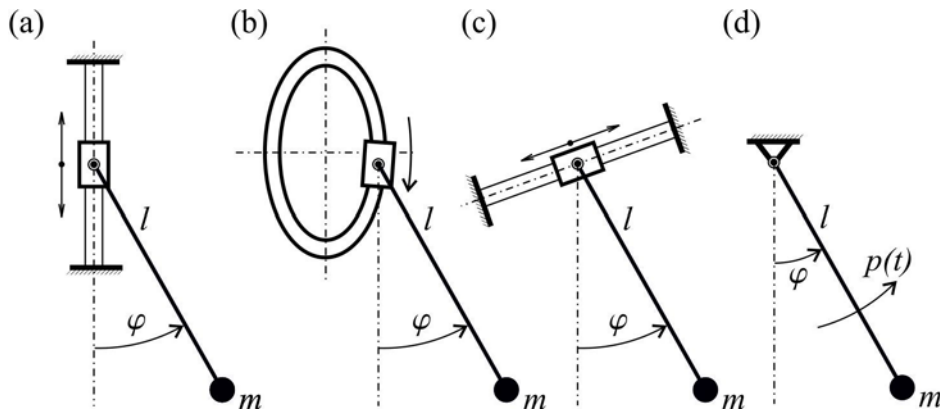


Figure 2. Physical model of the pendulum: (a-c) pendulum excited at the pivot point (a) vertically, (b) elliptically, (c) along a tilted axis, (d) pendulum excited by the external torque  $p(t)$ :  $m$  is the mass of the pendulum bob,  $l$  is the length of the pendulum arm.

In the dissipative case, e.g. when the energy dissipates due to the friction in the pivot, one has to excite the pendulum to preserve oscillatory or rotational motion. There are two possibilities of excitation: (i) by the motion of the pivot, i.e., the parametrical excitation as shown in Figure 2(a-c), (ii) by the torque applied directly to the mass  $m$  – Figure 2(d). The parametrical excitation can be implemented by the vertical (Figure 2(a)) [43,44], elliptical (Figure 2(b)) [32,73] or along a tilted line (Figure 2(c)) motion of the pivot [56]).

Despite the fact that both oscillatory and rotational motions are robust only a few percent of the published papers on pendula dynamics refer to the rotational motion. Rotating solutions of a pendulum have been studied mainly in the case of pendulum parametric excitation. Koch and Leven [39] used Melnikov's method to detect bifurcations where harmonic and subharmonic rotating solutions are born. The closed form expression for the lower boundary in frequency-amplitude excitation parameters space has been derived for the region of existence of the stable rotating solution. Capecchi and Bishop [12,13] studied rotating solutions analytically using harmonic balance method. Approximate analytical solutions have been compared with numerical results. They also constructed basins of attraction for different types of motion. Later Clifford and Bishop [15] and Garira and Bishop [29] investigated rotating solutions numerically and introduced the classification of such trajectories distinguishing purely rotating, oscillating rotating, straddling rotating and large amplitude rotating orbits. Szemplinska-Stupnicka et al. [71,72] conducted numerical studies of the parametrically excited pendulum, which have been illustrated using basins of attraction, bifurcation diagrams and attractor manifolds phase portraits. They have identified global bifurcations responsible for the onset of complex transient and/or steady state dynamics and various other aspects including fractal basin boundaries and coexistence of rotating solutions with other (including nonrotating) attractors. Extensive numerical simulations have been performed by Xu et al. [78-81]. Various parameter space plots for different sets of initial conditions and damping which allow to follow the development of attractors in the excitation amplitude-frequency parameters space have been calculated. The problem of dynamical integrity of both rotating and oscillating competing trajectories has been studied by Lenci and Rega [43] using a systematic construction of basins of attractions for varying parameters. The cross-erosion and the effects of secondary attractors in reducing the attractors safety, and thus its practical reliability, has been pointed out. Some analytical and experimental studies of the rotating solutions were also conducted by Xu et al. in [80,81]. In 2008, Lenci et al. [44] considered period-1 rotations analytically and obtained the approximation for the lower stability boundary associated with these period-1 rotations in the forcing parameter planes. De Paula et al. [55] have applied chaos control methods to avoid bifurcations that destabilize the rotating motion keeping the desired rotation over the extended parameter range. Pendula excited by a combination of the vertical and horizontal forcing at the pivot have been considered in the literature but they are far less researched [26,30,31,32,45,48,73]. Ge and Lin [30] numerically studied the response of a pendulum, whose pivot has been vertically excited and has been free to move horizontally. Mann and Koplów [48] used a combination of experimental measurements and analytical predictions (based on the method of multiple scales) to understand the results of the pitchfork bifurcation. Thompson et al. [73] have investigated the dynamics of the elliptically excited pendulum numerically concentrating on the change of stability boundaries of rotational motion due to the introduction of horizontal component. A pendulum excited by the combination of vertical and horizontal forcing at the pivot point has been considered by Pavlovskaja et al. [56]. Analytical approximations of period-1 rotations and their stability boundary on the excitation parameters plane have been derived using asymptotic analysis for the pendulum excited elliptically and along a tilted axis. One should mention the studies which have been concentrated on the oscillations of the inverted pendulum excited along a tilted axis (see e.g. [70,82]). Lythoof [47] have explained

why when a simple harmonic pendulum is viewed binocularly with a neutral-tint filter in front of one eye, the pendulum, instead of swinging to and fro in a plane, appears to swing in an ellipse, first advancing towards and then receding from the observer. A simple mechanical system consisting of the rotating pendulum has been used in the experimental studies of Lorenz chaos [14]. A model which comprises a rotating pendulum linked by an oblique spring pinned to its rigid support is investigated in [65]. This model provides a cylindrical dynamical system with both smooth and discontinuous regimes depending on the value of a system parameter and also the dynamics transient relying on the coupling strength between the rotating pendulum and the linked spring. Finally, one should mention the studies in which the pendulum is excited parametrically by the random signal [8,83,84]. To summarize these studies it should be pointed out that the rotational solutions exist over limited parameters range and there are numerous bifurcations of the system that destabilize a rotational motion.

The study of synchronization of oscillating pendula can be traced back to the works of the Dutch researcher Christian Huygens in XVIIth century [33,34]. He showed that a couple of mechanical clocks hanging from a common support were synchronized. Huygens had found that the pendulum clocks swung in exactly the same frequency and  $\pi$  out-of-phase, i.e., in antiphase synchronization. After the external perturbation, the antiphase state was restored within half an hour and remained indefinitely. Recently, several research groups revisited the Huygens' experiment [7,17-19,22-24,36-38,59,66,74,76,77]. Pogromsky et al. [61] designed a controller for synchronization problem for two pendula suspended on an elastically supported rigid beam. To explain Huygens' observations, Bennett et al. [4] built an experimental device consisting of two interacting pendulum clocks hanged on a heavy support which was mounted on a low-friction wheeled cart. The device moves by the action of the reaction forces generated by the swing of two pendula and the interaction of the clocks occurs due to the motion of the clocks base. It has been shown that to repeat the results of Huygens, high precision (the precision that Huygens certainly could not achieve) is necessary. Another device mimicking Huygens' clock experiment, the so-called 'coupled pendula of the Kumamoto University' [41], consists of two pendula whose suspension rods are connected by a weak spring, and one of the pendula is excited by an external rotor. The numerical results of Fradkov and Andrievsky [28] show simultaneous approximate in-phase and antiphase synchronization. Both types of synchronization can be obtained for different initial conditions. Additionally, it has been shown that for the small difference in the pendula frequencies they may not synchronize. A very simple demonstration device was built by Pantaleone [54]. It consists of two metronomes located on a freely moving light wooden base. The base lies on two empty soda cans which smoothly rolls on the table. Both in-phase and antiphase synchronizations of the metronomes have been observed. Synchronous configurations of a pair of double pendula has been identified in [40]. Finally, one should mentioned the first experimental observation of chimera states in mechanical system of a number of coupled metronomes [49].

Mechanical systems that contain rotating parts (for example vibro-exciter, unbalance rotors) are typical in engineering applications and for years have been the subject of intensive studies [16,42,75]. One problem of scientific interest, which among others occurs in such systems, is the phenomenon of synchronization of different rotating parts [2,5,51] and references within]. Despite different initial conditions, after a sufficiently long transient, the rotating parts move in the same way - complete synchronization or a permanent constant shift is established between their displacements, i.e., the angles of rotation - phase synchronization [2,5,21,22,51]. Synchronization occurs due to dependence of the periods of rotating elements motion and the displacement of the base on which these elements are mounted [27]. Prasad [62] considers the system of coupled counter-rotating oscillators and observes mixed synchronizations, i.e., some systems' variables are synchronized in-phase, while others are

out-of-phase. The dynamics of the system consisting of  $n$  rotating (in the same direction) pendula mounted on the movable beam have been considered in [5,20]. The pendula have been excited by the external torques which are linearly dependent on the angular velocities of the pendulums. As the result of such excitation, each pendulum rotates around its axis of rotation. It has been shown that both complete and phase synchronizations of the rotating pendula are possible. The approximate analytical conditions for both types of synchronizations and equations which allow the estimation of the phase differences between the pendula have been derived. Contrary to the case of the oscillatory pendula [17-19,22,23,37,38], phase synchronization is not limited to three and five clusters' configurations. The case of slowly rotating pendula and the influence of the gravity on their motion have been considered. The obtained results have been compared to those of Blekhman [5]. The dynamics of the similar system in which one pendulum rotates counter-clockwise, i.e., has a positive angular velocity, while the remaining pendula rotate clockwise with negative angular velocity has been studied in [21]. Two cases have been considered: (i) pendula rotate in the horizontal plane, i.e., the gravity has no influence on their motion, (ii) pendula rotate in the vertical plane and their weight causes the unevenness of their rotation, i.e., each pendulum slows down when the center of its mass goes up and accelerates when the center of its mass goes down. It has been shown that in such systems, despite opposite directions of rotation different types of synchronization occur. The dynamics of the pendula suspended on the nonlinear oscillators has been studied in [9,10,35]. The regions of stable synchronous rotational motion have been identified. In [69] the dynamics of the set of two pairs of double pendula mounted on the platform which oscillates vertically has been studied. Using a custom designed experimental rig different types of synchronous motion of rotating pendula have been identified. The extreme sensibility of the synchronized state on the system parameters and initial conditions has been pointed out.

In this review we consider the dynamics of the system consisting of  $n$  pendula mounted on the movable beam. The pendula are excited by the external torques which are linearly dependent on the angular velocities of the pendula. As the result of such excitation each pendulum rotates around its axis of rotation. We consider two cases: (i) all pendula rotate in the same direction, (ii) one pendulum rotates in the opposite direction to the other pendula. It has been shown that both complete and various types of phase synchronizations of the rotating pendula are possible. The synchronization mechanism base on the energy transfer between pendula via the oscillating beam has been identified. We derive the approximate analytical conditions for each type of synchronizations and equations which allow the estimation of the phase differences between the pendula. We consider the case of slowly rotating pendula and consider the influence of the gravity on their motion. Our results have been compared to those of [5]. Differences of both analyses have been pointed out and explained. The case when the excitation of one pendulum is weakening or even stops operating is also considered. We give evidence that the initial synchronization and the energy transfer between pendula can extend the rotational motion of this pendulum. We give evidence that our results are robust as they exist in the wide range of system parameters.

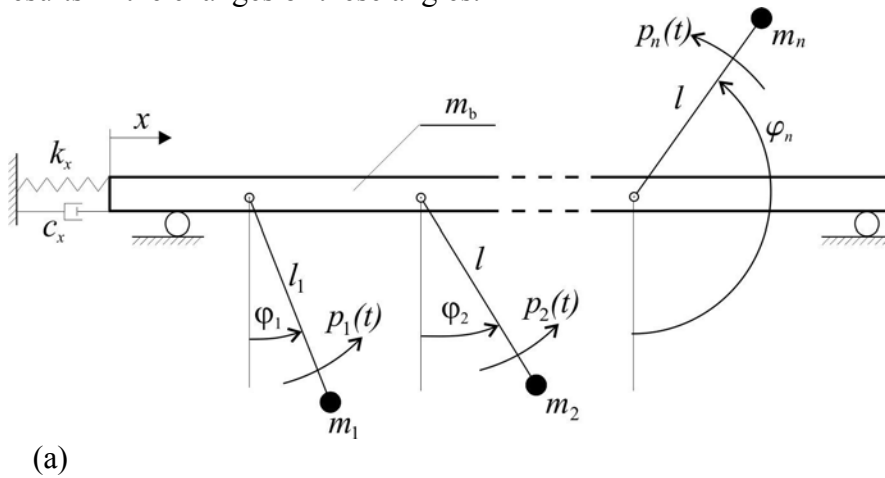
This review paper is organized as follows. Section 2 explains how the synchronization can be achieved in the system of the coupled pendula. We consider two cases: (i) externally excited pendula are mounted to the movable beam, (ii) unexcited pendula are mounted on oscillating platform. Both cases are illustrated by the examples of experimentally observed synchronous states. In Sec. 3 we describe the considered model and identify the synchronization mechanism. The approximate analytical conditions for each type of synchronizations are derived. The main Section 4 gives several numerical examples of the synchronous behavior. The cases of both identical and nonidentical pendula as well as of

identically and differently excited pendula are considered. Sec. 5 describes the behavior of the system when the excitation of one of the pendula weakens or vanishes. Finally, we summarize our results in Sec. 6.

## 2. Synchronous states of rotating pendula

Let us consider the systems shown in Figure 3(a-c). Each system consists of a rigid beam of mass  $m_B$  on which  $n$  rotating pendula are mounted. In Figure 3(a,b) the beam is connected to a stationary base by the spring (or springs) with stiffness coefficient  $k_x$  and a damper (or dampers) with a damping coefficient  $c_x$ . Due to the existence of the forces of inertia, which act on each pendulum pivot, the beam can move in horizontal (Figure 3(a)) or vertical (Figure 3(b)) directions (this motion is described by coordinate  $x$ ). The masses of the pendula are indicated as  $m_i$ ;  $l_i$  are the lengths of the pendula. The rotation of the  $i$ -th pendula is described by  $\varphi_i$ . The rotations of the pendula are damped by linear dampers (not shown in Figure 3) with damping coefficient  $c_{\varphi_i}$ . Each pendulum is driven by the drive torque inversely proportional to its velocity:  $p_{oi} - \dot{\varphi}_i p_{li}$ . If any other external forces do not act on the pendulum, then under the action of such a moment it rotates with constant angular velocity. As the system is in a gravitational field ( $g=9.81$  - acceleration of gravity), the weight of the pendulum causes the unevenness of its rotation: the pendulum slows down, when the center of mass rises up and accelerates when the center of mass falls down. The effect of gravity is important in the case of slow rotations of the pendula. For high rotational speed it can be neglected as in the studies of rotor dynamics [16,42,75 and references within]. It is assumed that  $p_{li} > 0.0$ . If  $p_{oi}$  torque is positive, the pendulum rotates to the left having a positive value of the instantaneous angular velocity, if  $p_{oi} < 0.0$ , the pendulum rotates to the right with a negative angular velocity. In the system shown in Figure 3(c) pendula are forced to rotate (and oscillate) by the parametrical excitation, i.e., the periodic motion of the base to which they are mounted.

To explain how the synchronization can be achieved in the systems of Figure 3(a,b) first consider the case of identical pendula and nonmovable beam. In this case all pendula have the same period of rotations (the pendula have the same masses and lengths). The rotations of the pendula are initiated by non-zero initial conditions and the pendula's evolutions tend to the limit cycles. The pendula are not coupled and the phase angles between their displacements have fixed values, depending on initial conditions. Any perturbation of the pendula results in the changes of these angles.





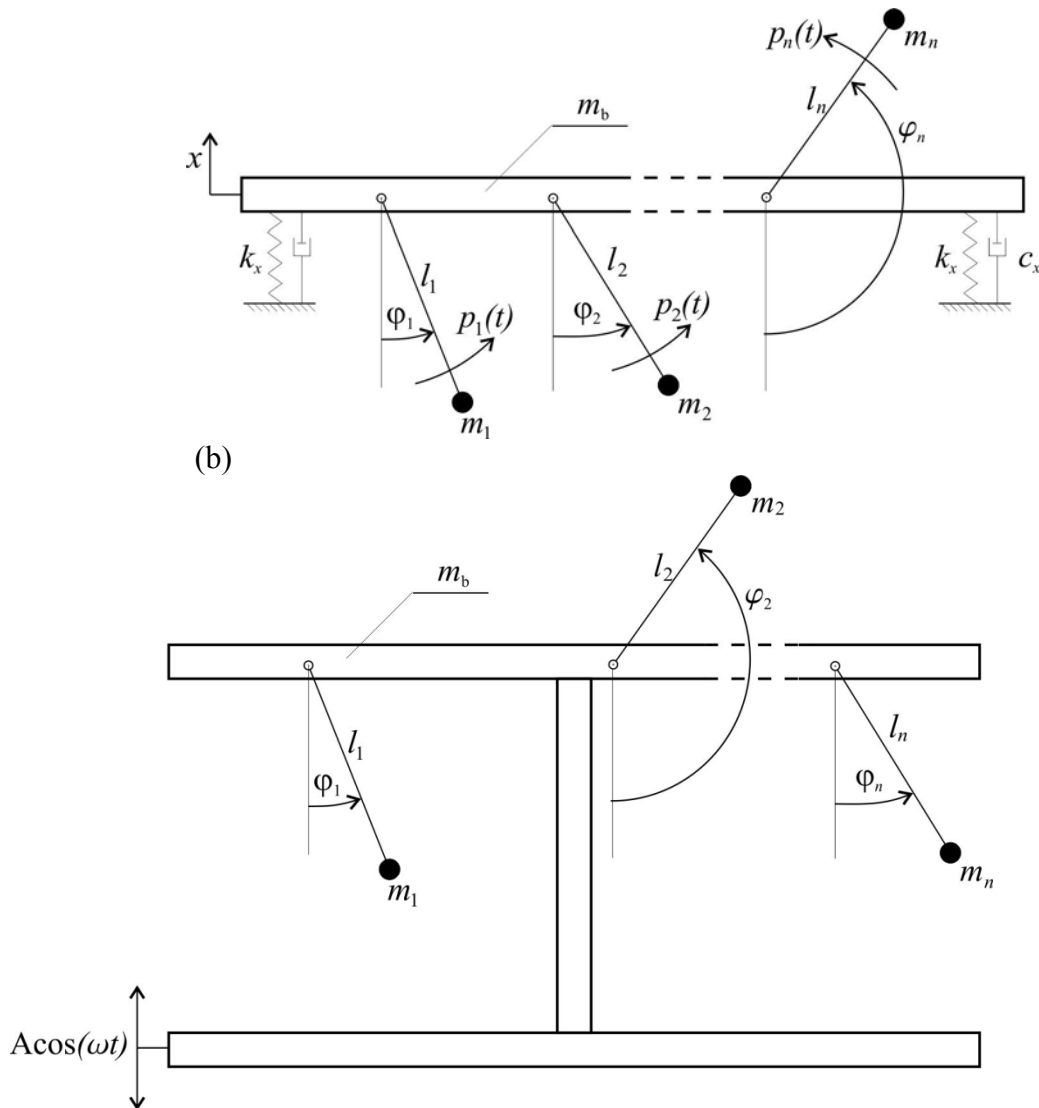


Figure 3. (a,b) externally forced pendula mounted to the beam which can move; (a) horizontally (b) vertically, parametrically excited pendula mounted to the beam which oscillates periodically.

When the beam can move (horizontally or vertically), the oscillations of the beam excited by the forces with which pendula act on it, cause the changes of the phase shifts between the pendula's displacements and differentiate the angular velocity of their rotations. When after the transient time, all pendula have the same angular velocity of rotation and there are constant phase shifts between the pendula's displacements, we can say that the pendula achieve synchronization [6,57,60,63,64]. The state of synchronization is achieved when the motion of the system is periodic and there are constant phase shifts between the pendula displacements [5,20,21]. The values of the phase shifts characterize the synchronous configuration and are independent of the initial conditions (unless the initial conditions belong to the basin of attraction of the particular configuration).

For systems like Figure 3(a,b) the synchronization of the rotating pendula has been observed experimentally in [85]. A simple rig consisting of three direct-current electrical motors mounted on the wooden plate which can oscillate vertically (shown in Figure 4) has been considered. The pendula are mounted at the end of the motor's rods. The control system (for details see [85]) has been used to vary the pendula's angular velocity. The sponges are used as springs and viscous dampers.



Figure 4. The experimental rig: three direct-current electrical motors mounted on the wooden plate which can oscillate vertically.

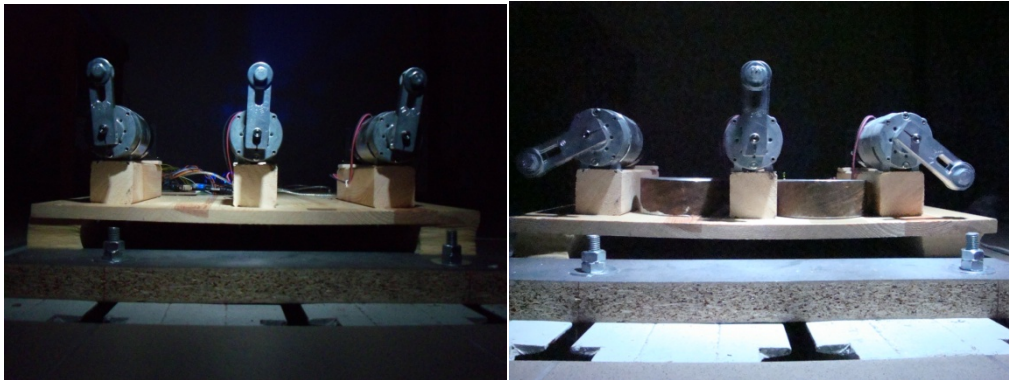


Figure 5. Experimentally observed synchronous configurations, (a) complete synchronization, (b) synchronization with the phase shifts between pendula equal to  $2\pi/3$ .

The examples of experimentally observed synchronous configurations are shown in Figure 5(a,b). Figure 5(a) presents the complete synchronization of three pendula. The configuration in which the phase shifts between pendula's displacement are equal to  $2\pi/3$  is illustrated in Figure 5(b).

In the case of Figure 3(c) we cannot speak about the synchronization between the pendula but the pendula can synchronize with the periodic parametrical forcing (phase locking) [52]. This can lead to the occurrence of the various synchronous states of rotating pendula [69].



Figure 6. Experimental implementation of the parametrically excited pendula of Figure 3(c).

In [69] the system like one in Figure 3(c), i.e., the system of four pendula arranged into a cross structure as shown in Figures 6 has been considered. The base, mounted on the shaker, is excited in the vertical direction by a parametric excitation  $A\cos(\omega t)$ . In the experiment, the rig has been mounted on the shaker LDS V780 Low Force Shaker. The shaker introduces

practically kinematic periodic excitation  $A \cos \omega t$ , where  $A$  and  $\omega$  are the amplitude and the frequency of the excitation, respectively. At initial moments the pendula have been assumed to be in the upper position, i.e.,  $\varphi_{1-4} = \pi \pm \pi/36$ . We fix the value of the excitation amplitude  $A=0.01 \pm 0.005$  [m] and consider excitation frequency  $\omega$  as a control parameter.

Rotating pendula can be 1:1 and 1:2 synchronized with the oscillations of the platform. In the considered system one can observe the synchronous states of both clockwise and counter-clockwise rotating pendula. In the experiment using a simple mechanical rig, the existence of different types of synchronous configurations of rotating nonidentical pendula, has been confirmed. Typical examples of different types of synchronous states are shown in Figures 7(a-d), where yellow arrows indicate the direction of rotation. For a qualitative classification of the pendula behavior, we use the following nomenclature; the pendula which rotate clockwise or counter-clockwise are marked by + and -, respectively, the pendula which are at rest are marked by 0. The angular velocity of the pendulum is given as follows:  $\dot{\varphi}_i = \omega t + b \sin(\omega t)$ , where  $i=1, \dots, 4$ , for the case of clockwise rotation and  $\dot{\varphi}_i = -\omega t + b \sin(-\omega t)$ , where the harmonic component describes the influence of the gravity on the motion of pendula ( $b$  is constant for all pendula as their masses are the same) [20,21]. Figure 7(a) presents the case when all pendula rotate in the same direction, i.e., (+,+,+,+). The pendula's displacements fulfill the relation  $\varphi_i - \varphi_j = 0$ , where  $i, j=1, 2, 3, 4, i \neq j$ . In Figure 7(b) one observes the synchronous motion when 3 pendula (1, 2, and 3) rotate in the same direction, while the fourth in the opposite one (+,+,+,-). In this case,  $\varphi_{1-3} + \varphi_4 = 0$  and pendulum 4 is in the state of mirror synchronization [21] with the cluster of synchronized pendula 1, 2 and 3. In Figure 7(c), we present the variation of the case (+,+,+,-) when three pendula rotate in the same rotation velocity while the fourth one rotates twice slower. Pendula 1, 2, and 3 are synchronized. The case when two pendula rotate clockwise and two counterclockwise is presented in Figure 7(d). The pairs of the pendula which rotate in the same directions are synchronized and are in the state of cluster antiphase synchronization [21], i.e.,  $\varphi_{1,2} + \varphi_{3,4} = \pi + b \sin(\omega t)$ .

All the observed synchronous states are stable but their basin of attraction are very small and the small perturbations (smaller than the accuracy of the shaker) can lead the system to the other configuration. The likelihood that the system will remain in a given configuration is very small and in the experiments practically equal to zero. In such systems one has to use the concept of basin stability [87]. This has been confirmed in the numerical simulations summarized in Figure 8 (for details see [67]).

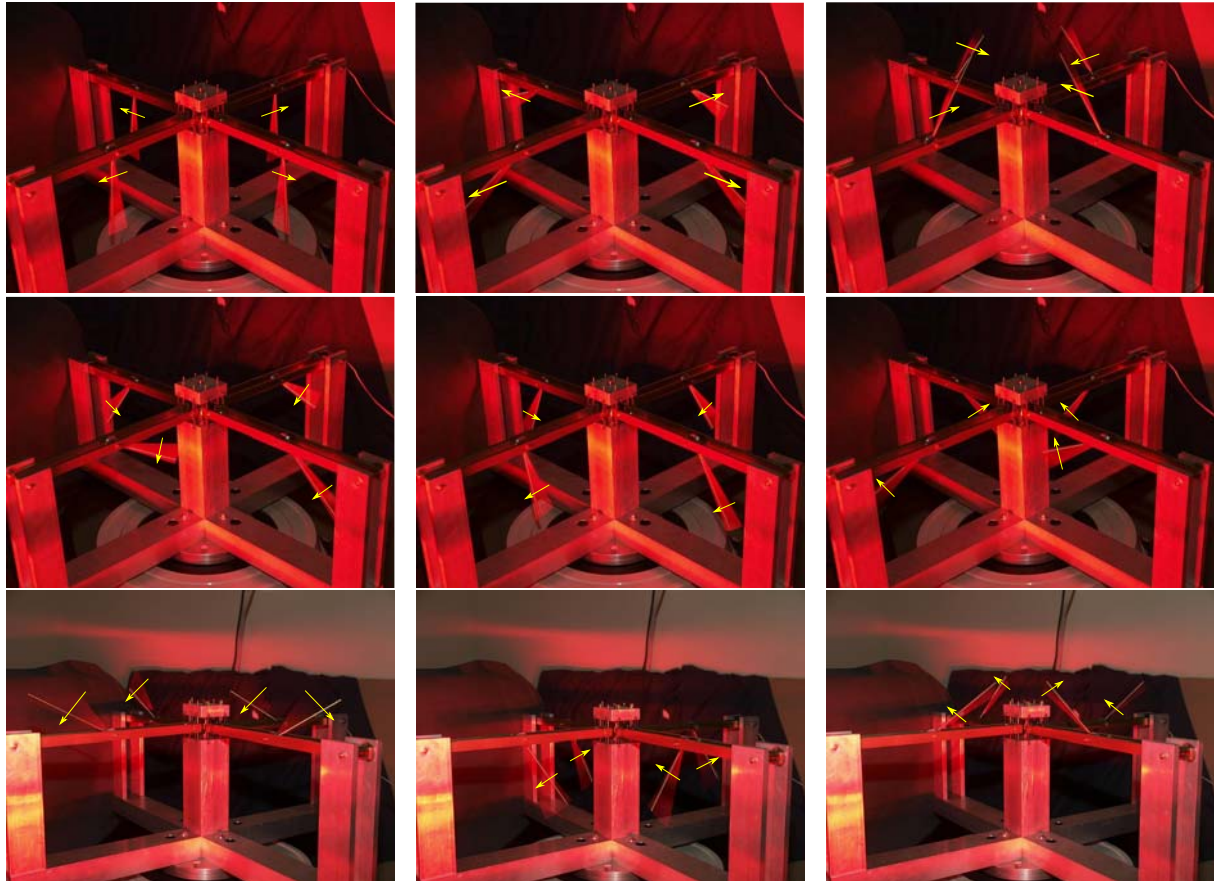


Figure 7. Different types of experimentally observed synchronous states; (a) pendula rotate clockwise (+,+,+,+),  $\omega=20.00$  [rad/s], (b) 3 pendula rotate clockwise while the fourth one counterclockwise (+,+,+,-),  $\omega=24.00$  [rad/s], (c) 3 pendula rotate clockwise ( $\omega=29.00$  [rad/s]) while the fourth one counterclockwise (+,+,+,-) with twice slower angular velocity, (d) 2 pendula rotate clockwise and 2 counterclockwise (+,+,-,-),  $\omega=35.00$  [rad/s].

The extreme sensitivity of the synchronized state on the system parameters and the initial conditions which introduces pseudo-randomness to the predictability of the synchronous state has been observed. The basins of attraction of different synchronous states are presented in Figure 8. It can be seen that the type of pendula synchronization very strongly depends on the excitation parameters. Generally, synchronous rotation of pendula is robust as it exists for the wide range of excitation parameters, but particular synchronous states are very sensitive to the changes of system parameters as shown in Figure 8.

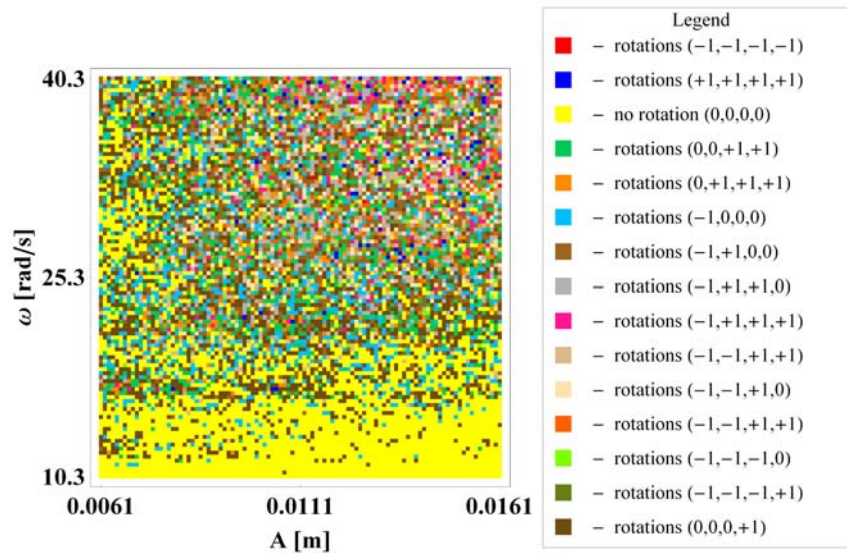


Figure 8. Basins of attraction of the combined synchronous states of 4 parametrically excited pendula.

In practical application of the systems based on the parametrically excited pendula one has to apply a feedback control mechanism. This mechanism should be capable to keep the pendula rotating permanently in the desired synchronous configuration.

### 3. Synchronization mechanism

#### 3.1. Equations of motion

Let consider the system shown in Figure 3(a). The equations of motion described above are as follows:

$$m_i l_i^2 \ddot{\phi}_i + m_i l_i \ddot{x} \cos \phi_i + c_{\phi_i} \dot{\phi}_i + m_i l_i g \sin \phi_i = p_{0i} - p_{1i} \phi_i, \quad (1)$$

$$\left( m_B + \sum_{i=1}^n m_i \right) \ddot{x} + c_x \dot{x} + k_x x = \sum_{i=1}^n m_i l_i \left( -\dot{\phi}_i \cos \phi_i + \dot{\phi}_i^2 \sin \phi_i \right), \quad (2)$$

where  $i=1,2,\dots,n$ . In our numerical simulations eqs.(1,2) have been integrated by the 4<sup>th</sup> order Runge-Kutta method. The obtained results confirmed the existence of the phenomenon of phase synchronization in the considered system and allowed the determination of phase angles between the synchronized pendula. Additionally the numerical integration of eqs.(1,2) allows the determination of the basins of attraction of different coexisting configurations of the synchronized pendula.

#### 3.2. Synchronization conditions

##### 3.2.1. Energy balance of pendula

Multiplying eq. (1) by the angular velocity of the pendula  $\dot{\phi}_i$  we obtain the equation of the energy balance:

$$m_i l_i^2 \ddot{\phi}_i \dot{\phi}_i + m_i l_i g \dot{\phi}_i \sin \phi_i = -c_{\phi_i} \dot{\phi}_i^2 - m_i l_i \ddot{x} \cos \phi_i \dot{\phi}_i + p_{0i} \dot{\phi}_i - p_{1i} \dot{\phi}_i^2, \quad (3)$$

where  $i=1,\dots,n$ . Assume that the motion of both pendula is periodic with period  $T$  and integrating eq.(3) over the period  $T$  we obtain the equation of the energy balance:

$$\begin{aligned} & \int_0^T m_i l_i^2 \ddot{\phi}_i \dot{\phi}_i dt + \int_0^T m_i l_i g \dot{\phi}_i \sin \phi_i dt = \\ & = -\int_0^T c_{\phi_i} \dot{\phi}_i^2 dt - \int_0^T m_i l_i \ddot{x} \cos \phi_i \dot{\phi}_i dt + \int_0^T (p_{0i} \dot{\phi}_i - p_{1i} \dot{\phi}_i^2) dt. \end{aligned} \quad (4)$$

Left hand side of eq.(4) represents the increase of the total energy of the  $i$ -th pendulum. For the periodic oscillations of the pendula (and the beam) the angular velocities of the rotating pendula fluctuate around the constant mean value so this increase has to be equal zero

$$\int_0^T m_i l_i^2 \ddot{\phi}_i \dot{\phi}_i dt + \int_0^T m_i l_i g \dot{\phi}_i \sin \phi_i dt = 0. \quad (5)$$

The first component of the right hand side of eq. (4) gives the energy dissipated by the viscous dampers  $c_{\phi_i}$ :

$$W_i^{DAMP} = \int_0^T c_{\phi_i} \dot{\phi}_i^2 dt. \quad (6)$$

The next component of the right hand side of eq. (4) describes the energy transferred by the  $i$ -th pendulum to the beam (when it is positive) or the energy transferred from the beam to the  $i$ -th pendulum:

$$W_i^{SYN} = \int_0^T m_i l_i \ddot{x} \cos \phi_i \dot{\phi}_i dt. \quad (7)$$

The last component of the right hand side of eq.(4) gives the energy supplied to the  $i$ -th pendulum by the driving torque:

$$W_i^{DRIVE} = \int_0^T (p_{0i}\dot{\varphi}_i - p_{1i}\dot{\varphi}_i^2) dt. \quad (8)$$

Substituting eqs. (5-8) into eq. (4) i.e.,

$$W_i^{DRIVE} = W_i^{DAMP} + W_i^{SYN}. \quad (9)$$

one obtains pendula' energy balances.

### 3.2.2. Energy balance of the beam

Multiplying eq.(2) by beam's velocity  $\dot{x}$  one gets:

$$\left( m_B + \sum_{i=1}^n m_i \right) \ddot{x}\dot{x} + c_x \dot{x}^2 + k_x x\dot{x} = \sum_{i=1}^n m_i l_i \dot{x} \left( -\ddot{\varphi}_i \cos \varphi_i + \dot{\varphi}_i^2 \sin \varphi_i \right) \quad (10)$$

and assuming that beam's oscillations are periodic and integrating eq.(10) over period  $T$  we obtain the energy balance of the beam:

$$\int_0^T \left( m_B + \sum_{i=1}^n m_i \right) \ddot{x}\dot{x} dt + \int_0^T k_x x\dot{x} dt = - \int_0^T c_x \dot{x}^2 dt + \int_0^T \left( \sum_{i=1}^n m_i l_i \left( -\ddot{\varphi}_i \cos \varphi_i + \dot{\varphi}_i^2 \sin \varphi_i \right) \right) \dot{x} dt. \quad (11)$$

Left hand side of eq.(11) represents the increase of the total energy of the beam. As the oscillations are periodic this increase should be equal zero:

$$\int_0^T \left( m_B + \sum_{i=1}^n m_i \right) \ddot{x}\dot{x} dt + \int_0^T k_x x\dot{x} dt = 0 \quad (12)$$

First component on the left hand side of eq.(11) describes the energy dissipated by the viscous damper  $c_x$  during one period of oscillations:

$$W_{beam} = \int_0^T c_x \dot{x}^2 dt. \quad (13)$$

The next component gives the energy which is supplied to the beam by the pendula (the sum of the works performed during the period  $T$  by the forces with which pendula act on the beam):

$$\sum_{i=1}^{i=n} (W_i^{SYN}) = \int_0^T \left( \sum_{i=1}^n m_i l_i \left( -\ddot{\varphi}_i \cos \varphi_i + \dot{\varphi}_i^2 \sin \varphi_i \right) \right) \dot{x} dt. \quad (14)$$

Substituting eqs.(12-14) into eq. (11) we get the energy balance of the beam in the following form:

$$W_{beam} = \sum_{i=1}^{i=n} (W_i^{SYN}). \quad (15)$$

Substituting eq.(9) into eq. (15), i.e.,

$$W_1^{DRIVE} + W_2^{DRIVE} = W_1^{DAMP} + W_1^{DAMP} + W_{beam}. \quad (16)$$

we get the energy balance of system (1,2).

### 3.2.3. Synchronization conditions - linearized model

In this section we derive the approximate analytical conditions for synchronization of rotating pendula. Following the idea of Blekhman [5] to explain the phenomena of synchronization we determine and analyze the work done by the momentum with which the  $i$ -th pendulum acts on beam -  $W_i^{SYN}$ .

Let us assume that the damping in the system is small, i.e.,



$$W_{beam} \approx 0.0, \quad (17)$$

$$W_i^{DAMP} \approx 0.0.$$

When the oscillations are periodic and there is no energy dissipation there is no need for the energy supply, so

$$W_i^{DRIVE} = 0. \quad (18)$$

From eqs. (9) we have

$$W_i^{SYN} = 0. \quad (19)$$

(i) *Pendula rotating in the same directions*

As in [5], we assume that the pendula's angular velocities are constant, i.e., the fluctuations of the pendula's angular velocities caused by the motion in the gravitational field are so small that can be neglected. Hence, the pendula's accelerations are equal to zero and in the case, when the pendula rotate in the same direction, one gets linear functions describing the pendula's angles of rotation:

$$\begin{aligned} \dot{\varphi}_i &= \omega, \\ \varphi_i &= \omega t + \beta_i, \\ \ddot{\varphi}_i &= 0. \end{aligned} \quad (20)$$

Right hand side of eq.(2) describes the force with which  $n$  pendula are acting on beam:

$$F = \sum_{i=1}^n m_i l_i (-\ddot{\varphi}_i \cos \varphi_i + \dot{\varphi}_i^2 \sin \varphi_i) \quad (21)$$

Substituting eq. (20) into eq.(21) one gets:

$$F = \sum_{i=1}^n (m_i l_i \omega^2 \sin(\omega t + \beta_i)) \quad (22)$$

Substituting eq. (22) into eq. (2) and denoting

$$U = m_B + \sum_{i=1}^n m_i,$$

one gets:

$$U\ddot{x} + c_x \dot{x} + k_x x = \sum_{i=1}^n (m_i l_i \omega^2 \sin(\omega t + \beta_i)) \quad (23)$$

Assuming that the damping coefficient  $c_x$  is small the oscillations of the beam can be described in the following way:

$$\begin{aligned} x &= \frac{\omega^2}{k_x - \omega^2 U} \left( \sum_{i=1}^n (m_i l_i \sin(\omega t + \beta_i)) \right), \\ \ddot{x} &= \frac{-\omega^4}{k_x - \omega^2 U} \left( \sum_{i=1}^n (m_i l_i \sin(\omega t + \beta_i)) \right). \end{aligned} \quad (24)$$

In the equation of motion of each pendula (1) we have the component which has been identified as a synchronization momentum. Substituting eqs. (20,24) into eq. (7) and denoting

$$A = \frac{-\omega^4}{k_x - \omega^2 U}$$

one gets:



$$W_k^{SYN} = m_k l_k \int_0^T A \left[ \sum_{i=1}^n (m_i l_i \sin(\omega t + \beta_i)) \right] \omega \cos(\omega t + \beta_k) dt = 0. \quad (25)$$

After some calculations one gets

$$W_k^{SYN} = m_k l_k \pi A \left( \cos \beta_k \sum_{i=1}^n m_i l_i \sin \beta_i - \sin \beta_k \sum_{i=1}^n m_i l_i \cos \beta_i \right) = m_k l_k \pi A \sum_{i=1}^n m_i l_i \sin(\beta_i - \beta_k) = 0. \quad (26)$$

Eq. (26) allows the calculation of the phase angles  $\beta_k$  for which the synchronization takes place and the pendula rotate periodically. Eq. (26) is fulfilled for

$$\beta_1 = \beta_2 = \dots = \beta_n \quad (27)$$

and the pendula reach complete synchronization or when

$$\sum_{i=1}^n m_i l_i \cos \beta_i = 0, \quad \sum_{i=1}^n m_i l_i \sin \beta_i = 0, \quad (28)$$

and we observe phase synchronization. Note that the synchronization conditions given by eqs. (27-28) are identical to those obtained by Blekhman using small parameter methods [5].

In the case of identical pendula condition (28) is simplified to the following form

$$1.0 + \cos \beta_2 + \cos \beta_3 + \dots + \cos \beta_n = 0, \quad (29)$$

$$\sin \beta_2 + \sin \beta_3 + \dots + \sin \beta_n = 0.$$

It can be shown that eqs. (29) are fulfilled for the following phase angles

$$\beta_i = \frac{2\pi(i-1)}{n}, i = 1 \dots n. \quad (30)$$

For  $n=2$  (two pendula) eq.(30) gives  $\beta_1=0$ ,  $\beta_2=0$  and  $\beta_1=0$ ,  $\beta_2=\pi$ .

For  $n=3$  (three pendula) eq.(30) gives  $\beta_1=0$ ,  $\beta_2=0$  (as observed in Figure 5(a)) and  $\beta_1=0$ ,  $\beta_2=2\pi/3$  and  $\beta_3=4\pi/3$  (Figure 5(b)).

In the considered case the synchronization state of the pendula' motion is the periodic motion of the system (1,2) in which phase angles  $\beta_i$  fluctuate around constant mean values (characteristic for a given configuration). The mean values of  $\beta_i$  are independent of initial conditions (in the basin of attraction of the particular configurations) and not sensitive to the external perturbations. In this state, when the pendula are identical there is no energy transfer between the pendula via the beam.

### (ii) Pendula rotating in different directions

In the case when  $m$  of the total  $n$  pendula rotates in the opposite direction to the rest (i.e.,  $n-m$ ) of the pendula the phase differences between pendula in the synchronous configurations have to be calculated from different equations. Let assume the pendulum 1 rotates clockwise and the other pendula counterclockwise. In this case the linearized equations describing pendula's displacements and angular velocities are as follows:

$$\begin{aligned} \dot{\varphi}_1 &= \omega, \\ \dot{\varphi}_2 &= \dot{\varphi}_3 = \dots = \dot{\varphi}_n = -\omega, \\ \varphi_1 &= \omega t + \beta_1, \\ \varphi_2 &= -\omega t + \beta_2, \\ &\dots \\ \varphi_n &= -\omega t + \beta_n, \\ \ddot{\varphi}_1 &= \ddot{\varphi}_2 = \dots = \ddot{\varphi}_n = 0.0. \end{aligned} \quad (31)$$

Repeating the calculations presented in Sec. 3.3.2.1. one gets the following equations (equivalent to eqs. (26)):

$$\begin{aligned}
 W_1^{SYN} &= A\pi(m_1 l_1 m_1 l_1 \sin(\beta_1 - \beta_1) + m_1 l_1 m_2 l_2 \sin(\beta_1 + \beta_2) + \dots + m_1 m_n \sin(\beta_1 + \beta_n)) = 0 \\
 W_2^{SYN} &= A\pi(-m_2 l_2 m_1 l_1 \sin(\beta_2 + \beta_1) + m_2 l_2 m_2 l_2 \sin(\beta_2 - \beta_2) + \dots + m_2 m_n \sin(\beta_2 - \beta_n)) = 0 \\
 W_3^{SYN} &= A\pi(-m_3 l_3 m_1 l_1 \sin(\beta_3 + \beta_1) + m_3 l_3 m_2 l_2 \sin(\beta_3 - \beta_2) + \dots + m_3 l_3 m_n l_n \sin(\beta_3 - \beta_n)) = 0 \quad (32) \\
 &\dots \\
 W_n^{SYN} &= A\pi(-m_n l_n m_1 l_1 \sin(\beta_n + \beta_1) + m_n l_n m_2 l_2 \sin(\beta_n - \beta_2) + \dots + m_n l_n m_n l_n \sin(\beta_n - \beta_n)) = 0
 \end{aligned}$$

Eqs.(32) allow the calculation of the value of phase angles  $\beta_i$  at which the motion of pendulums synchronization occurs, and thus the motion of the system is periodic.

In the case of  $n=2$  identical pendula, and assuming that  $\beta_1=0$ , eqs.(32) get the form of two identical equations:

$$\begin{aligned}
 \sin(\beta_2) &= 0 \\
 \sin(\beta_2) &= 0
 \end{aligned} \quad (33)$$

which are fulfilled in two cases: (i)  $\beta_2=0$  - the *mirror-synchronization (M)*, (ii)  $\beta_2=\pi$  - the *antiphase synchronization (A)* as given in Table 1.

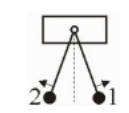
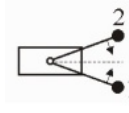
type of synchronization	phase difference between pendula	pendula's configuration
<i>mirror-synchronization (M)</i>	$\beta_1=0, \beta_2=0$	
<i>antiphase synchronization (A)</i>	$\beta_1=0, \beta_2=\pi$	

Table 1. Types of synchronization observed for  $n=2$  pendula rotating in opposite directions.

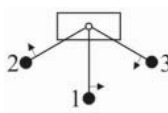

type of synchronization	phase difference between pendula	pendula's configuration
<i>tree-synchronization (T)</i>	$\beta_1=0, \beta_2=-\pi/3, \beta_3=-5\pi/3$	
<i>cluster-antiphase synchronization (CA)</i>	$\beta_1=0, \beta_2=\beta_3=\pi$	

Table 2. Types of synchronization observed for  $n=3$  pendula (pendulum 1 rotates in opposite direction to pendula 2 and 3).

For three identical pendula, assuming that  $\beta_i=0$ , eqs.(32) get the following form:

$$\begin{aligned}
\sin(\beta_2) + \sin(\beta_3) &= 0 \\
\sin(\beta_2) - \sin(\beta_2 - \beta_3) &= 0 \\
\sin(\beta_3) - \sin(\beta_3 - \beta_2) &= 0
\end{aligned} \tag{34}$$

which are fulfilled for:

(i)  $\beta_2 = -\pi/3$  and  $\beta_3 = -5\pi/3$  - the *tree-synchronization (T)*, (ii)  $\beta_2 = \beta_3 = \pi$  - the *cluster-antiphase synchronization (CA)* as given in Table 2.

## 4. Numerical examples

### 4.1. Two pendula rotating in the same direction

In this example we consider the system (1-2) with the following parameter values:  $m_1=m_2=1.00$ ,  $l_1=l_2=0.25$ ,  $c_{\varphi 1}=c_{\varphi 2}=0.01$ ,  $p_{01}=p_{02}=5.00$ ,  $p_{11}=p_{12}=0.50$ ,  $m_B =6.00$ . One can calculate that  $\dot{\varphi}_N = 10.0$  and  $U=8.0$ . We consider different values of stiffness coefficient  $k_x$  of the spring connecting the beam  $m_B$  with a fixed foundation so the beam can oscillate above or below the resonance, i.e., the frequency

$$\alpha_x = \sqrt{\frac{k_x}{U}} \quad (35)$$

is smaller or larger than the pendulum's 1 angular velocity  $\dot{\varphi}_N$ . The damping coefficient  $c_x$  has been selected in such a way as to be equivalent to the arbitrarily selected logarithmic decrement of damping  $\Delta=\ln(1.5)$ . As such a damping does not significantly change the period of the beam's free oscillations  $c_x$  can be calculated from the formula

$$c_x = \frac{\Delta\sqrt{k_x U}}{\pi}. \quad (36)$$

Typical time series of pendula' velocities and displacements are shown in Figure 9(a,b). The unit of time on the horizontal axis is the number  $N = \dot{\varphi}_N t/2\pi$ , i.e., the number of complete revolutions of the pendulum rotating with constant angular velocity  $\dot{\varphi}_N$ . Figure 9(a) shows the angular velocities of pendula  $\dot{\varphi}_1$  and  $\dot{\varphi}_2$  for a system with low stiffness coefficient  $k_x=100.0$ , so  $\alpha_x = \sqrt{10.0/8.0} = 3.53 < 10.0 = \dot{\varphi}_N$ . The following initial conditions have been considered:  $\varphi_{10}=0$ ,  $\varphi_{20}=\pi/4$ ,  $\dot{\varphi}_{10} = \dot{\varphi}_{20} = 0.0$ . As one can see, after the transient the phase difference between the pendula' velocities tends to  $\pi$ . Figure 9(b) shows the angular displacement of pendulum 2,  $\varphi_2 - \varphi_1$ , related to the displacement of the first pendulum. One can notice that after the decay of the transient, this angle oscillates around a constant average value  $\pi$  and the system reaches the state of antiphase synchronization. This state for small values of  $k_x$  is reachable for any initial conditions. Shown in both figures the fluctuations of angular velocities and displacements, are caused by the weight of pendula, i.e., pendulum speeds during the motion down and slows when its mass rise up.

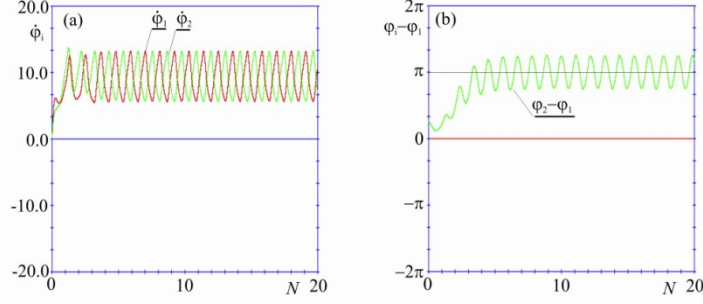


Figure 9. Time series of pendula' velocities and displacements calculated from eqs (1,2):  $m_1=m_2=1.00$ ,  $l_1=l_2=0.25$ ,  $c_{\phi_1}=c_{\phi_2}=0.01$ ,  $p_{01}=p_{02}=5.00$ ,  $p_{11}=p_{12}=0.50$ ,  $m_B=6.00$ ,  $\dot{\phi}_n=10.0$  and  $U=8.0$  (the unit of time on the horizontal axis is the number  $N = \dot{\phi}_N t / 2\pi$ , i.e., the number of complete revolutions of the pendulum rotating with constant angular velocity  $\dot{\phi}_N$ ); (a) angular velocities  $\dot{\phi}_1$  and  $\dot{\phi}_2$  for a system (1,2) with low stiffness coefficient  $k_x=100.0$ ,  $\phi_{10}=0$ ,  $\phi_{20}=\pi/4$ ,  $\dot{\phi}_{10} = \dot{\phi}_{20} = 0$ ; (b) angular displacement of pendulum 2:  $\phi_2 - \phi_1$  related to the displacement of the first pendulum.

The pendula' configurations characteristic for the system (1-2) with  $n=2$  pendula and its basins of attraction are shown in Figure 10(a-d). Figure 10(a) presents the configuration of antiphase synchronization with  $\beta_1=0$  and  $\beta_2=\pi$ . Notice that the same values of  $\beta_1$  and  $\beta_2$  can be calculated analytically from eq.(30) and condition (29) is fulfilled. The configuration complete synchronization is presented in Figure 10(b). This configuration is observed for larger values of coefficient  $k_x$  when condition (27) is fulfilled. Figure 10(c) shows the basins of attraction of the complete (white color) and anti-phase (gray color) synchronization states in the system with a stiffness coefficient of  $k_x=3600.0$ . The basins are shown in the  $\phi_{10}-\phi_{20}$  plane with fixed initial velocities  $\dot{\phi}_{10} = \dot{\phi}_{20} = 0$ . These basins for systems with different values of the stiffness coefficient  $k_x$ , shown on the plane  $k_x-\phi_{20}$  ( $\phi_{10}=0$ ,  $\dot{\phi}_{10} = \dot{\phi}_{20} = 0$ ) are presented in Figure 10(d). The results of Figure 10(d) and predictions of [5] are significantly different. Blekhman [5] predicts the existence of complete (for  $k_x \dot{\phi}_N = U \dot{\phi}_N^2 < 800.0$ ) and antiphase (for  $k_x \dot{\phi}_N = U \dot{\phi}_N^2 > 800.0$ ) independently of initial conditions. Meanwhile, Figure 10(d) shows, that the boundary between the basins of attraction of complete and antiphase synchronizations is located significantly below the value of  $k_x \dot{\phi}_N$  and is not horizontal. For  $k_x < k_{x1} \approx 400.0$ , independently of initial conditions one observes the antiphase synchronization while for  $k_{x1} < k_x < k_{x2} \approx 600.0$  there exists the coexistence of complete and antiphase synchronizations. In the interval  $k_{x2} < k_x < k_{x3} \approx 1840.0$  independently of initial conditions the system (1,2) reaches the state of complete synchronization and for larger values of  $k_x > k_{x3}$  we have the coexistence of both synchronization states again.

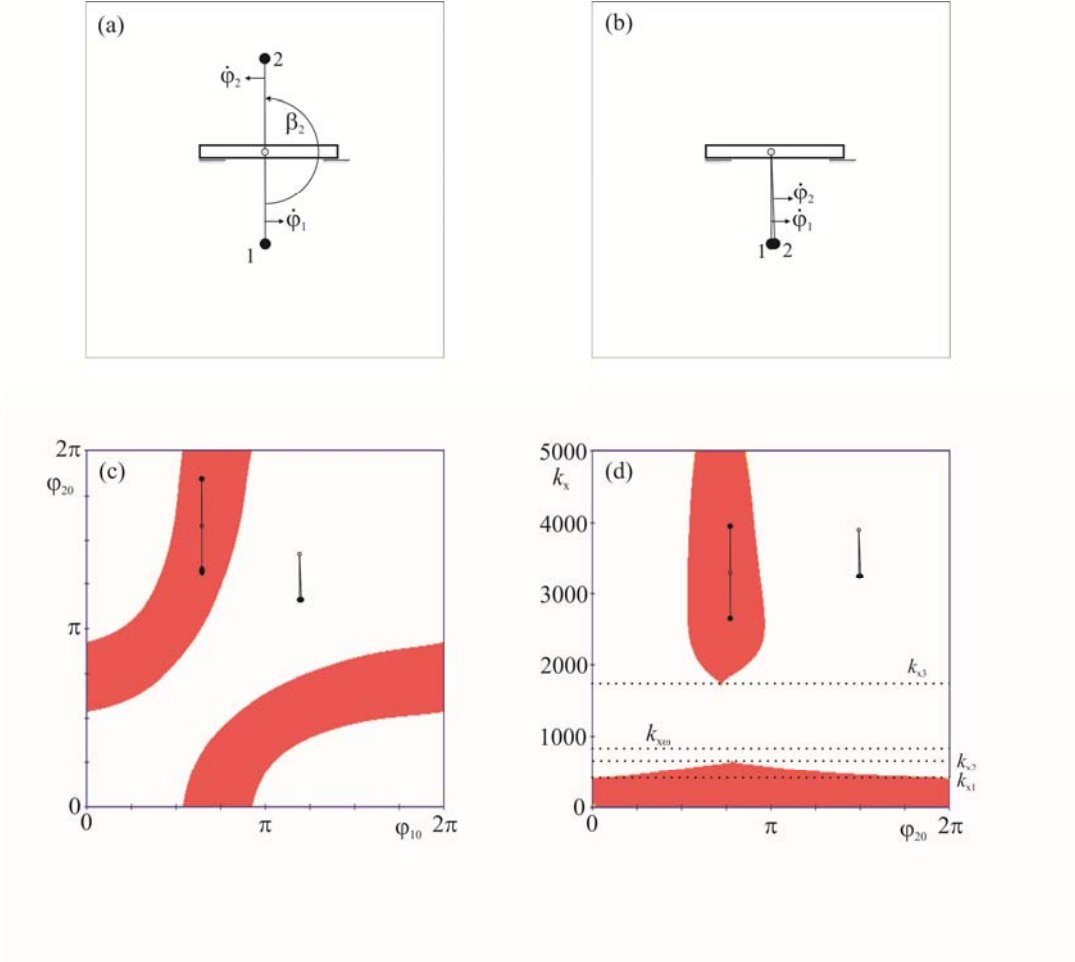


Figure 10. The pendula' configurations characteristic for the system (1,2) with  $n=2$  pendula and its basins of attraction; (a) configuration of antiphase synchronization with  $\beta_1=0$  and  $\beta_2=\pi$ , (b) complete synchronization, (c) basins of attraction of the complete (white color) and anti-phase (gray color) synchronization states,  $k_x=3600.0$  (the basins are shown in the  $\varphi_{10} - \varphi_{20}$  plane with fixed initial velocities  $\dot{\varphi}_{10} = \dot{\varphi}_{20} = 0$ , (d) basins attraction for different values of the stiffness coefficient  $k_x$ , shown on the plane  $k_x - \varphi_{20}$ ,  
 $(\varphi_{10} = \dot{\varphi}_{10} = \dot{\varphi}_{20} = 0)$

#### 4.2. Three pendula rotating in the same direction

Let us consider the system (1-2) with the following parameter values:  $m_1=m_2= m_3=1.00$ ,  $l_1=l_2=l_3=0.25$ ,  $c_{\varphi 1}=c_{\varphi 2}=c_{\varphi 3}=0.01$ ,  $p_{01}=p_{02}= p_{03}=5.00$ ,  $p_{11}=p_{12}= p_{13}=0.50$ ,  $m_B =6.00$ . One can calculate that  $\dot{\varphi}_N = 10.0$  and  $U=9.0$  (due to  $n=3$ ). The values of stiffness and damping coefficients  $k_x$  and  $c_x$  have been taken as in previous section.

Typical time series of pendula' velocities and displacements in the case of phase synchronization are shown in Figure 11(a,b). Figure 11(a) shows the angular velocities of pendula  $\dot{\varphi}_1, \dot{\varphi}_2$  and  $\dot{\varphi}_3$  for a system with low stiffness coefficient  $k_x=100.0$  and  $\alpha_x = \sqrt{10.0/9.0} = 3.33 < 10.0 = \dot{\varphi}_N$ . The following initial conditions have been considered:  $\varphi_{10} = 0, \varphi_{20} = \frac{\pi}{4}, \varphi_{30} = \frac{\pi}{2}, \dot{\varphi}_{10} = \dot{\varphi}_{20} = \dot{\varphi}_{30} = 0$ . As in the previous plots (Figure 9(a,b)) the unit of time on the horizontal axis is the number  $N = \dot{\varphi}_N t / 2\pi$ , i.e., the number of complete revolutions of the pendulum rotating with constant angular velocity  $\dot{\varphi}_N$ . As one can see, after the decay of transients the phase difference between the pendula velocities tends to

the constant value of  $2\pi/3$ . Figure 11(b) shows the angular displacement of pendula,  $\varphi_2 - \varphi_1$  and  $\varphi_3 - \varphi_1$ , related to the displacement of the first pendulum. One can notice that these angles in what follows referred as the relative displacements oscillate around a constant average values  $2\pi/3$  and  $4\pi/3$ . Such a state of phase synchronization is obtained for  $k_x=100.0$  and arbitrary initial conditions. Shown in both figures the angular velocity fluctuations and movements in relative terms, are caused by the motion in gravitational field. Numerically estimated phase shifts  $\beta_2=2\pi/3$  and  $\beta_3=4\pi/3$  are in good agreement with the values calculated analytically from eqs.(30).

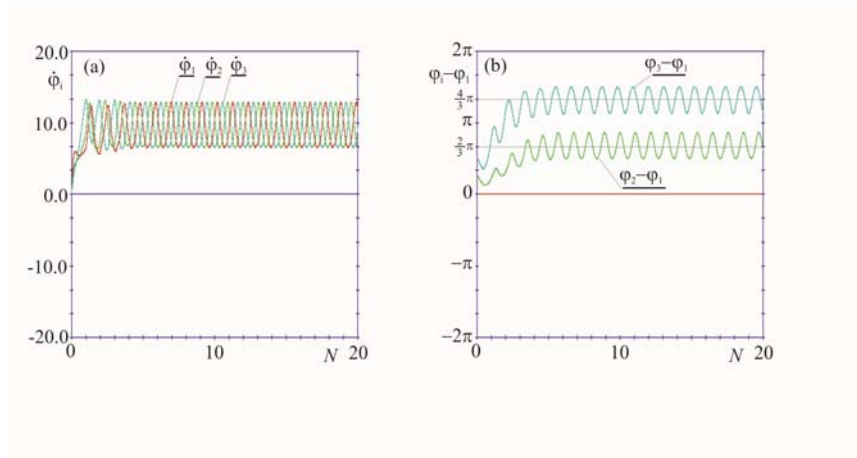


Figure 11. Time series of pendula' velocities and displacements in the case of phase synchronization,. (a) angular velocities of pendula  $\dot{\varphi}_1$ ,  $\dot{\varphi}_2$  and  $\dot{\varphi}_3$  for a system (1,2) with low stiffness coefficient  $k_x=100.0$  and  $\alpha_x = 3.33$ ,  $\varphi_{10} = 0$ ,  $\varphi_{20} = \frac{\pi}{4}$ ,  $\varphi_{30} = \frac{\pi}{2}$ ,  $\dot{\varphi}_{10} = \dot{\varphi}_{20} = \dot{\varphi}_{30} = 0$  (the unit of time on the horizontal axis is the number  $N = \dot{\varphi}_N t / 2\pi$ , i.e., the number of complete revolutions of the pendulum rotating with constant angular velocity  $\dot{\varphi}_N$ ), (b) angular displacement of pendula  $\varphi_2 - \varphi_1$  and  $\varphi_3 - \varphi_1$  related to the displacement of the first pendulum,  $\beta_2=2\pi/3$ ,  $\beta_3=4\pi/3$ .

In another example, it is assumed that  $k_x=3600.0$ , so  $\alpha_x = \sqrt{3600.0/9.0} = 20.0 > 10.0 = \dot{\varphi}_N$  and the system of the beam and three pendula eqs. (1,2) is below the resonance. We consider the following initial conditions:  $\varphi_{10} = 0$ ,  $\varphi_{20} = \frac{\pi}{4}$ ,  $\varphi_{30} = \frac{\pi}{2}$ , Figure 12(a,b) shows that after a transitional period the angular velocities of all three pendula are the same and the relative displacements  $\varphi_2 - \varphi_1$  and  $\varphi_3 - \varphi_1$  tend to zero, so one observes the state of complete synchronization. Due to the existence of gravitational field we observe the fluctuations of the pendula' motion caused by their weights.

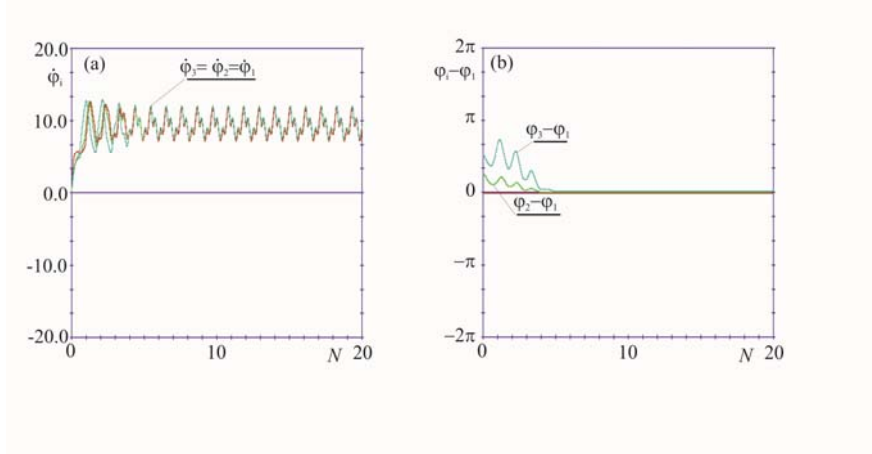


Figure 12. Time series of pendula' velocities and displacements in the case of the complete synchronization,. (a) angular velocities of pendula  $\dot{\varphi}_1, \dot{\varphi}_2$  and  $\dot{\varphi}_3$  for a system (1,2) with low stiffness coefficient  $k_x=3600.0$  and  $\alpha_x = 20.0, \varphi_{10} = 0, \varphi_{20} = \frac{\pi}{4}, \varphi_{30} = \frac{\pi}{2}, \dot{\varphi}_{10} = \dot{\varphi}_{20} = \dot{\varphi}_{30} = 0$  (the unit of time on the horizontal axis is the number  $N = \dot{\varphi}_N t / 2\pi$ , i.e., the number of complete revolutions of the pendulum rotating with constant angular velocity  $\dot{\varphi}_N$ ),  
 (b) angular displacement of pendula  $\varphi_2 - \varphi_1$  and  $\varphi_3 - \varphi_1$  related to the displacement of the first pendulum,  $\beta_2 = \beta_3 = 0$ .

In the system (1,2) with a stiffness coefficient of  $k_x=3600.0$  and different initial conditions (for example  $\varphi_{10} = 0, \varphi_{20} = \frac{\pi}{2}, \varphi_{30} = \pi, \dot{\varphi}_{10} = \dot{\varphi}_{20} = \dot{\varphi}_{30} = 0$  one observes a different type of synchronization as shown in Figure 13(a,b). After a transitional period angular velocities  $\dot{\varphi}_1$  and  $\dot{\varphi}_3$  tend to each other and are different than  $\dot{\varphi}_2$ ; relative displacement  $\varphi_3 - \varphi_1$  reaches a constant value  $2\pi$ , so  $\varphi_3 = \varphi_1$ , and  $\varphi_2 - \varphi_1 = \pi$ . Two pendula 1 and 3 create a cluster which is in anti-phase with pendulum 2.

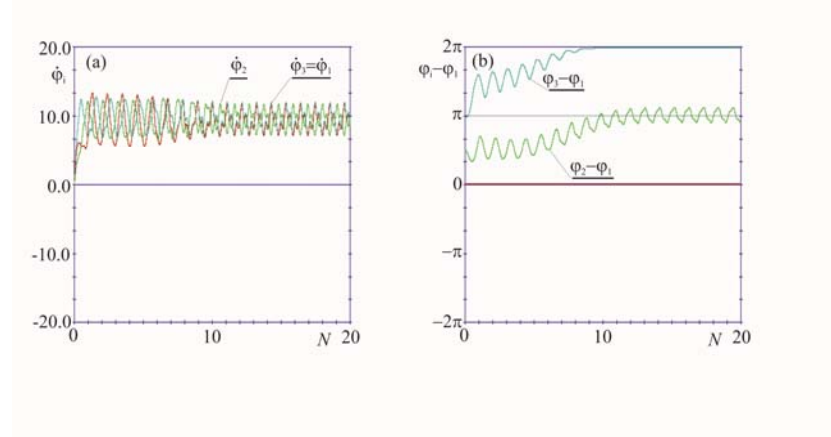


Figure 13. Time series of pendula' velocities and displacements in the case of the antiphase synchronization of pendulum 2 with a cluster consisting of pendula 1 and 3; (a) angular velocities of pendula  $\dot{\varphi}_1, \dot{\varphi}_2$  and  $\dot{\varphi}_3$  for a system (1-2) with low stiffness coefficient  $k_x=3600.0$  and  $\alpha_x = 20.0, \varphi_{10} = 0, \varphi_{20} = \frac{\pi}{2}, \varphi_{30} = \pi, \dot{\varphi}_{10} = \dot{\varphi}_{20} = \dot{\varphi}_{30} = 0$  (the unit of time on the horizontal axis is the number  $N = \dot{\varphi}_N t / 2\pi$ , i.e., the number of complete revolutions of the pendulum rotating with constant angular velocity  $\dot{\varphi}_N$ ),  
 (b) angular displacement of pendula  $\varphi_2 - \varphi_1$  and  $\varphi_3 - \varphi_1$  related to the displacement of the first pendulum,  $\beta_2 = \pi, \beta_3 = 2\pi$ .



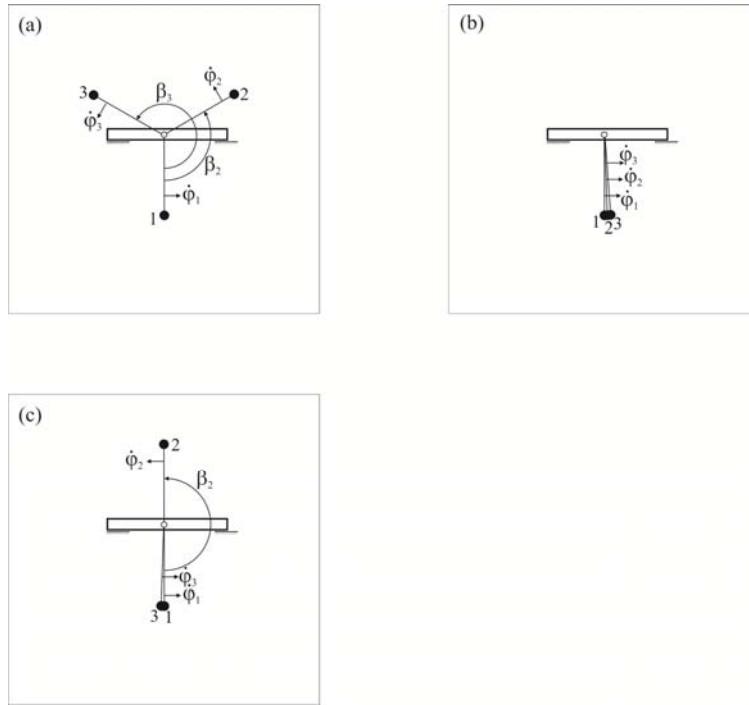


Figure 14. Synchronization configurations in the system (1,2) with  $n=3$  pendula; (a) phase synchronization with phase shifts between pendula:  $\beta_1=0$ ,  $\beta_2=2\pi/3$  and  $\beta_3=4\pi/3$ , (b) complete synchronization ( $\beta_1=\beta_2=\beta_3=0$ ), (c) antiphase synchronization of a single pendulum with the cluster of two other pendula,  $\beta_1=0$ ,  $\beta_2=\pi$  and  $\beta_3=0$ .

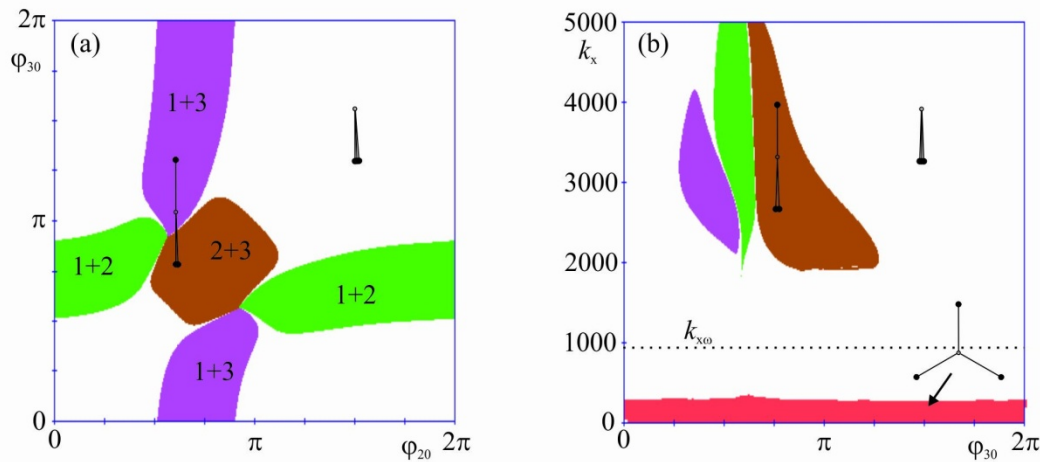


Figure 15. Basins of attraction of the different states of pendula' synchronization, (a) basins of attraction of complete (white color) and anti-phase (gray color with different shades for different pairs of pendula in the cluster) synchronization states for a system (1,2),  $k_x=3600.0$  (the basins are shown in the  $\varphi_{20} - \varphi_{30}$  plane,  $\varphi_{10} = 0, \dot{\varphi}_{10} = \dot{\varphi}_{20} = \dot{\varphi}_{30} = 0$ , (b) basins of attraction of complete (white color), anti-phase (gray color in different shades for different pairs of pendula in the cluster) and phase (dark gray color at the bottom) for different values of stiffness coefficient  $k_x$ ,  $\varphi_{10} = 0, \varphi_{20} = \pi, \dot{\varphi}_{10} = \dot{\varphi}_{20} = \dot{\varphi}_{30} = 0$ .

Our numerical results show that in the system (1-2) with  $n=3$  pendula three different configurations of synchronized pendula are possible, as shown in Figure 14(a-c). Figure 14(a) presents the phase synchronization with phase shifts between pendula:  $\beta_1=0$ ,  $\beta_2=2\pi/3$  and  $\beta_3=4\pi/3$  (condition (21) is fulfilled) which exists for sufficiently small values of  $k_x < 370$  (regardless of initial conditions). Complete synchronization ( $\beta_1=\beta_2=\beta_3$  and condition (20) is fulfilled) which exists for the appropriate values of  $k_x$  ( $370 < k_x < 1880$ ) regardless of initial conditions and which for sufficiently large values of  $k_x$  ( $k_x > 1880$ ) coexists with antiphase synchronization is described in Figure 14(b). In contrast to the previously studied systems with oscillating pendula [17-19] one can observe the phenomenon of antiphase synchronization of a single pendulum with the cluster of two other pendula. Figure 14(c) presents the anti-phase synchronization  $\beta_1=0$  (or  $\beta_2=0$  or  $\beta_3=0$ ) and two other phase shift angles equal to  $\pi$  (condition (21) is fulfilled). This configuration co-exists with a complete synchronization for sufficiently large values of  $k_x$  ( $k_x > 1880$ ). Depending on initial conditions the cluster is created of pendula 1-2, 1-3 or 2-3.

The basins of attraction of different states of pendula' synchronization are shown in Figure 15(a,b). Figure 15(a) shows the basins of attraction of complete (white color) and anti-phase (gray color with different shades for different pairs of pendula in the cluster) synchronization states for a system with stiffness coefficient  $k_x=3600.0$ . The basins are shown in the  $\varphi_{20} - \varphi_{30}$  plane ( $\varphi_{10} = 0, \dot{\varphi}_{10} = \dot{\varphi}_{20} = \dot{\varphi}_{30} = 0$ ). Figure 15(b) shows the basins of attraction of complete (white color), anti-phase (gray color in different shades for different pairs of pendula in the cluster) and phase (dark gray color at the bottom) for different values of stiffness coefficient  $k_x$ . The following initial conditions have been considered:  $\varphi_{10} = 0, \varphi_{20} = \pi, \dot{\varphi}_{10} = \dot{\varphi}_{20} = \dot{\varphi}_{30} = 0$ .

The results obtained by the numerical integration of equations of motion (1,2) are significantly different from the results obtained by the method of small parameter [5]. For example Blekhman [5] predicts the existence of complete and phase synchronization (the second one with the same phase shifts as in our studies, i.e.,  $2\pi/3$  and  $4\pi/3$ ). It has been stated that for the systems with stiffness coefficient  $k_{x\dot{\varphi}_N} = U\dot{\varphi}_N^2 < 900.0$  independently of initial conditions the phase synchronization occurs while for larger values of  $k_{x\dot{\varphi}_N}$  the complete synchronization takes place. Contrary to this statement Figure 15(a,b) shows that the boundary between the basins of attraction phase and complete synchronization takes place at the level  $k_x=370.0$  (almost three times lower).

Another significant difference between our results and these of [5] is the existence of anti-face synchronization of a single pendulum and a cluster consisting of two pendula ([5] does not prescribe such configuration). For  $k_x > 1880.0$  this configuration co-exists with a complete synchronization of all pendula. Notice that the method of small parameter used in [5] does not allow the identification of the coexisting configurations.

### 4.3. Large system of pendula rotating in the same direction

We studied the systems with up to 100 rotating pendula. It has been found that for larger  $n$  same types of synchronization are observed. Their examples are shown in Figures 16-18. Figure 16(a,b) presents the phase synchronization of  $n=20$  pendula in the system (1-2) with  $k_x=1000.0$ ,  $M=20.0$ , and the following initial conditions:  $\varphi_{i0} = \frac{i\pi}{20}$ ,  $\dot{\varphi}_{i0} = 0$ . Figure 16(a) shows that pendula' velocities  $\dot{\varphi}_1, \dots, \dot{\varphi}_{20}$  oscillate around the average value close to  $\dot{\varphi}_N$ . Angular displacements  $\varphi_i - \varphi_1$  tend to the constant values which differ by  $\pi/10$  as can be seen in Figure 16(b). The complete synchronization of 20 pendula is described in Figure 17(a,b).

We consider the system (1-2) with  $k_x = 20000.0$ ,  $M = 20.0$  and initial conditions :  $\varphi_{i0} = \frac{7i\pi}{180}$ ,  $\dot{\varphi}_{i0} = 0.0$ . The velocities of all pendula  $\dot{\varphi}_1, \dots, \dot{\varphi}_{20}$  oscillate around the constant average value  $\dot{\varphi}_N$  (Figure 17(a)) and angular displacements  $\varphi_i - \varphi_1$  tend to zero, i.e., the displacements of all pendula are the same (Figure 17(b)). The example of the synchronization in clusters is presented in Figure 18(a,b). We consider the same system as in the previous example with the following initial conditions:  $\varphi_{i0} = \frac{i\pi}{20}$ ,  $\dot{\varphi}_{i0} = 0.0$ . Figure 18(a) shows that pendula' velocities  $\dot{\varphi}_1, \dots, \dot{\varphi}_{20}$  oscillate around the average value close to  $\dot{\varphi}_N$ . The angular displacements  $\varphi_i - \varphi_1$  tend to two constant values 0 or  $\pi$  as can be seen in Figure 18(b). Two clusters of synchronized pendula have been created (they consist of 7 and 13 pendula). The clusters are synchronized in antiphase.

Contrary to the case of oscillating pendula [17,18] rotating pendula are not grouped in three or five clusters only. The lack of this restriction causes that in the system (1,2) depending on initial condition one can observe a great variety of different clusters' configurations. The number of configurations grows with a number of pendula  $n$ .

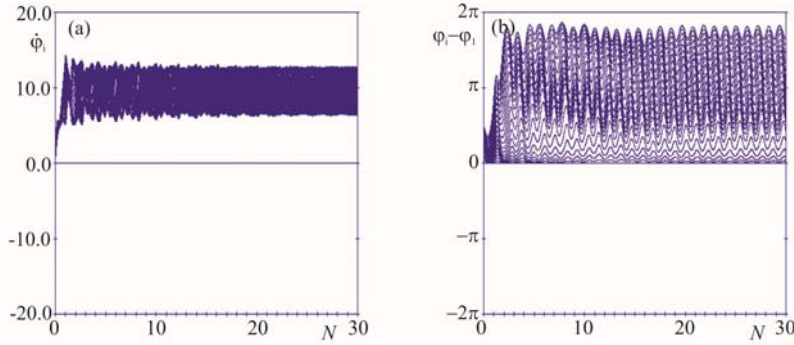


Figure 16. Phase synchronization of  $n=20$  pendula in the system (1-2):  $m_1=m_2=\dots=m_{20}= 1.00$ ,  $l_1=l_2=\dots=l_{20}=0.25$ ,  $c_{\varphi 1}=c_{\varphi 2}=\dots=c_{\varphi 20}=0.01$ ,  $p_{01}=p_{02}=\dots=p_{020}=5.00$ ,  $p_{11}=p_{12}=\dots=p_{120}=0.50$ ,  $m_b = 20.00$ ,  $k_x=1000.0$ ,  $\varphi_{i0} = \frac{i\pi}{20}$ ,  $\dot{\varphi}_{i0} = 0.0$ ; (a) pendula' velocities  $\dot{\varphi}_i$ , (b) angular displacements

$$\varphi_i - \varphi_1.$$

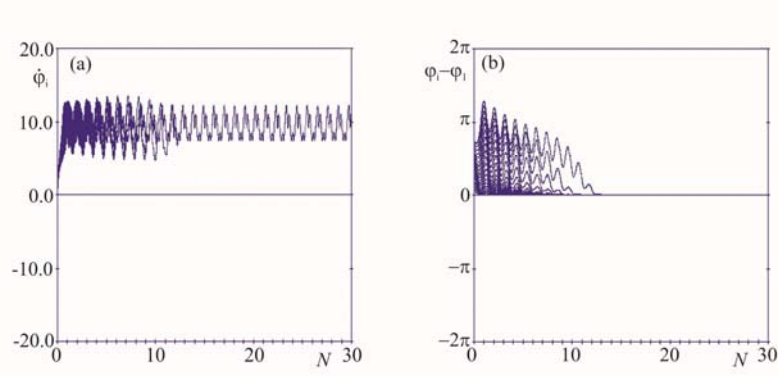


Figure 17. Complete synchronization of 20 pendula in system (1-2):  $m_1=m_2=\dots=m_{20}= 1.00$ ,  $l_1=l_2=\dots=l_{20}=0.25$ ,  $c_{\varphi 1}=c_{\varphi 2}=\dots=c_{\varphi 20}=0.01$ ,  $p_{01}=p_{02}=\dots=p_{020}=5.00$ ,  $p_{11}=p_{12}=\dots=p_{120}=0.50$ ,  $m_B=20.00$ ,  $k_x=20000.0$ ,  $\varphi_{i0} = \frac{7i\pi}{180}$ ,  $\dot{\varphi}_{i0} = 0.0$ ; (a) pendula velocities  $\dot{\varphi}_i$ , (b) angular displacements  $\varphi_i - \varphi_1$ .

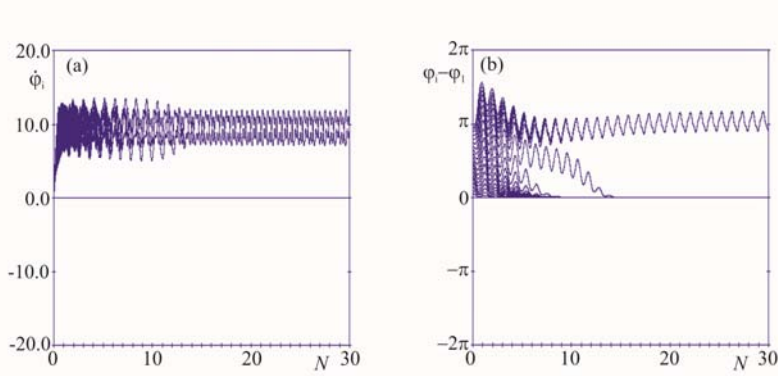


Figure 18. Cluster synchronization of 20 pendula in system (1-2):  $m_1=m_2=\dots=m_{20}= 1.00$ ,  $l_1=l_2=\dots=l_{20}=0.25$ ,  $c_{\varphi 1}=c_{\varphi 2}=\dots=c_{\varphi 20}=0.01$ ,  $p_{01}=p_{02}=\dots=p_{020}=5.00$ ,  $p_{11}=p_{12}=\dots=p_{120}=0.50$ ,  $m_b=20.00$ ,  $k_x=20000.0$ ,  $\varphi_{i0} = \frac{i\pi}{20}$ ,  $\dot{\varphi}_{i0} = 0.0$ ; (a) pendula velocities  $\dot{\varphi}_i$ , (b) angular displacements  $\varphi_i - \varphi_1$ . Clusters of 7 and 13 pendula are synchronized in antiphase.

#### 4.4 Two pendula rotating in the opposite directions

Now, let us consider the system (1-2) with the following parameter values:  $m_1=m_2=1.00$ ,  $l_1=l_2=0.25$ ,  $c_{\varphi 1}=c_{\varphi 2}=0.01$ ,  $p_{01}=5.00$ ,  $p_{02}= -5.00$ ,  $p_{11}=p_{12}=0.2$ ,  $m_B=6.00$ . One can calculate that  $\dot{\varphi}_{1N} = 10.0$ ,  $\dot{\varphi}_{2N} = -10.0$  and  $U=8.0$ . The values of stiffness and damping coefficients  $k_x$  and  $c_x$  have been taken as in previous section.

Figure 19(a) presents time series of the pendula's angular velocities  $\dot{\varphi}_1$  and  $\dot{\varphi}_2$  for the small value of the stiffness coefficient  $k_x=500.0$ , so  $\alpha_x = \sqrt{500.0/8.0} = 7.91 < 10.0 = \dot{\varphi}_{1N}$ . The pendula rotate in opposite directions with constant velocities  $\dot{\varphi}_{10} = \dot{\varphi}_{1N} = 10.0 [s^{-1}]$ ,  $\dot{\varphi}_{20} = \dot{\varphi}_{2N} = -10.0 [s^{-1}]$  starting from the initial positions:  $\varphi_{10}=0$ ,  $\varphi_{20}=\pi/4$ . One can see that after

the initial transient (several rotations) caused by the oscillations of the beam the pendula's velocities fluctuate (due to the gravity) around the initial values  $\dot{\varphi}_{1N}$  and  $\dot{\varphi}_{2N}$ . Figure 19(b) shows time series of the sum of pendula's displacements  $\varphi_2 + \varphi_1$ . One can see that this sum (after the initial transient) is constant and equal to zero so  $\varphi_2 = -\varphi_1$ . This type of synchronization is the *mirror-synchronization* ( $M$ ) as the rotational motion of pendulum 2 is the mirror image of the rotations of pendulum 1 as can be seen at the diagram shown in Figure 19(b). For the small value of the stiffness coefficient  $k_x=500.0$  and different initial conditions  $\varphi_{10}=0$ ,  $\varphi_{20}=-43\pi/36$  one can observe different type of synchronization as shown in Figure 12(c,d). After the initial transient the pendula's velocities (as in the previous case) fluctuate around the initial values  $\dot{\varphi}_{1N}$  and  $\dot{\varphi}_{2N}$  (Figure 19(c)). The sum of pendula's displacements  $\varphi_2 + \varphi_1$  fluctuates around the constant averaged value  $\langle \varphi_2 + \varphi_1 \rangle = -\pi$  as shown in Figure 19(d). We call this type of synchronization the *antiphase-synchronization* ( $A$ ). For the larger values of  $k_x$  the next type of synchronization can be observed. Figure 20(a,b) illustrates pendula's synchronization for large values of the stiffness coefficient  $k_x=3000.0$  and  $\alpha_x = \sqrt{3000.0/8.0} = 19.36 > 10.0 = \dot{\varphi}_{1N}$ . We consider the following initial conditions:  $\varphi_{10}=0$ ,  $\varphi_{20}=-3\pi/2$ . After the initial transient the sum of pendula's displacements  $\varphi_2 + \varphi_1$  fluctuates around constant averaged value  $\langle \varphi_2 + \varphi_1 \rangle$  close to  $-3\pi/2$  as shown in Figure 20(a). We call this type of synchronization the *third-quarter-synchronization* ( $3Q$ ). When pendulum 1 passes through the static equilibrium position pendulum 2 approaches the horizontal plane of symmetry ( $\varphi_1 = 0 \Rightarrow \varphi_2 \approx -3\pi/2$ ).

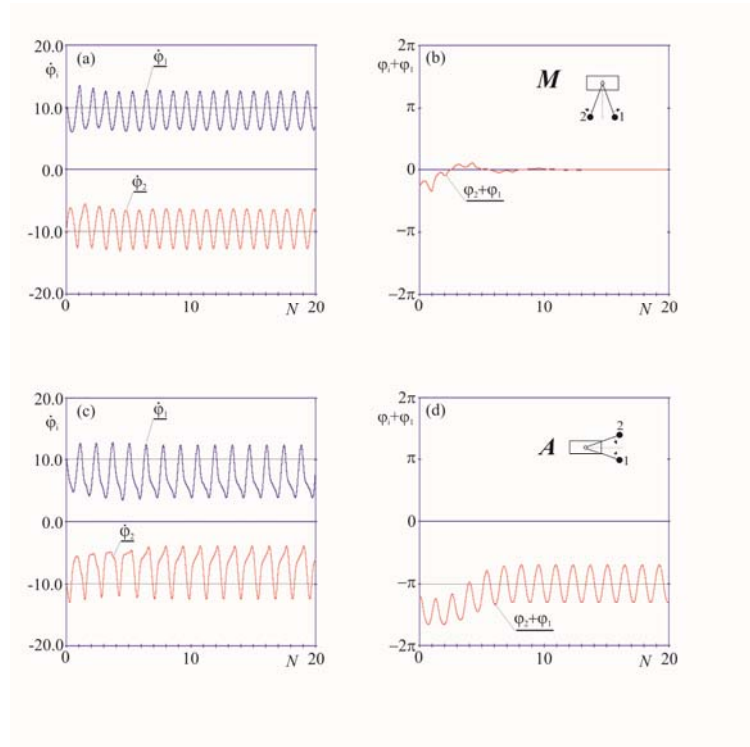


Figure 19. Mirror-synchronization ( $M$ ) and antiphase-synchronization ( $A$ ) of 2 pendula; (a) pendula's velocities during mirror-synchronization,  $k_x=500$ ,  $\varphi_{10}=0$ ,  $\varphi_{20}=-\pi/4$ ; (b) pendula's displacements during mirror-synchronization,  $k_x=500$ ,  $\varphi_{10}=0$ ,  $\varphi_{20}=-\pi/4$ ; (c) pendula's velocities during antiphase-synchronization,  $k_x=500$ ,  $\varphi_{10}=0$ ,  $\varphi_{20}=-1.19$ ; (d) pendula's displacements during antiphase-synchronization,  $k_x=500$ ,  $\varphi_{10}=0$ ,  $\varphi_{20}=-1.19$ .

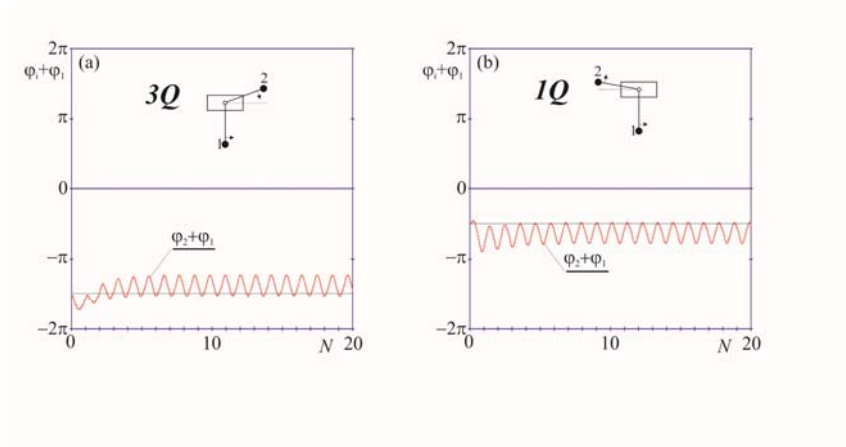


Figure 20. Third-quarter-synchronization ( $3Q$ ) and first-quarter-synchronization ( $1Q$ ) of 2 pendula; (a) pendula's displacements during third-quarter-synchronization:  $k_x=3000.0$ ,  $\varphi_{10}=0$ ,  $\varphi_{20}=-3\pi/2$ ; (b) pendula's displacements during first-quarter-synchronization:  $k_x=3000.0$ ,  $\varphi_{10}=0$ ,  $\varphi_{20}=-\pi$ .

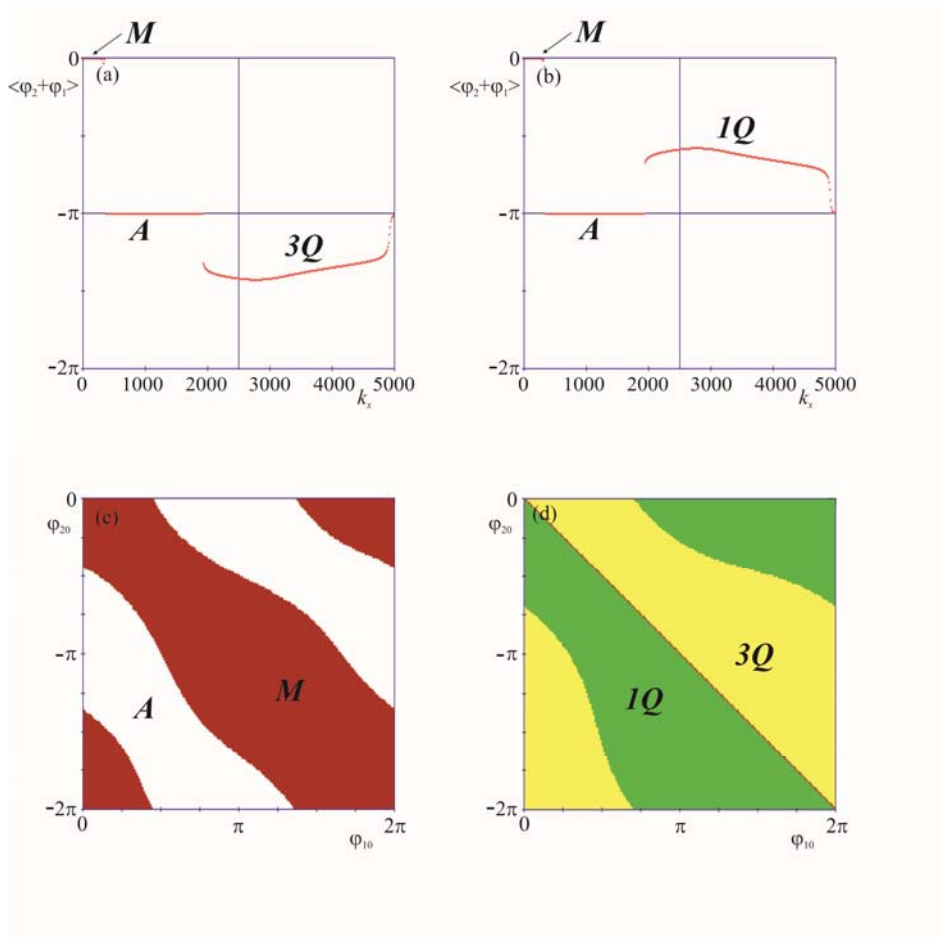


Figure 21. The influence of the stiffness coefficient  $k_x$  on the type of synchronization of 2 pendula: (a) average value of the sum of the pendula's displacements  $\langle \varphi_2 + \varphi_1 \rangle$  versus  $k_x$ :  $\varphi_{10}=0$ ,  $\varphi_{20}=-3\pi/2$ ; (b) average value of the sum of the pendula's displacements  $\langle \varphi_2 + \varphi_1 \rangle$  versus  $k_x$ :  $\varphi_{10}=0$ ,  $\varphi_{20}=-\pi$ ; (c) mirror- and antiphase- synchronization for different initial conditions:  $k_x=500$ ; (d) third- and first- quarter-synchronization for different initial conditions:  $k_x=3000$ .

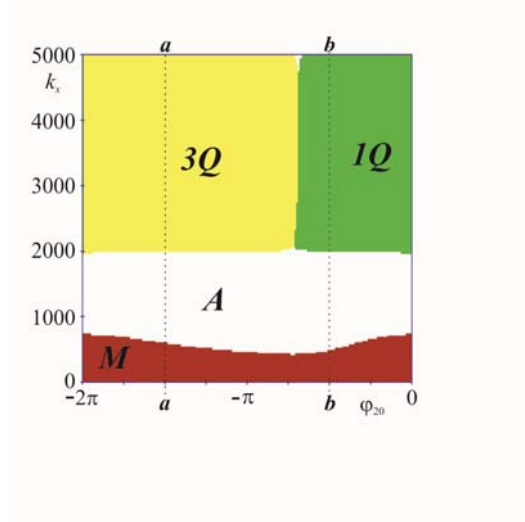


Figure 22. Different types of synchronization of 2 pendula versus stiffness coefficient  $k_x$  and initial position of pendulum 2  $\varphi_{20}$ : initial position of pendulum 1  $\varphi_{10}=0$ .

For different initial conditions:  $\varphi_{10}=0$ ,  $\varphi_{20}=-\pi/2$ , after the initial transient the sum of pendula's displacements  $\varphi_2 + \varphi_1$  fluctuates around constant averaged value  $\langle \varphi_2 + \varphi_1 \rangle$  closed to  $-\pi/2$  as shown in Figure 20(b). This type of synchronization has been called the *first-quarter-synchronization* ( $1Q$ ). When pendulum 1 passes through the static equilibrium position pendulum 2 leaves the horizontal plane of symmetry ( $\varphi_1=0 \Rightarrow \varphi_2 \approx -\pi/2$ ). The pendula's configurations during ( $1Q$ ) and ( $3Q$ ) synchronizations are shown at diagrams in Figure 13(a,b). ( $3Q$ ) and ( $1Q$ ) synchronizations are not observed when one neglects the effect of gravity or when the pendula rotate in the horizontal plane. In both cases the pendula's velocities oscillate around the initial values  $\dot{\varphi}_{1N}$  and  $\dot{\varphi}_{2N}$  as in the examples shown in Figure 12(a,c).

The influence of the stiffness coefficient  $k_x$  and initial conditions on the type of synchronization is discussed in Figure 21(a-d). Figure 21(a) presents the averaged value of the sum of pendula's displacements  $\langle \varphi_2 + \varphi_1 \rangle$  versus stiffness coefficient  $k_x$ . For all values of  $k_x$  the motion of the system is initiated from the same initial conditions. In Figure 21(a) we show the averaged value of the sum of pendula's displacements  $\langle \varphi_2 + \varphi_1 \rangle$  versus the stiffness coefficient  $k_x$  for the following initial conditions:  $\varphi_{10}=0$ ,  $\varphi_{20}=-3\pi/2$ . One can see that for the small values of the stiffness coefficient  $k_x < 360.0$ , the value of  $\langle \varphi_2 + \varphi_1 \rangle = 0$  and the system is in the state of mirror-synchronization ( $M$ ). For  $k_x = 360.0$  the value of  $\langle \varphi_2 + \varphi_1 \rangle$  jumps to  $-\pi$  and in the interval  $360.0 < k_x < 1910.0$  we observe antiphase-synchronization ( $A$ ). For  $k_x = 1910.0$  the next jump of  $\langle \varphi_2 + \varphi_1 \rangle$  (to the value of  $-4\pi/3$ ) occurs and the type of synchronization is changed to the third-quarter-synchronization ( $3Q$ ). In the interval  $1910.0 < k_x < 5000.0$  [N/m] in the state of the third-quarter-synchronization ( $3Q$ ) the value of  $\langle \varphi_2 + \varphi_1 \rangle$  initially decreases down to the value  $-1.41\pi$  and later increases up to the value  $-\pi$ , so we observe the return to the state of antiphase-synchronization ( $A$ ). Figure 21(b) shows the value of  $\langle \varphi_2 + \varphi_1 \rangle$  versus  $k_x$  for different initial conditions (we change the value of  $\varphi_{20}$  from  $\varphi_{20}=-3\pi/2$  to  $\varphi_{20}=3\pi/2$ ). As in Figure 21(a) for small values of  $k_x$  first we observe the state of the mirror-synchronization ( $M$ ) and next the antiphase-synchronization ( $A$ ). The jump of the value of  $\langle \varphi_2 + \varphi_1 \rangle$  to  $-0.65$ , observed for  $k_x = 1960.0$ , indicates the change of the type of synchronization to the first-quarter ( $1Q$ ). In the interval  $1960.0 < k_x < 5000.0$  in the state of the first-quarter-synchronization, the value of  $\langle \varphi_2 + \varphi_1 \rangle$  initially increases up to  $-0.57$  and next decreases down to  $-\pi$ , so we observe the return to the state of antiphase-synchronization ( $A$ ). Figure 21(c)



presents the influence of the initial conditions  $\varphi_{10}$  and  $\varphi_{20}$  on the type of synchronization for the small value  $k_x=500.0$  (types  $(M)$  and  $(A)$  are observed) while Figure 21(d) shows basins of  $(3Q)$  and  $(1Q)$  for large value of  $k_x=3000.0$ .

The influence of the stiffness coefficient  $k_x$  and initial position of pendulum 2 -  $\varphi_{20}$  on the type of synchronization is discussed in Figure 22. We assume the initial position of the pendulum 1 -  $\varphi_{10}=0$ . One can see that for small values of the stiffness coefficient  $k_x<425.0$  and any value of  $\varphi_{20}$  the mirror-synchronization  $(M)$  occurs. In the interval  $425.0<k_x<760.0$ , depending on initial condition  $\varphi_{20}$  one observes mirror  $(M)$  or antiphase  $(A)$  synchronization.  $(A)$  and  $(M)$  types of synchronization observed for  $k_x=500.0$  are shown in Figure 21(c). In the interval  $760.0<k_x<1960.0$  for any value of  $\varphi_{20}$  antiphase-synchronization  $(A)$  occurs. For  $k_x>1960.0$  depending on initial condition  $\varphi_{20}$  we observe the third-quarter  $(3Q)$  or the first-quarter  $(1Q)$  synchronization.  $(1Q)$  and  $(3Q)$  types of synchronization observed for  $k_x=3000.0$  are shown in Figure 21(d).

#### 4.5. Three pendula rotating in various directions

In the simulations of the system of three pendula, we use the same parameter values as in previous example, and additionally consider  $p_{03}=-5.00$ , i.e., pendulum 1 rotates counterclockwise and pendula 2 and 3 clockwise.

Figure 23(a-d) shows time series of the sum of pendula's displacements  $\varphi_2 + \varphi_1$  and  $\varphi_3 + \varphi_1$  during four different synchronous states. In Figure 23(a) we present time series for the case of small stiffness coefficient  $k_x=200.0$ , so  $\alpha_x = \sqrt{200.0/9.0} = 4.71 < 10.0 = \dot{\varphi}_{1N}$  and the following initial conditions:  $\varphi_{10}=0$ ,  $\varphi_{20}=-\pi/3$ ,  $\varphi_{30}=-4\pi/3$ . After the initial transient the sum of pendula's displacements  $\varphi_2 + \varphi_1$  fluctuates around constant averaged value approximately equal to  $-\pi/3$ , and the sum  $\varphi_3 + \varphi_1$ , fluctuates around the averaged value close to  $-1.66$ . This type of synchronization we call the tree synchronization  $(T)$ . The pendula's configuration for  $\varphi_1=0$  is shown at the diagram in Figure 23(a). Increasing the value of the stiffness coefficient to  $k_x=1000.0$  (so  $\alpha_x = \sqrt{1000.0/9.0} = 10.54 > 10.0 = \dot{\varphi}_{1N}$  and the beam oscillations are above the resonance) and changing the initial positions of the pendula to  $\varphi_{10}=0$ ,  $\varphi_{20}=-\pi$ ,  $\varphi_{30}=-\pi/2$  (other initial conditions are the same as in Figure 23(a) one observes the synchronous state in which pendula 2 and 3 (rotating to the left) create the cluster (their displacements are identical) as shown in Figure 23(b). The sum of the displacements of any pendulum in cluster and pendulum 1  $\varphi_2 + \varphi_1 = \varphi_3 + \varphi_1$  fluctuates around constant average value  $\langle \varphi_2 + \varphi_1 \rangle = \langle \varphi_3 + \varphi_1 \rangle$  approximately equal to  $-\pi$  and we observe the cluster-antiphase-synchronization  $(CA)$ . The pendula's configuration during this type of synchronization for  $\varphi_1=0$  is shown at the diagram in Figure 23(b). Additionally in the system with three pendula one can observe four new types of synchronization which occur due to the existence of gravity and the change of the amplitude and phase of the beam's oscillations (as the result of the increased value of the stiffness coefficient  $k_x$ ). For  $k_x=3000.0$  and initial conditions  $\varphi_{10}=0$ ,  $\varphi_{20}=-1.38$ ,  $\varphi_{30}=-1.44$ , we observe the type of synchronization similar to  $(T)$  synchronization but with obtuse angles between pendulum 1 and pendula 2,3 as shown at the diagram in Figure 23(c). We call this synchronization the *yankee 32* ( $Y32$ ) -synchronization. For different initial conditions one can observe the pendula's configuration which is the mirror image of  $(Y32)$ , i.e., pendulum 3 is on the right side and pendulum 2 on the left side of the diagram. This configuration is called the *yankee 23* ( $Y23$ ) -synchronization. For the same value of the stiffness coefficient  $k_x$  and initial conditions:  $\varphi_{10}=0$ ,  $\varphi_{20}=-1.38$ ,  $\varphi_{30}=-\pi$  we observe the type of



synchronization shown in Figure 23(d). This synchronization is similar to (CA) synchronization, but the angle between the cluster (of pendula 2 and 3) and pendulum 1 is approximately equal to  $-3\pi/2$  (the *cluster-right-synchronization* (CR)) or  $-\pi/2$  (the *cluster-left-synchronization* (CL)).

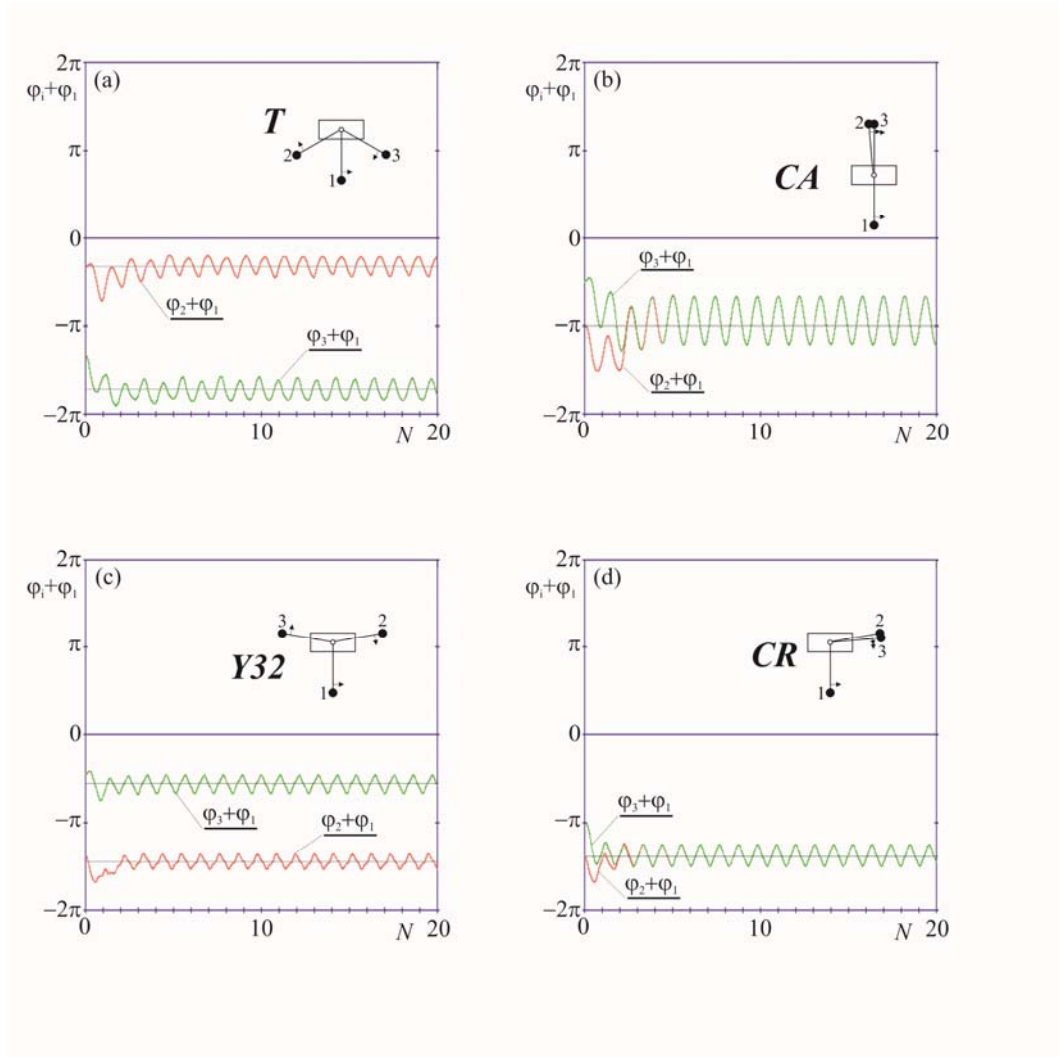


Figure 23: Different types of synchronization of 3 rotating pendula: (a) tree synchronization ( $T$ ),  $k_x=200.0$ [N/m],  $\varphi_{10}=0$ ,  $\varphi_{20}=-\pi/3$ ,  $\varphi_{30}=-4\pi/3$ ; (b) cluster-antiphase-synchronization (CA),  $k_x=1000.0$ [N/m],  $\varphi_{10}=0$ ,  $\varphi_{20}=-\pi$ ,  $\varphi_{30}=-\pi/2$ ; (c) yankee-32-synchronization (Y32),  $k_x=3000.0$ [N/m],  $\varphi_{10}=0$ ,  $\varphi_{20}=-1.38$ ,  $\varphi_{30}=-1.44$ ; (d) cluster-right-synchronization (CR),  $k_x=3000.0$ [N/m],  $\varphi_{10}=0$ ,  $\varphi_{20}=-1.38$ ,  $\varphi_{30}=-\pi$ .

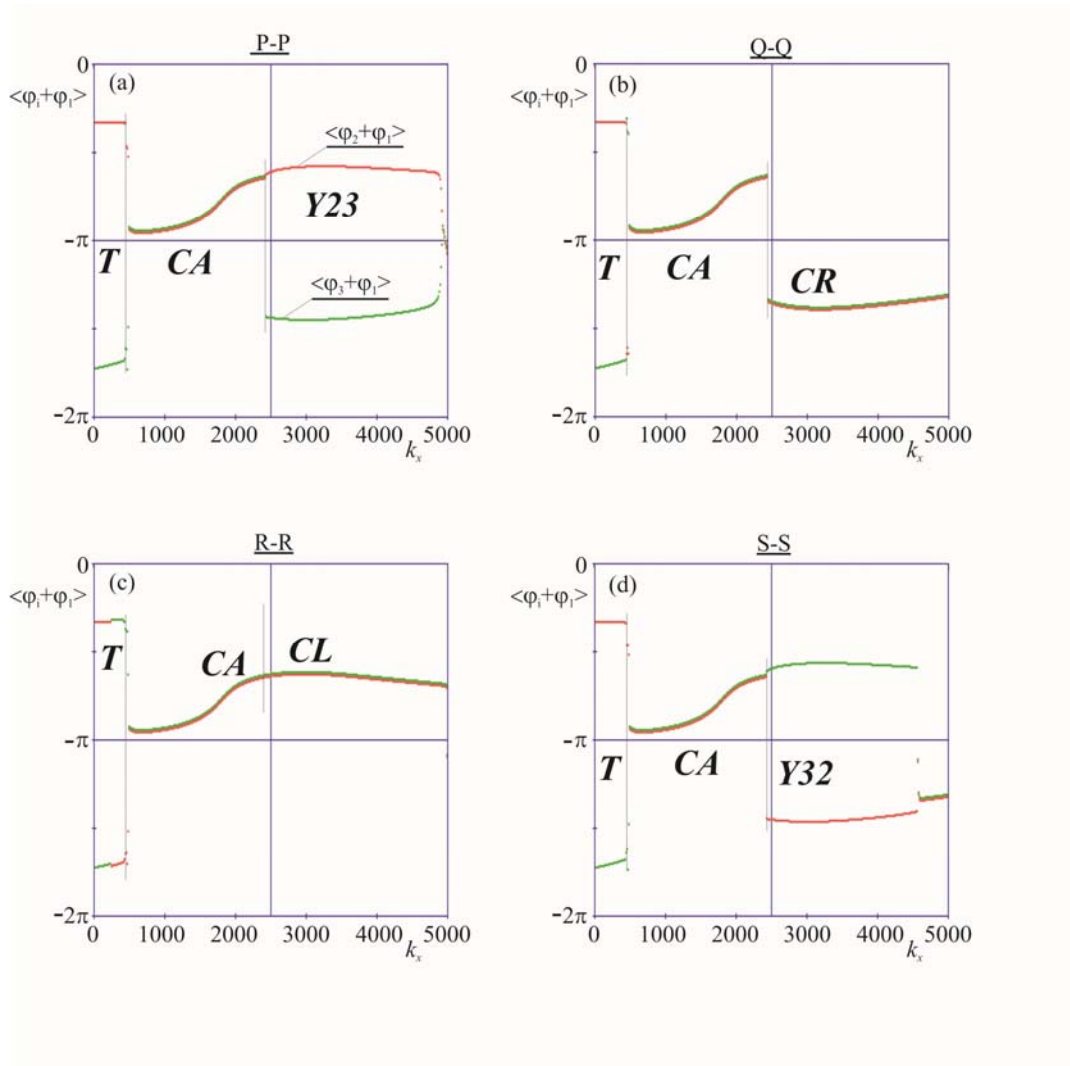


Figure 24: The influence of the stiffness coefficient  $k_x$  on the type of synchronization of 3 pendula shown as the average values of the sums of pendula's displacements  $\langle \varphi_2 + \varphi_1 \rangle$  and  $\langle \varphi_3 + \varphi_1 \rangle$  versus  $k_x$ : (a)  $\varphi_{10}=0, \varphi_{20}=-0.75, \varphi_{30}=-1.87$ ; (b)  $\varphi_{10}=0, \varphi_{20}=-0.75, \varphi_{30}=-\pi$ ; (c)  $\varphi_{10}=0, \varphi_{20}=-0.75, \varphi_{30}=-0.44$ ; (d)  $\varphi_{10}=0, \varphi_{20}=-0.75, \varphi_{30}=-0.22$ .

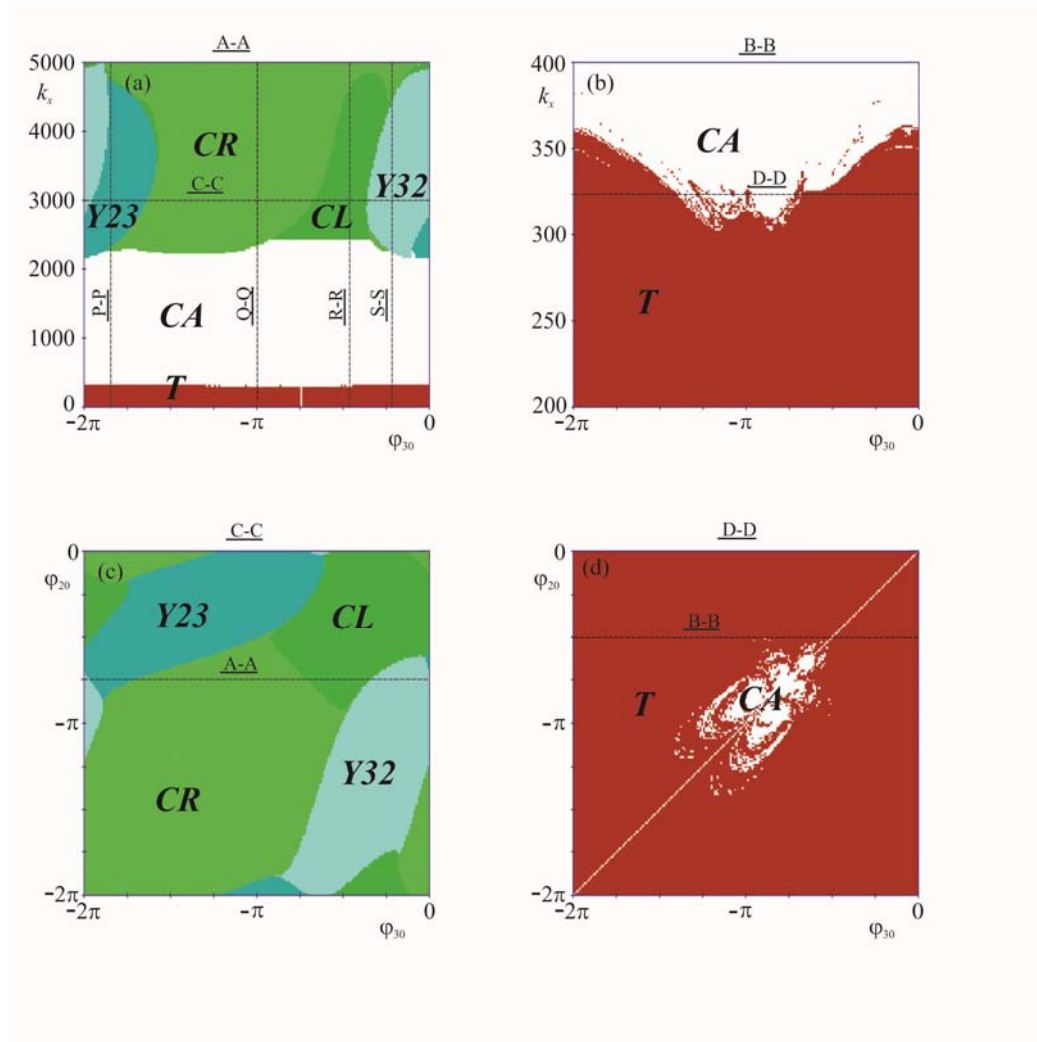


Figure 25: Dependence of the type of synchronization on the stiffness ratio  $k_x$  and initial conditions: (a) type of synchronization versus  $k_x$  and  $\varphi_{30}$ :  $\varphi_{10}=0$ ,  $\varphi_{20}=-0.75$ ; A-A cross-section of map (c); (b) the enlargement of map (a) for small values of  $k_x$ , B-B cross-section map (d); (c) the type of synchronization for different initial conditions  $\varphi_{20}$  and  $\varphi_{30}$ ;  $\varphi_{10}=0$ ,  $k_x=3000$ , C-C cross-section map (a); (d) the type of synchronization as function  $\varphi_{20}$  and  $\varphi_{30}$ ;  $\varphi_{10}=0$ ,  $k_x = 325$ , D-D cross-section map (b).

Figure 24(a-d) shows the influence of stiffness coefficient  $k_x$  on the type of the synchronous state. The averaged values of the sums of pendula's displacements  $\langle \varphi_2 + \varphi_1 \rangle$  and  $\langle \varphi_3 + \varphi_1 \rangle$  versus  $k_x$  are shown. For all values of  $k_x$  the motion of the system is initiated from the same initial conditions. In the system with small stiffness coefficient  $k_x$  one observes ( $T$ ) type synchronization as can be seen in Figure 24(a-d). For larger values of  $k_x$  we observe ( $CA$ ) synchronization and finally for  $k_x > 2200 \div 2400$  (exact value depends on  $\varphi_{30}$ ) two other types of synchronization ( $CR$ ) and ( $Y32$ ) and their mirror images ( $CL$ ) and ( $Y23$ ) are possible. Figure 24(a-d) shows that the values  $\langle \varphi_2 + \varphi_1 \rangle$  and  $\langle \varphi_3 + \varphi_1 \rangle$  are changing with the change of  $k_x$ , so the descriptions of the pendula's configurations in different types of synchronizations with the statements about the angles close to  $\pi$  in the case of ( $CA$ ) or  $3\pi/2$  and  $\pi/2$  in the case of ( $CR$ )

and (*CL*) present only the qualitative differences. Particularly in Figure 24(c) the distinction between (*CA*) and (*CL*) synchronization is arbitrary, due to the continuous change of the angle between cluster (pendula 2 and 3) and pendulum 1. In the other cases the distinction between different types of synchronization is justified by the jump changes of angles  $\langle \varphi_2 + \varphi_1 \rangle$  and (or)  $\langle \varphi_3 + \varphi_1 \rangle$ . The cross sections shown in Figure 24(a-d) are indicated in Figure 25(a). Figure 25(a) shows the basins of existence of different types of synchronization on the plane  $k_x - \varphi_{30}$ . We consider the following initial conditions  $\varphi_{10}=0$ ,  $\varphi_{20}=-1.75$ . Figure 25(b) shows the enlargement of Figure 25(a) for  $200 < k_x < 400$ . From Figure 25(a,b) one can conclude that for stiffness coefficient  $k_x < 2200 \div 2400$  one can observe either (*T*) ( $k_x < 300 \div 370$ ) or (*CA*) synchronization ( $300 \div 370 < k_x < 2200 \div 2400$ ). The type of synchronization depends on the value of  $k_x$  only in the neighborhood of the boundaries between basins (*T*) and (*CA*) as shown in 25(b) and 25(d). Figure 25(d) presents the cross section of Figure 25(b) on level  $k_x=325$  which shows the coexistence of (*T*) and (*CA*) synchronizations for different initial conditions  $\varphi_{20}$  and  $\varphi_{30}$ . For larger values of  $k_x$  we observe the coexistence of four types of synchronization as can be seen in Figure 25(a,c). Figure 25(c) is the cross section of Figure 18(a) at level  $k_x=3000$ .

#### 4.6. Large system of pendula rotating in different directions

In an attempt to generalize the results of previous sections to the system with larger number of pendula we perform simulations of such systems. In Figure 26(a) we show the sums of pendula's displacements  $\varphi_i + \varphi_1$  ( $i=2 \dots 6$ ) for the system with small stiffness  $k_x=200.0$ . The following initial conditions have been used:  $\varphi_{10}=0$ ,  $\varphi_{20}=-0.16$ ,  $\varphi_{30}=-0.32$ ,  $\varphi_{40}=-0.48$ ,  $\varphi_{50}=-0.64$ ,  $\varphi_{60}=-0.80$ . One can see that after the initial transient (several rotations) the sums of pendula's displacements fluctuate around constant values close to  $0$ ,  $\pm\pi$  and  $\pm 2\pi/3$ . This type of synchronization is equivalent to the tree-synchronization (*T*). Figure 26(b) presents that the increase of the stiffness coefficient to  $k_x=2000.0$  leads to the change of the type of synchronization to the cluster-antiphase (*CA*). Figure 26(c,d) shows that with further increase of the stiffness coefficient, e.g. to the value  $k_x=3000.0$  the type of synchronization depends on the initial conditions as one can observe either (*CL*) (Figure 26(c)) or *Yankee* (Figure 26(d)) synchronization.

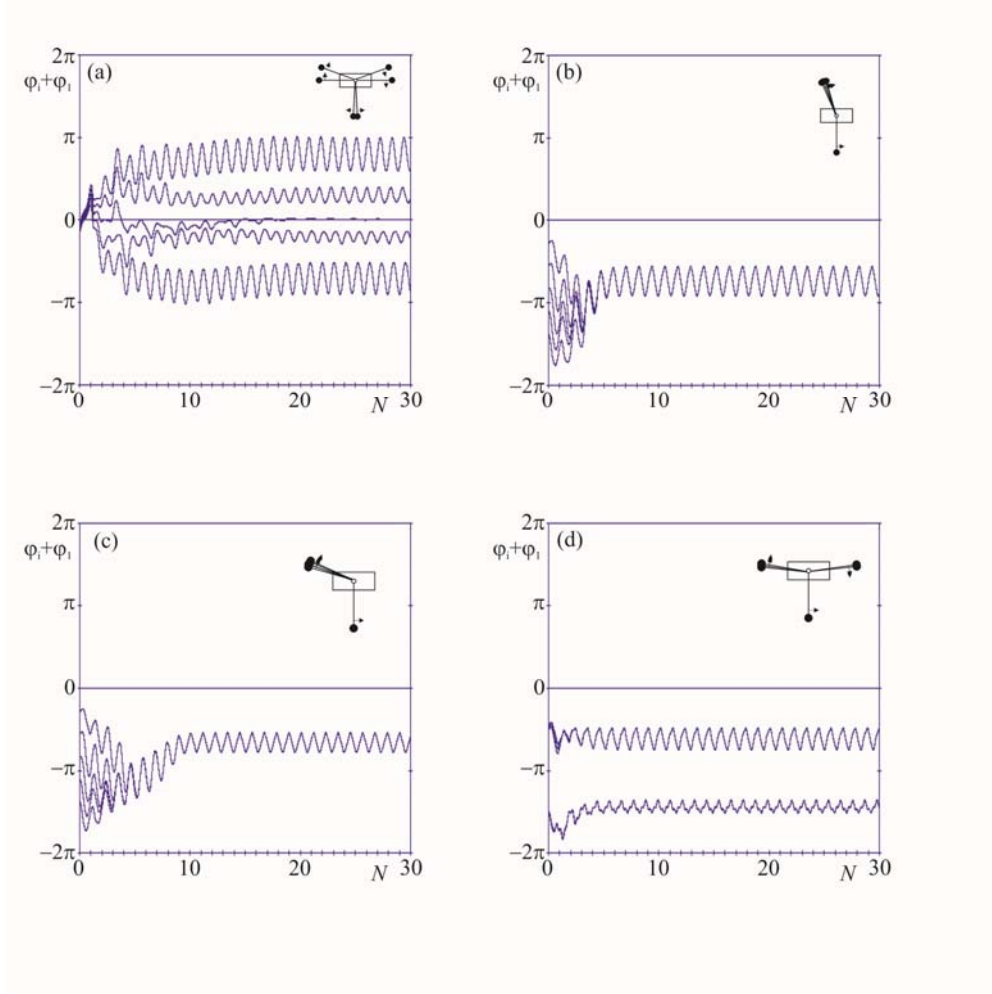


Figure 26: Different types of synchronization for the system with six pendula; (a) pendula's displacements during the tree-synchronization,  $k_x=200.0$ ,  $\varphi_{10}=0$ ,  $\varphi_{20}=-0.16$ ,  $\varphi_{30}=-0.32$ ,  $\varphi_{40}=-0.48$ ,  $\varphi_{50}=-0.64$ ,  $\varphi_{60}=-0.80$ , (b) pendula's displacements during the cluster-antiphase-synchronization,  $k_x=2000.0$ ,  $\varphi_{10}=0$ ,  $\varphi_{20}=-0.27$ ,  $\varphi_{30}=-0.55$ ,  $\varphi_{40}=-0.83$ ,  $\varphi_{50}=-1.11$ ,  $\varphi_{60}=-1.38$ , (c) pendula's displacements during the cluster-left-synchronization,  $k_x=3000.0$ ,  $\varphi_{10}=0$ ,  $\varphi_{20}=-0.27$ ,  $\varphi_{30}=-0.55$ ,  $\varphi_{40}=-0.83$ ,  $\varphi_{50}=-1.11$ ,  $\varphi_{60}=-1.38$ , (d) pendula's displacements during the yankee-synchronization,  $k_x=3000.0$ ,  $\varphi_{10}=0$ ,  $\varphi_{20}=-0.44$ ,  $\varphi_{30}=-0.52$ ,  $\varphi_{40}=-\pi$ ,  $\varphi_{50}=-3\pi/2$ ,  $\varphi_{60}=-1.52$ .

Generally in the systems with large number of pendula we observe the same types of synchronizations as described for three pendula in previous sections. Probability of the appearance of the Yankee type of synchronization decreases with the increase of the number of pendula.

#### 4.7. Two pendula with different driving torques, rotating in the same direction

In the last example, let us consider the case of two pendula with the same lengths and masses but with different driving torques. In our numerical simulations eqs.(1,2) have been integrated by the 4<sup>th</sup> order Runge-Kutta method. The obtained results confirmed the existence of the phenomenon of phase synchronization in the considered system and allowed the determination of phase angles between the synchronized pendula. Additionally, the numerical

integration of eqs.(1,2) allows the determination of the basins of attraction of different coexisting configurations of the synchronized pendula. We use the following parameters' values:  $l_1=l_2=5.0$ ,  $c_{\varphi_1}=c_{\varphi_2}= 0.012$ ,  $m_1=m_2=1.0$ ,  $m_b=10.0$ ,  $c_x=21.5$ . In different examples we consider two values of  $k_x=2400.0$  or  $400.0$ . Pendulum 1 is driven by the torque given by  $p_{01}=5.0$ ,  $p_{11}=0.4$ . The parameters of the driving torque of pendulum 2 have been taken as control parameters.

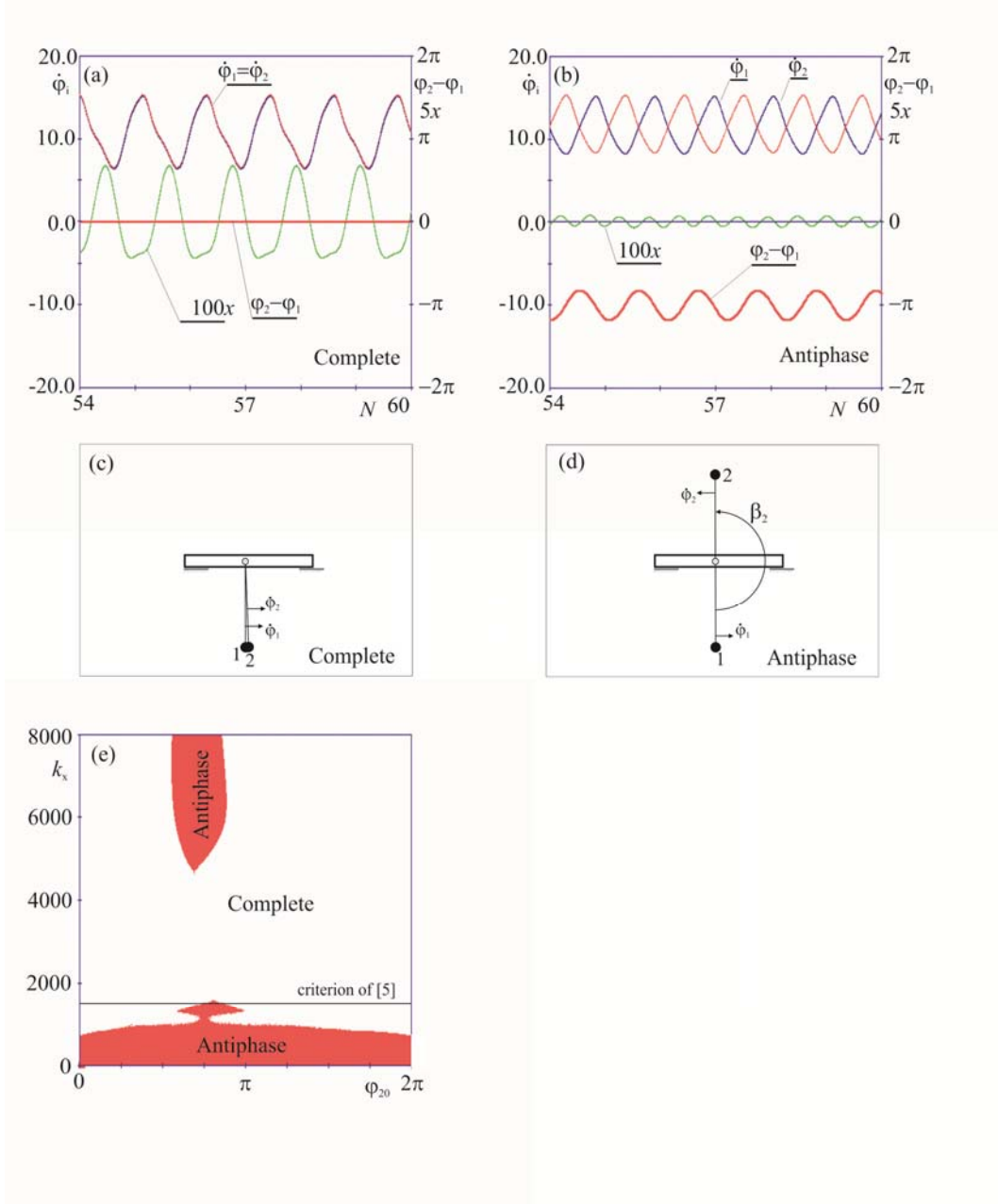


Figure 27. Two types of synchronous configurations of identically driven pendula:  $l_1=l_2=0.25$ ,  $c_{\varphi_1}=c_{\varphi_2}= 0.012$ ,  $m_1=m_2=1.0$ ,  $m_b=10.0$ ,  $c_x=21.5$ ,  $p_{01}=5.0$ ,  $p_{11}=0.4$ ,  $p_{02}=5.0$ ,  $p_{12}=0.4$ ; (a) time series of the pendula' angular velocities  $\dot{\varphi}_1$ ,  $\dot{\varphi}_2$  during the state of complete synchronization ( $\varphi_2 - \varphi_1 = 0$ ),  $k_x=2400.0$ , (b) time series of the pendula' angular velocities  $\dot{\varphi}_1$ ,  $\dot{\varphi}_2$  during the state of antiphase synchronization ( $\varphi_2 - \varphi_1 = \pi$ ),  $k_x=400.0$ , (c) pendula' configuration during the complete synchronization, (d) pendula' configuration during the antiphase synchronization, (e) basins of attraction of complete and antiphase synchronizations;  $p_{01}=5.0$ ,  $p_{11}=0.4$ ,  $p_{02}=5.0$ ,  $p_{12}=0.4$ ,  $\varphi_{10}=0$ ,  $\dot{\varphi}_{10} = 0$ ,  $\dot{\varphi}_{20} = 0$ ,  $x_0=0$ ,  $\dot{x}_0 = 0$ .

Figure 27(a-e) presents two types of the synchronous configurations which have been predicted in Sec. 3. In Figure 27(a) we show the time series of the pendula' angular velocities  $\dot{\varphi}_1, \dot{\varphi}_2$  during the state of complete synchronization ( $\varphi_2 - \varphi_1 = 0$ ) obtained for  $p_{01}=p_{02}=5.0$ ,  $p_{11}=p_{12}=0.4$ ,  $k_x=2400.0$ . Notice that these velocities are equal ( $\dot{\varphi}_1 = \dot{\varphi}_2$ ) and fluctuate (due to the gravity and the beam's oscillations) around the nominal value  $\dot{\varphi}_n = 12.5$ . The time series  $x$  is also shown (for better visibility it has been enlarged 5 times). The pendula' configuration during this type of synchronization is shown in Figure 27(c). Figure 27(b) shows the time series of the pendula' angular velocities  $\dot{\varphi}_1, \dot{\varphi}_2$  during the state of antiphase synchronization ( $\varphi_2 - \varphi_1 = \pi$ ) obtained for  $p_{01}=p_{02}=5.0$ ,  $p_{11}=p_{12}=0.4$ ,  $k_x=400.0$ . These velocities fluctuate around nominal value  $\dot{\varphi}_n = 12.5$  and the fluctuations are in the antiphase. The difference between the pendula' displacements fluctuates around mean value equal to  $\pi$ , i.e., ( $\varphi_2 - \varphi_1 \approx \pi$ ). The amplitudes of the beam's oscillations are much smaller than in the previous case. The pendula' configuration during this type of synchronization is shown in Figure 27(d). In Figure 27(e) we show the basins of attraction of different types of synchronization. The basins of complete and antiphase synchronizations are shown respectively in white and red colors. The basins are presented in the plane showing the stiffness coefficient  $k_x$  versus initial value of displacement  $\varphi_{20}$ . The rest of the initial conditions are as follows  $\varphi_{10}=0$ ,  $\dot{\varphi}_{10}, \dot{\varphi}_{20} = 0$ ,  $x_0=0$ ,  $\dot{x}_0 = 0$ . For small values of  $k_x$ , (smaller than 19) the system reaches the state of antiphase synchronization for all values of  $\varphi_{20}$ . Similarly in the interval  $1600 < k_x < 4680$  independently of  $\varphi_{20}$  we observe complete synchronization. In the intervals  $760 < k_x < 1600$  and  $4680 < k_x < 8000$  the type of synchronous configuration depends on  $\varphi_{20}$ . These results can be compared to that of [5]. On the base of analytical analysis he has shown that the basin boundary between complete and antiphase synchronization is determined by the constant value of  $k_x$  (independent of initial conditions), for which angular velocity  $\dot{\varphi}_{n1,2} = \frac{p_{01}}{p_{11}} = 12.5$  is the resonant frequency of the linear oscillator consisting of the spring with stiffness coefficient  $k_x$  and mass  $m_b=10.0$ . For the considered parameters' values it is equal to  $k_x=10.0 \times 12.5^2=1560.0$ . This criterion is indicated in Figure 27(e) by the horizontal line.

In further studies we consider the pendula which are driven by different torques. In Figure 28(a) we show the time series of the pendula' angular velocities  $\dot{\varphi}_1, \dot{\varphi}_2$  during the state of almost complete synchronization ( $\varphi_2 - \varphi_1 \approx 0$ ) obtained for:  $p_{01}=5.0$ ,  $p_{11}=0.4$ ,  $p_{02}=3.75$ ,  $p_{12}=0.3$ . Notice that the values of the parameters are different but the ratios are the same  $\dot{\varphi}_{n1,2} = \frac{p_{01}}{p_{11}} = \frac{p_{02}}{p_{12}} = 12.5$ . In comparison to the case of Figure 27(a) we observe only small differences in angular velocities of both pendula. With the increase of  $p_{12}$  (the decrease of the nominal angular velocity  $\dot{\varphi}_{2N}$  of pendula 2) these differences increase and the phase shift between pendula becomes clearly visible. Finally, for  $p_{12}=0.355$  synchronization mechanism based on the energy transfer between the pendula (via the beam) fails and the synchronization is no longer observed and we observe the quasiperiodic motion. The example of quasiperiodic motion is shown in Figure 28(b) for  $p_{12}=0.36$ . The action of the synchronization mechanism is still visible. The energy transfer from pendulum 1 to pendulum 2 tries to increase the angular velocity of pendulum 2 and allows both pendula to rotate with the same velocity. This action is manifested by long intervals in which the difference of pendula' displacements  $\varphi_2 - \varphi_1$  fluctuates between constant values. However, the energy transfer is not sufficient and we observe the rapid increase (nearly a jump) of the difference  $\varphi_2 - \varphi_1$  by  $2\pi$ . One can say that at some instances pendulum 2 loses one rotation in comparison to pendulum 1. Figure 28(c) presents the pendula' and the beam energy balances versus parameter  $p_{12}$ . Pendulum 1 increases the common angular velocity to the value larger than the nominal velocity  $\dot{\varphi}_{n2}$  of pendulum 2 so the value of energy  $W_2^{\text{DRIVE}}$  decreases up to  $W_2^{\text{DAMP}}$  (for  $p_{12}=0.319$ ), energy



$W_2^{\text{SYN}}$  becomes zero and takes no part in the excitation of the beam's oscillations. Next energy  $W_2^{\text{SYN}}$  becomes negative, i.e., the driver torque of pendulum 2 supplies less energy than the energy dissipated by the damper of pendulum 2. To keep both pendula rotating with the same velocity pendulum 1 has to supply energy to pendulum 2. The energy  $W_1^{\text{SYN}}$  is divided between the beam and pendulum 2, i.e., pendulum 1 drives both the beam and pendulum 2. Figure 28(d) presents the example of the energy balance for the case with negative  $W_2^{\text{SYN}}$  for  $p_{12}=0.33$ .

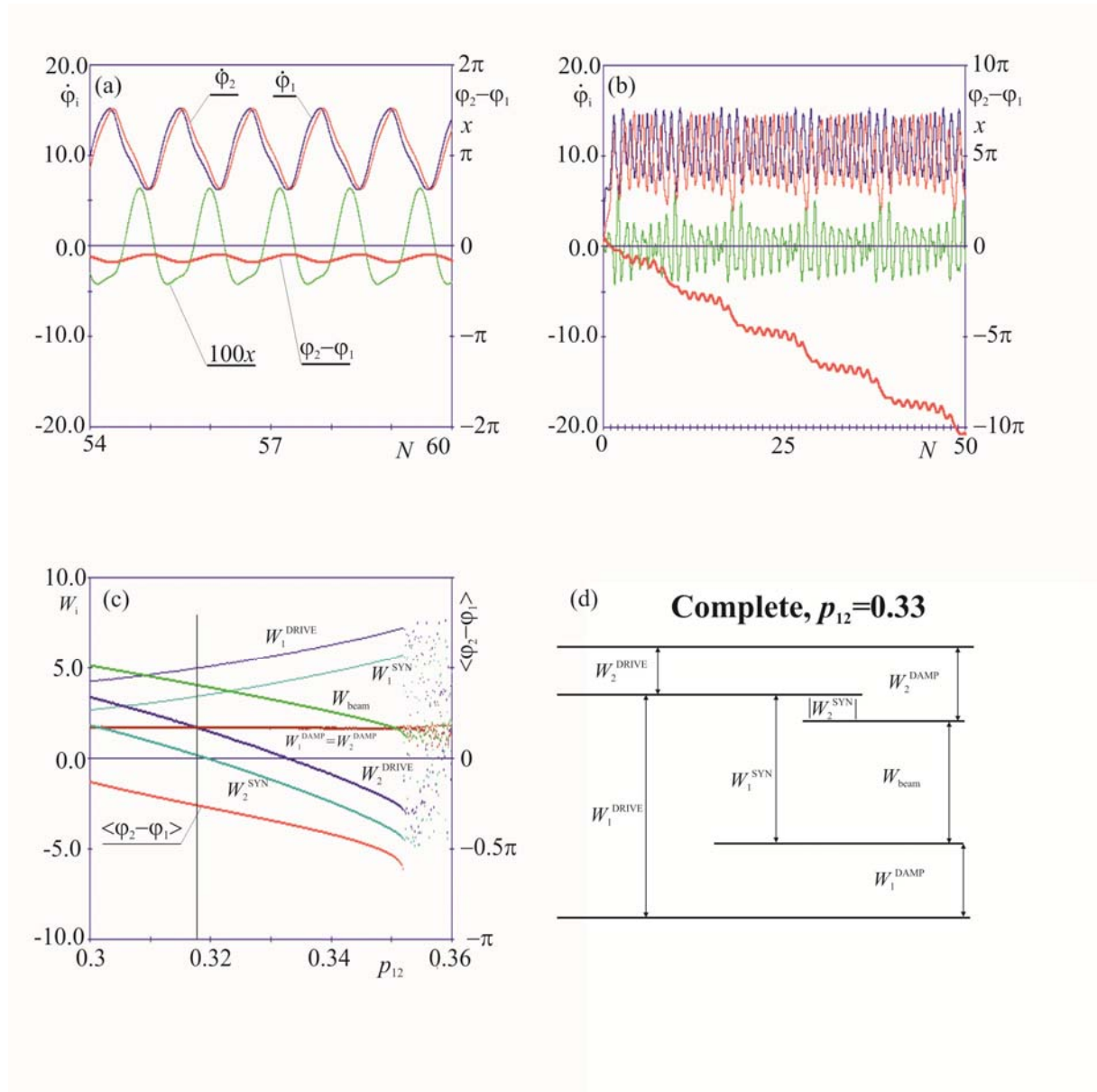


Figure 28. Almost complete synchronization in the system with pendula with different driving torques:  $\dot{\phi}_{10} = 12.0$ ,  $p_{01}=5.0$ ,  $p_{02}=3.75$ ,  $p_{11}=0.4$ ; (a) time series of the pendula's angular velocities  $\dot{\phi}_1$ ,  $\dot{\phi}_2$  during the state of almost complete synchronization ( $\varphi_2 - \varphi_1 \approx 0$ ),  $p_{12}=0.3$ , (b) time series of the pendula's angular velocities  $\dot{\phi}_1$ ,  $\dot{\phi}_2$  at the threshold between almost complete synchronization and quasiperiodic motion,  $p_{12}=0.356$ ; (c) energy balance of the system versus  $p_{12}$ , (d) the example of the energy balance in the case when  $W_2^{\text{SYN}} < 0$ .



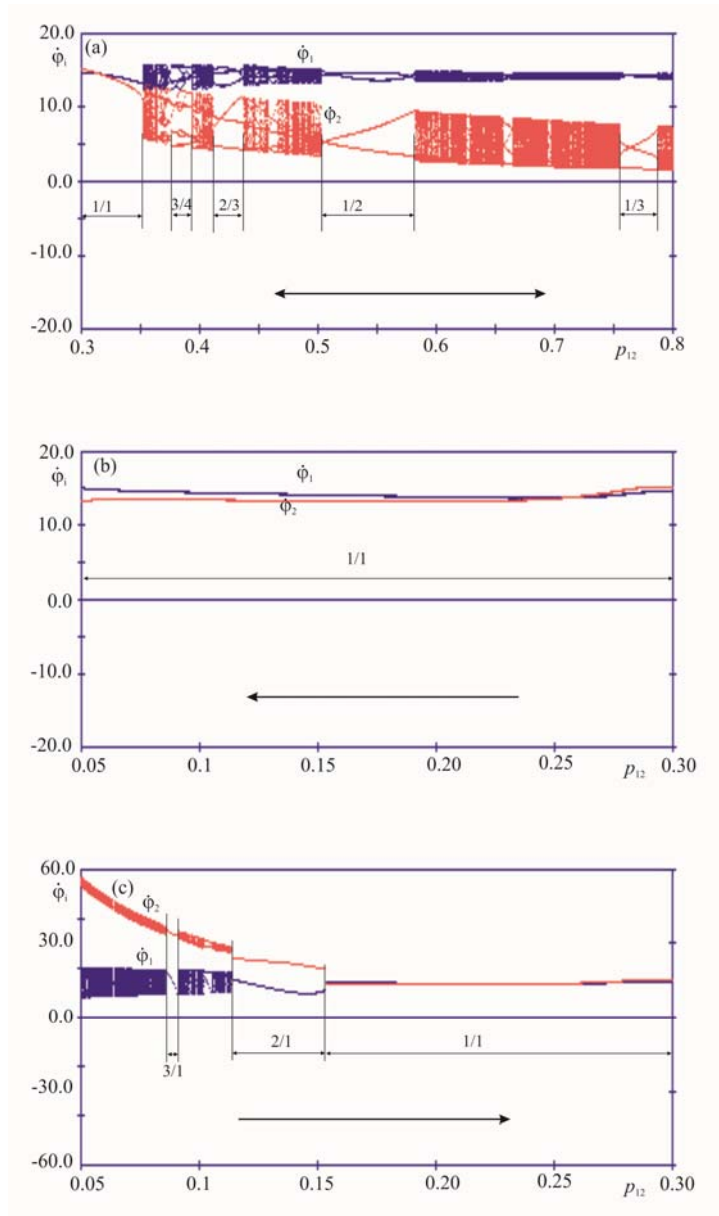


Figure 29. Bifurcation diagrams:  $\dot{\phi}_1, \dot{\phi}_2$  (at the time instances when pendulum 1 passes through the equilibrium position, i.e., when  $\varphi_l = 2\pi j, j=1, 2, \dots$ ) versus  $p_{12}$ :  $k_x=2400.0, p_{01}=5.0, p_{11}=0.4, p_{02}=3.75; \varphi_{10}=0, \dot{\varphi}_{10} = 0, \dot{\varphi}_{20} = 0, x_0=0, \dot{x}_0 = 0$ ; (a) the value of  $p_{12}$  is increased from 0.3 to 0.8 and next decreased from 0.8 to 0.3, the intervals of 1/1 almost complete synchronization and intervals of 1/2, 1/3, 2/3, 3/4 synchronizations are indicated, (b) the value of  $p_{12}$  is decreased from 0.3 to 0.05, interval of 1/1 almost complete synchronization is indicated, (c) the value of  $p_{12}$  is increased from 0.05 to 0.3, intervals of 3/1, 2/1 and 1/1 synchronizations are indicated.

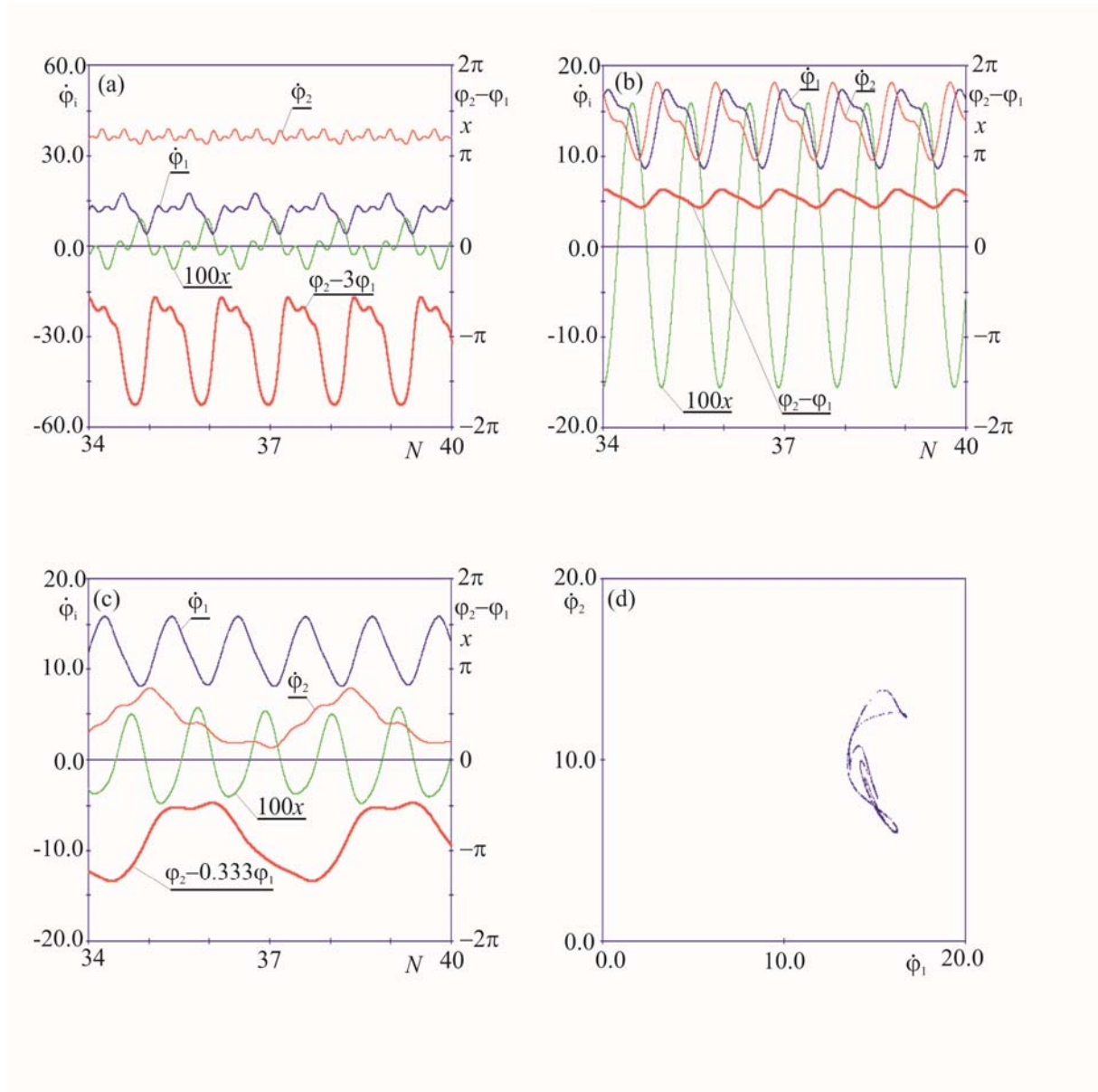


Figure 30. The examples of different types of system behaviors shown in Figure 29(a-c):  $\dot{\phi}_{10} = 12.0$ ,  $k_x=2400.0$ ,  $p_{01}=5.0$ ,  $p_{11}=0.4$ ,  $p_{02}=3.75$ ; (a) time series of the pendula' angular velocities  $\dot{\phi}_1$ ,  $\dot{\phi}_2$  during the state of 3/1 synchronization,  $p_{12}=0.088$ ,  $\varphi_{10}=0$ ,  $\dot{\phi}_{10} = 12.0$ ,  $\varphi_{20}=1.57$ ,  $\dot{\phi}_{20} = 2.0$ ,  $x_0=0$ ,  $\dot{x}_0=0$ , (b) time series of the pendula' angular velocities  $\dot{\phi}_1$ ,  $\dot{\phi}_2$  during the state of almost complete synchronization ( $\varphi_2 - \varphi_1 \approx 0$ ) 1/1 synchronization (coexisting with 3/1 synchronization),  $p_{12}=0.088$ ,  $\varphi_{10}=0$ ,  $\dot{\phi}_{10} = 12.0$ ,  $\dot{\phi}_{10} = 14.8$ ,  $\varphi_{20}=1.80$ ,  $\dot{\phi}_{20} = 13.2$ ,  $x_0=0.05$ ,  $\dot{x}_0 = 0.95$ , (c) time series of the pendula' angular velocities  $\dot{\phi}_1$ ,  $\dot{\phi}_2$  during the state 1/3 synchronization,  $p_{12}=0.76$ ,  $\varphi_{10}=0$ ,  $\dot{\phi}_{10} = 0$ ,  $\varphi_{20}=1.57$ ,  $\dot{\phi}_{20} = 0$ ,  $x_0=0.0$ ,  $\dot{x} = 0$ , (d) Poincaré map of quasiperiodic motion,  $p_{12}=0.36$ ,  $\varphi_{10}=0.0$ ,  $\dot{\phi}_{10} = 2.0$ ,  $\varphi_{20}=0.0$ ,  $\dot{\phi}_{20} = 2.0$ ,  $x_0=0$ ,  $\dot{x}_0 = 0$ .

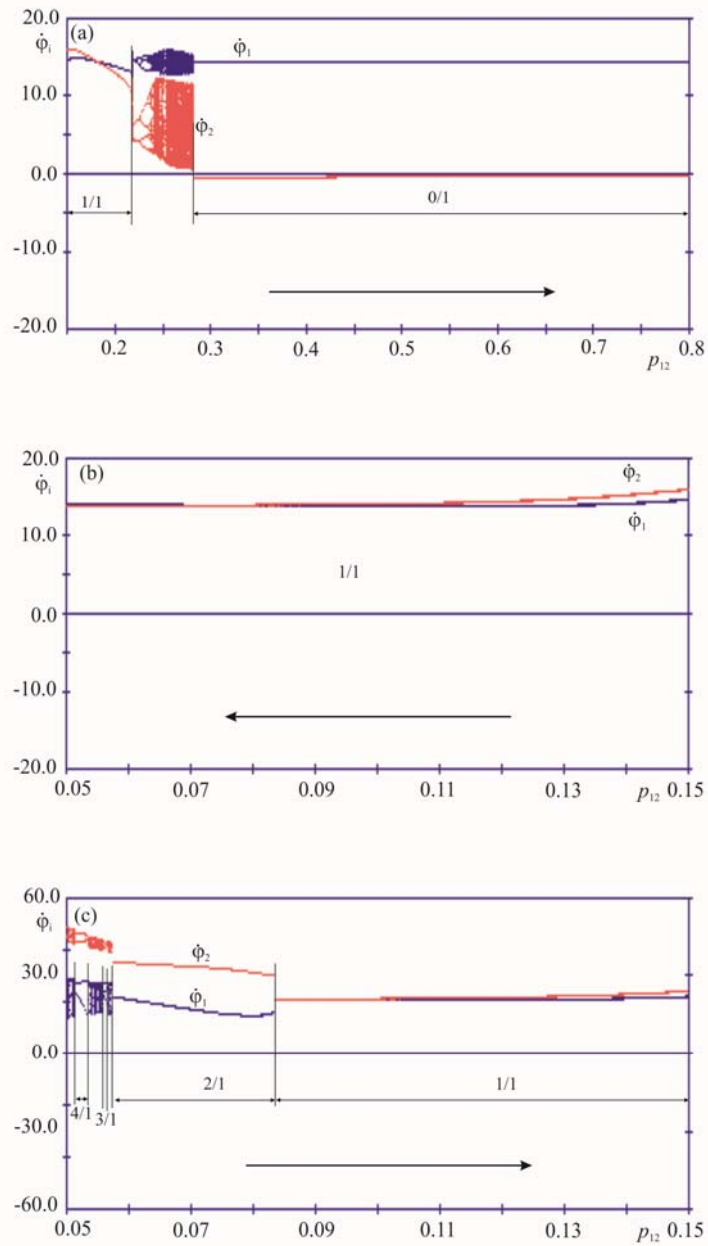


Figure 31. Bifurcation diagrams:  $\dot{\phi}_1, \dot{\phi}_2$  (at the time instances when pendulum 1 passes through the equilibrium position, i.e., when  $\varphi_1 = 2\pi n$ ) versus  $p_{12}$ ,  $k_x = 2400.0$ ,  $p_{01} = 5.0$ ,  $p_{11} = 0.4$ ,  $p_{02} = 0.36$ ; (a) the value of  $p_{12}$  is increased from 0.15 to 0.8,  $\varphi_{10} = 0$ ,  $\dot{\varphi}_{10} = 12.0$ ,  $\varphi_{20} = 0$ ,  $\dot{\varphi}_{20} = 0$ ,  $x_0 = 0$ ,  $\dot{x} = 0$ , (b) the value of  $p_{12}$  is decreased from 0.15 to 0.05,  $\varphi_{10} = 0$ ,  $\dot{\varphi}_{10} = 12.0$ ,  $\varphi_{20} = 0$ ,  $\dot{\varphi}_{20} = 2.0$ ,  $x_0 = 0$ ,  $\dot{x} = 0$ , (c) the value of  $p_{12}$  is increased from 0.05 to 0.15,  $\varphi_{10} = 0$ ,  $\dot{\varphi}_{10} = 36.0$ ,  $\varphi_{20} = 0$ ,  $\dot{\varphi}_{20} = 36.0$ ,  $x_0 = 0$ ,  $\dot{x} = 0$ .

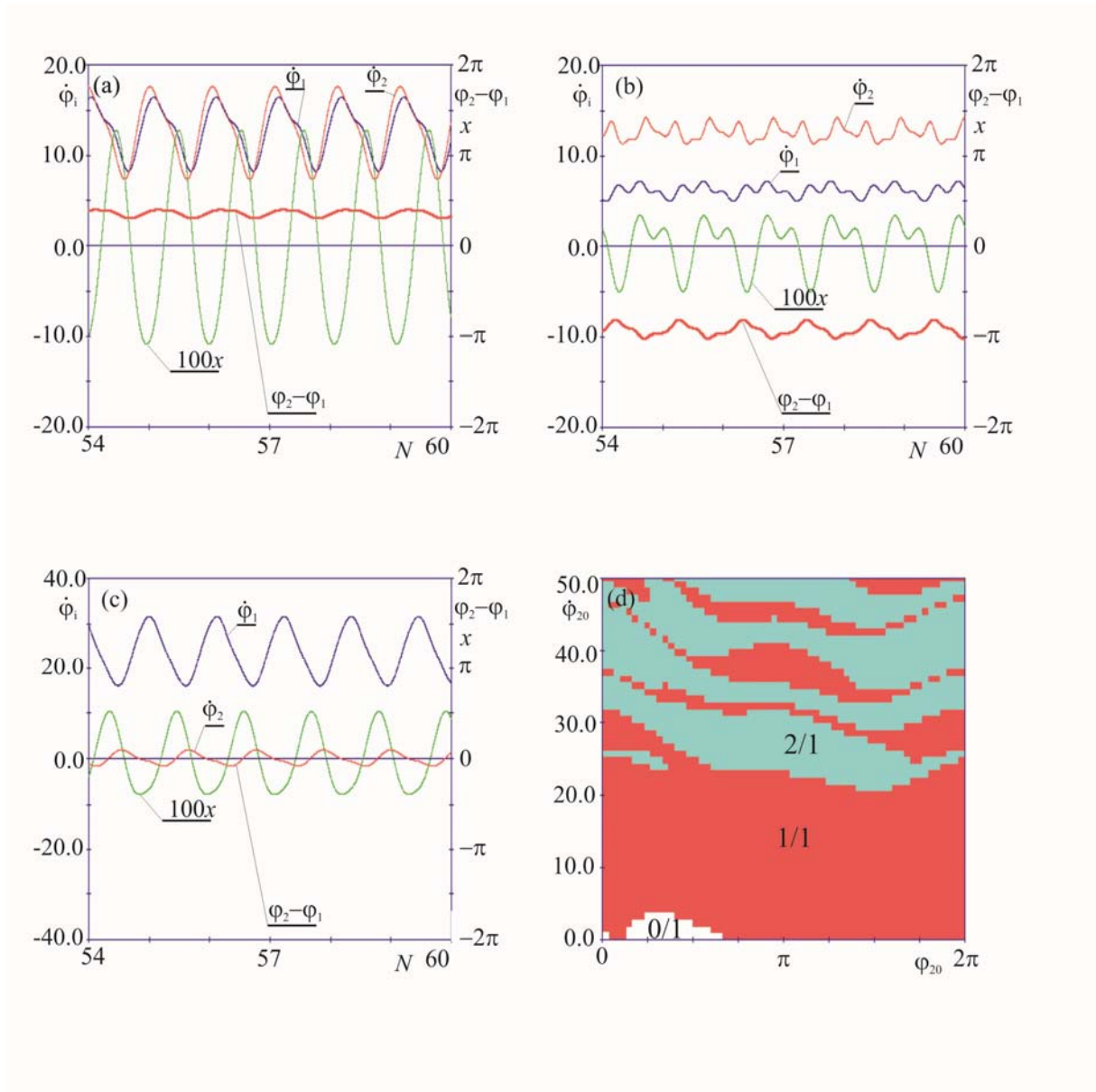


Figure 32: The examples of different types of coexisting attractors shown in Figure 31(a-c):  
 $k_x=2400.0, p_{01}=5.0, p_{11}=0.4, p_{02}=0.36, p_{12}=0.068$ ; (a) time series of the pendula' angular velocities  $\dot{\phi}_1, \dot{\phi}_2$  during the state of 1/1 almost synchronization,  $p_{12}=0.088, \phi_{10}=0, \dot{\phi}_{10}=0, \phi_{20}=3.14, \dot{\phi}_{20}=18.0, x_0=0, \dot{x}=0$ , (b) time series of the pendula' angular velocities  $\dot{\phi}_1, \dot{\phi}_2$  during the state of 2/1 synchronization,  $\phi_{10}=0, \dot{\phi}_{10}=0, \phi_{20}=3.14, \dot{\phi}_{20}=24.0, x_0=0, \dot{x}=0$ , (c) time series of the pendula' angular velocities  $\dot{\phi}_1, \dot{\phi}_2$  during 0/1 state,  $\phi_{10}=0, \dot{\phi}_{10}=0, \phi_{20}=1.57, \dot{\phi}_{20}=0, x_0=0, \dot{x}=0$ , (d) basins of attraction of the attractors of (a-c),  $\phi_{10}=0.0, \phi_{10}=12.0, x_0=0, \dot{x}=0$ .

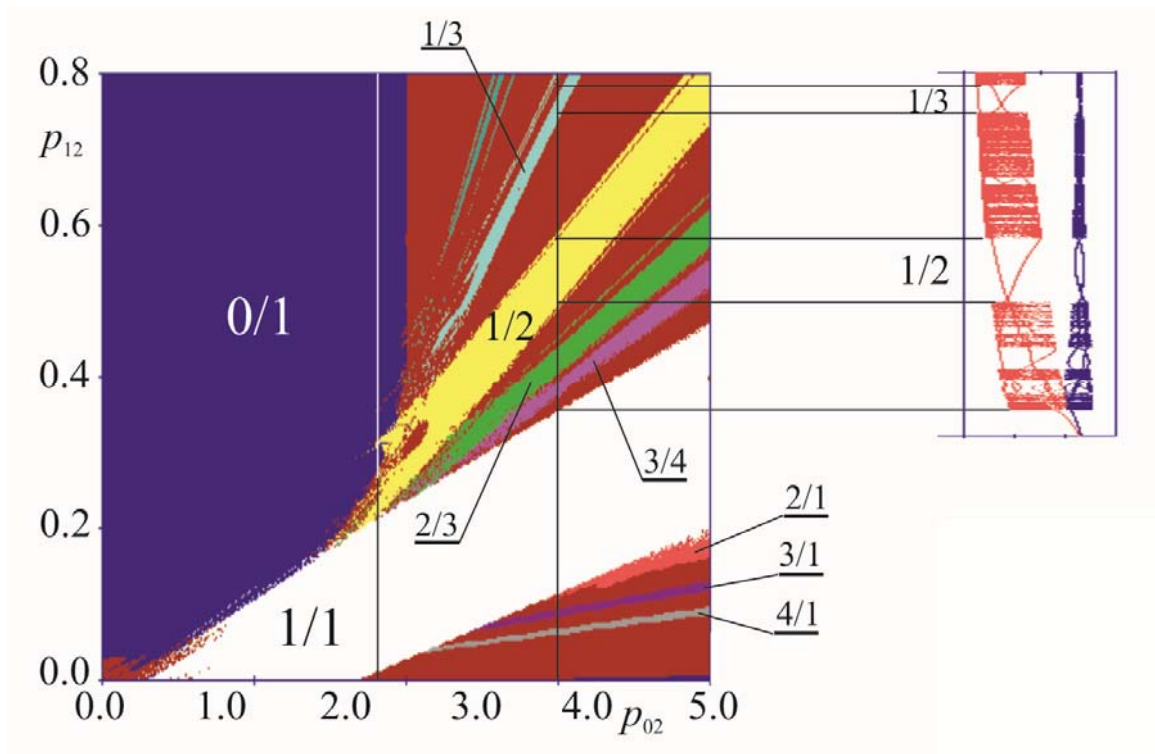


Figure 33. Type of synchronization for different values of driving torques: map  $p_{02}$  versus  $p_{12}$ , initially the driving torques of both pendula are identical  $p_{01}=p_{02}=5.0$ ,  $p_{11}=p_{12}=0.4$ ,  $\varphi_{10}=0$ ,  $\dot{\varphi}_{10} = 12.0$ ,  $\varphi_{20}=0$ ,  $\dot{\varphi}_{20} = 12.0$ ,  $x_0=0$ ,  $\dot{x} = 0$  (in the initial moment both pendula are passing through the equilibrium with the same angular velocity equal to  $\frac{1}{2}\dot{\varphi}_{n1}$  and after the transient the system reaches 1/1 complete synchronization).

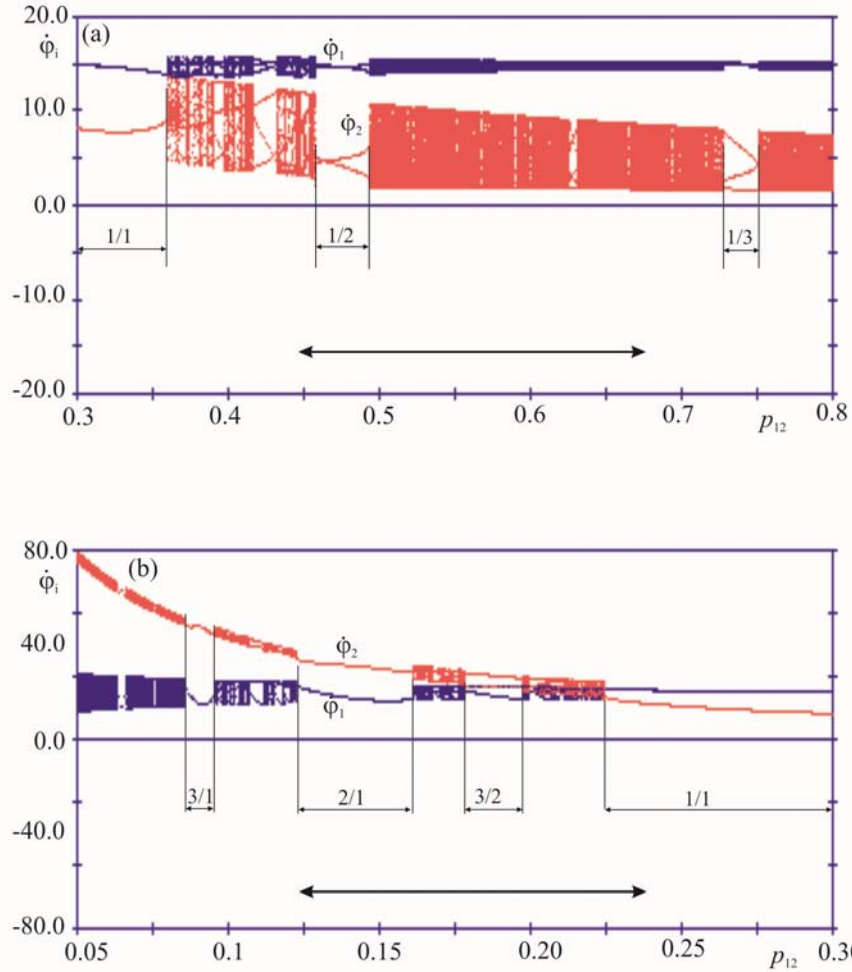


Figure 34. Bifurcation diagrams:  $\phi_1, \phi_2$  (at the time instances when pendulum 1 passes through the equilibrium position, i.e., when  $\varphi_1 = 2\pi j, j=1, 2, \dots$ ) versus  $p_{12}$ :  $k_x=400.0, p_{01}=5.0, p_{11}=0.4, p_{02}=3.75$ ;  $\varphi_{10}=0, \dot{\varphi}_{10} = 0, \dot{\varphi}_{20} = 0, x_0=0, \dot{x} = 0$ ; (a) the value of  $p_{12}$  is increased from 0.3 to 0.8 and next decreased from 0.8 to 0.3, the intervals of 1/1 almost complete synchronization and intervals of 1/2, 1/3, synchronizations are indicated, (b) the value of  $p_{12}$  is decreased from 0.3 to 0.05 and next increased from 0.05 to 0.3, intervals of 3/1, 3/1, 2/1 and 3/2 synchronizations are indicated.

The bifurcation diagrams shown in Figure 29(a-c) describe the behavior of the system with drive torques ( $p_{01}=5.0, p_{11}=0.4, p_{02}=3.75$ ) in the wide range of the values of  $p_{12}$ . We show the values of  $\phi_1, \phi_2$  (at the time instances when pendulum 1 passes through the equilibrium position, i.e., when  $\varphi_1=2\pi j, j=1, 2, \dots$ ) versus  $p_{12}$ . The calculations have been started with the state of complete synchronization. The diagram of Figure 29(a) has been calculated for increasing values of  $p_{12}$  in the interval  $[0.3, 0.8]$ . The single lines determine the regions of synchronization while the blurred columns of markers indicate the lack of synchronization. One can observe the following types of synchronization: (i) 1/1 almost complete synchronization for  $0.3 < p_{12} < 0.355$ , (ii) 1/2 synchronization for  $0.5 < p_{12} < 0.58$ , (iii) 1/3 synchronization for  $0.75 < p_{12} < 0.78$ , (iii) 2/3 synchronization for  $0.41 < p_{12} < 0.44$ , (iv) 3/4 synchronization for  $0.78 < p_{12} < 0.396$ . Symbol 1/1 indicates that pendulum 2 rotate with the same mean angular velocity as pendulum 1, i.e., in the time interval of one rotation of pendulum 2 pendulum 1 performs one rotation, and the symbol  $r/q$ , where  $r, q=2, 3$  indicates that in the time interval of  $r$  rotation of pendulum 2 pendulum 1 performs  $q$  rotations.  $r/q$



synchronous regions exist in the windows in the interval of existence of quasiperiodic regime. Our numerical calculations indicate that such windows (most of them very small) are dense in the considered interval. In the range  $0.3 < p_{12} < 0.8$  we have not observed other attractors coexisting with those shown in Figure 29(a). The decrease of the values  $p_{12}$  from 0.8 to 0.3 gives an identical bifurcation diagram as in the case of the increase. The bifurcation diagram of Figure 29(b) has been calculated for the decreasing values of  $p_{12}$  (from 0.3 to 0.05). One observes 1/1 almost complete synchronization in the whole interval  $0.3 > p_{12} > 0.05$ . The increase of  $p_{12}$  from 0.05 to 0.5 allows the calculation of Figure 29(c). In the interval  $0.05 < p_{12} < 0.16$  we observe different behavior to that shown in Figure 29(b), which indicates the coexistence of different attractors, e.g.; in the interval  $0.085 < p_{12} < 0.09$  we have the coexistence of 1/1 and 3/1 synchronizations and in the interval  $0.114 < p_{12} < 0.155$  synchronous configurations 1/1 and 2/1 coexist. One can also observe the coexistence of 1/1 synchronization (shown in Figure 29(b)) and quasi-periodic rotations. Figure 30(a-c) shows the examples of time series of the pendula' angular velocities  $\dot{\varphi}_1, \dot{\varphi}_2$  showing different types of synchronizations. Figure 30(a) presents time series during 3/1 synchronization for  $p_{12}=0.088$  (as shown in Figure 29(c)). In Figure 30(b) 1/1 synchronization (which coexists with quasiperiodic behavior for  $p_{12}=0.088$ ) is described. 1/3 synchronization for  $p_{12}=0.76$  is illustrated in Figure 30(c) (compare with Figure 29(a)). Poincare map of the quasiperiodic behavior is shown in Figure 30(d) ( $p_{12}=0.36$ ). Notice that the points of the map forms closed curve with the complicated structure.

The bifurcation diagrams shown in Figure 31(a-c) for the pendula which are driven by different torques. We take  $p_{01}=5.0, p_{11}=0.4$  (as in calculations shown in Figure 29(a-c)) but consider different value of  $p_{02}=0.36$ . Note that in this case the value of maximum dimensionless torque which can be generated by the driving device  $p_{02}$  is smaller than the maximum value of the torque generated by the weight of pendulum 2 (equal to  $m_2 g l_2$ ). This indicates that there exist initial conditions for which pendulum 2 stops to rotate at  $\varphi_{2crit}$  given by relation  $m_2 g l_2 \sin \varphi_{2crit} = p_{02}$ . Calculating the diagram shown in Figure 31(a) we increase the value of  $p_{12}$  in the interval  $[0.15, 0.8]$  and observe three basic types of system (3,4) behavior: (i) 1/1 almost complete synchronization for  $0.15 < p_{12} < 0.22$ , (ii) quasiperiodic motion  $0.228 < p_{12} < 0.272$ , (iii) the state indicated as 0/1, i.e., pendulum 2 does not rotate (is at rest) in the interval  $0.272 < p_{12} < 0.8$ . In further calculations we decrease the value of  $p_{12}$  from 0.8 to 0.05 and observe that in the whole interval pendulum 2 is at rest. This indicates that in the whole interval  $0.15 < p_{12} < 0.272$  there is the coexistence of the state 0/1 with the states shown in 31(a). When calculating the diagram shown in Figure 31(b) we decrease the value of  $p_{12}$  from 0.15 to 0.05. In the whole interval one observes 1/1 almost complete synchronization. The diagram presented in Figure 31(c) has been calculated for  $p_{12}$  increasing from 0.05 to 0.15. Note that in the interval  $0.05 < p_{12} < 0.084$  we observe different behavior to that presented in Figure 31(b), e.g., very narrow intervals of 4/1 synchronization and 3/1 synchronization and for  $0.058 < p_{12} < 0.082$  – 2/1 synchronization. Figure 31(a-c) shows that the system (3-4) has the following coexisting attractors: (i) for  $0.05 < p_{02} < 0.082$  we observe three attractors: 0/1, 1/1 and one of the attractors shown in Figure 31(c), (ii) for  $0.082 < p_{02} < 0.272$  we have two attractors: 0/1 and one of the attractors shown in Figure 31(a,b), (iii) for  $0.272 < p_{02} < 0.8$  there is only one attractor 0/1, i.e., pendulum 2 stops independently of initial conditions.

In Figure 32(a-c) we show the time series of the pendula' angular velocities  $\dot{\varphi}_1, \dot{\varphi}_2$  for different type of coexisting attractors which exist for  $p_{12}=0.068$ . Figure 32(a,b) presents respectively 1/1 and 2/1 synchronizations. The state 0/1 (with non-rotating pendulum 2) is shown in Figure 32(c). The basins of attraction of these attractors are presented in Figure 32(d). The basins are shown on the plane  $\varphi_{20}-\dot{\varphi}_{20}$  (other initial conditions  $\varphi_{10}, \dot{\varphi}_{10}, x_0, \dot{x}_0$  are equal to zero).

Figure 33 presents map  $p_{02}$  versus  $p_{12}$  which describes how the type of synchronization is changing with the change of the parameters of driving torques. We assume that initially the driving torques of both pendula are identical  $p_{01}=p_{02}=5.0$ ,  $p_{11}=p_{12}=0.4$ . We consider the following initial conditions:  $\varphi_{10}=0$ ,  $\dot{\varphi}_{10} = 12.0$ ,  $\varphi_{20}=0$ ,  $\dot{\varphi}_{20} = 12.0$ ,  $x_0=0.0$ ,  $\dot{x}_0 = 0$ , i.e., in the initial moment both pendula are passing through the equilibrium with the same angular velocity close to  $\dot{\varphi}_{Ni}$  and after the transient the system reach 1/1 almost complete synchronization. Next, we change (the jump change) the values of parameters  $p_{02}$  and  $p_{12}$ . We observed the following cases. In the region indicated in white the synchronization 1/1 has been preserved. The type of synchronization has been changed (regions indicated by  $r/q$ ). Pendulum 2 stops (black region indicated) as 0/1 or the pendula start to rotate quasiperiodically (red region). For example, along line  $p_{o2}=0.9$  the system shows 1/1 almost complete synchronization or pendulum 2 stops (0/1 configuration) and along the line  $p_{o2}=3.75$  one observes the behavior described in Figure 29(a,c).

Finally, Figure 34(a,b) presents the bifurcation diagrams calculated in the same way as the diagram shown in Figure 29(a-c) but in this case we start with the antiphase synchronization. The diagram of Figure 34(a) has been calculated for increasing values of  $p_{12}$  in the interval  $[0.3, 0.8]$ . One can observe the following types of synchronization: (i) 1/1 complete synchronization for  $0.3 < p_{12} < 0.364$ , (ii) 1/2 synchronization for  $0.464 < p_{12} < 0.488$ , (iii) 1/3 synchronization for  $0.716 < p_{12} < 0.744$ .  $r/q$  synchronous regions exist in the windows in the interval of existence of quasiperiodic regime. The decrease of values  $p_{12}$  from 0.8 to 0.3 gives the identical bifurcation diagram as in the case of the increase. The bifurcation diagram of Figure 34(b) has been calculated for decreasing values of  $p_{12}$  (from 0.3 to 0.05). One observes 1/1 antiphase synchronization in the interval  $0.3 > p_{12} > 0.228$ . The increase of the values  $p_{12}$  from 0.05 to 0.3 gives identical bifurcation diagram as in the case of the decrease. Contrary to the case when the calculations started from the complete synchronization we have not observed the coexistence of attractors.

In Figure 29(a-c) 31(b,c) and 34(a-b) all presented periodic solutions represents resonances on the torus. They originates and terminates as the result of the saddle-node bifurcations (as in the classical Arnold's tongues). In Figure 31(a) for  $0 < p_{12} < 0.221$  we observe 1/1 resonance. Next the periodic solution is destroyed in saddle-node bifurcation and we observe the small interval of behavior. Another saddle-node bifurcation leads to 2/1 resonance and finally after the sequence of period-doubling bifurcations (we observe 4/2, 8/4 and 16/8 resonances) the system show chaotic behavior. Bifurcations have been identified using path following software AUTO-07P and confirmed by the calculations of Lyapunov exponents.



## 5. Synchronization extends the life time of rotation

Synchronization occurs widely in natural and technological world, from the rhythm of applause [53], rhythm of the crowd of walkers on the bridge [25,68], flashing of fireflies [11] to the nanomechanical or chemical oscillators [67,86], but it has not been shown that the synchronization can extend the life time of the desirable behavior of the coupled systems. In this section we give evidence that the initial synchronous state extends the lifetime of rotational behavior of the coupled pendula in the case when the excitation of one or few pendula is suddenly (breakdown of energy supply) or gradually (as the effect of aging and fatigue) switched off. We show that for the properly chosen coupling (in our system parameters  $k_x$  and  $m_b$ ) the energy transfer from the excited pendula allow unexcited pendula to rotate. The initial synchronous configuration is replaced by phase synchronization with different phase shifts between pendula and the rotational velocity of the synchronized pendula is decreased. These two factors can be considered as the indicator of the breakdown of excitation in one or few pendula. As a proof of concept we examine the following examples. The presented results have been obtained from the numerical integration of equations of motion (1,2).

### *Example 1. Two pendula rotating in the same direction*

In this example we reconsider the system (1,2) consisting of two identical pendula rotating in the same direction. We consider system (1-2) with the following parameter values:  $m_1=m_2=1.00$ ,  $l_1=l_2=0.25$ ,  $c_{\varphi 1}=c_{\varphi 2}=0.03$  and different values of the mass of the beam  $m_b$  and the stiffness coefficient  $k_x$ . The damping coefficient  $c_x$  has been selected in such a way as to be equivalent to the arbitrarily selected logarithmic decrement of damping  $\Delta=\ln(1.5)$  (the decrement characteristic for the linear oscillator with mass equal to the total mass of the system shown in Figure 3(a) mounted to the spring with the stiffness coefficient  $k_x$ . The excitation parameters of pendulum 1 are equal to  $p_{01}=5.0$ ,  $p_{11}=0.2$ . These parameters of pendulum 2, i.e.,  $p_{02}$  and  $p_{12}$  are taken as control parameters.

Figure 35(a-d) presents three different types of synchronous configurations for the excitation torques characterized by:  $p_{01}=p_{02}=5.0$ ,  $p_{11}=p_{12}=0.2$ . In Figure 35(a) we show the time series of pendula's angular velocities  $\dot{\varphi}_1, \dot{\varphi}_2$  for  $k_x=7000$  and  $m_b=12$  in the state of the complete synchronization (C). Angular velocities of both pendula are identical, their oscillations are caused by the effect of gravity and oscillations of the beam. The pendula's displacements fulfill the relation  $\varphi_2 - \varphi_1 = 0$  and the beam performs small periodic oscillations (displacement  $x(t)$  is magnified 10 times). Additionally, the synchronous configuration at the time when the pendula are moving through the lower stable equilibrium is shown. Figure 35(b) shows the same time series in the case of antiphase synchronization (A) for  $k_x=1000$  and  $m_b=16$ . Pendula's angular velocities  $\dot{\varphi}_1, \dot{\varphi}_2$  oscillate around the same mean value. The phase shift between these oscillations is equal to  $\pi$ . The phase shift between pendula's displacements  $\varphi_2 - \varphi_1$  oscillate around  $\pi$  (i.e.,  $\varphi_2 - \varphi_1 - \pi = 0$ ). The amplitudes of the beam's oscillations are smaller than in the case of complete synchronization. In Figure 35(c) both pendula perform quasiperiodic rotations for  $k_x=6500$  and  $m_b=17$ . The pendula's average angular velocities (calculated for the large number of rotations) are equal, so the pendula perform the same number of rotations in the given time. As both pendula perform the same number of rotations in the given time we can call this case the quasiperiodic synchronization (QS). Quasiperiodic oscillations of the pendula's angular velocities are clearly visible at the Poincare map shown in Figure 35(d). This map shows the pendula's angular velocities  $\dot{\varphi}_1, \dot{\varphi}_2$  versus the phase shifts between pendula's displacements  $\varphi_2 - \varphi_1 - \pi = 0$

calculated at the time when pendulum 1 is moving through the lower equilibrium position (i.e., for  $\varphi_1=2j\pi, j+1, 2, \dots$ ).

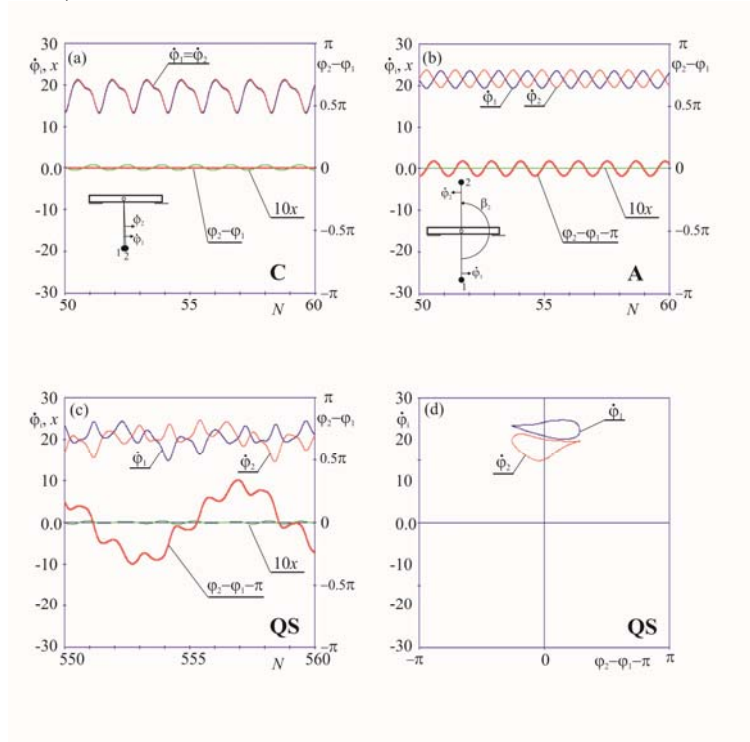


Figure 35. Time series of pendula's displacements  $\varphi_1, \varphi_2$ , angular velocities  $\dot{\varphi}_1, \dot{\varphi}_2$  and beam's displacement  $x$  (magnified 10 times):  $p_{01}=5.0, p_{11}=0.2, p_{02}=5.0, p_{12}=0.2, \varphi_{10}=0, \varphi_{20}=0.5\pi, \dot{\varphi}_{10} = \dot{\varphi}_{20} = 25, x_0 = \dot{x}_0 = 0$ , (a) complete synchronization  $k_x=7000.0, m_b=12.0$ , (b) antiphase synchronization  $k_x=1000.0, m_b=16.0$ , (c,d) synchronous quasiperiodic rotation  $k_x=6500.0, m_b=17.0$ , (d) Poincare map for the case of (c).

Figure 36(a,b) shows the dependence of the synchronous configuration on the parameters  $k_x$  and  $m_b$ . The calculations have been performed for  $p_{01}=5.0, p_{11}=0.2, p_{02}=5.0, p_{12}=0.2$  and initial conditions  $\varphi_{10}=0, \varphi_{20}=0.5\pi, \dot{\varphi}_{10} = \dot{\varphi}_{20} = 25, x_0 = \dot{x}_0 = 0$  (Figure 36(a)) and  $\varphi_{10}=0, \varphi_{20}=0.5\pi, \dot{\varphi}_{10} = 25, \dot{\varphi}_{20} = -25, x_0 = \dot{x}_0 = 0$ , i.e., the pendula initially rotate in different directions (Figure 36(b)). The regions of complete (C), antiphase (A), quasiperiodic (QS) synchronizations are indicated respectively in green, navy blue and violet colors. Notice the navy blue – violet band in the vicinity of the diagonal. In this region the complete synchronization (see Figure 36(a)) coexists with either antiphase or quasiperiodic synchronization.

Determination of the domain in parameters space  $(k_x, m_b)$ , in which different synchronous configurations coexist, is not straightforward and require precise calculations. Blekhman [5] suggested that the boundary of the complete and antiphase is given by the condition  $\dot{\varphi}_N = p_{01}/p_{11} = a_x$ , where  $a_x$  is the resonant frequency of the linear oscillator consisting of mass  $m_b+nm$  suspended on the spring with stiffness coefficient  $k_x$ . This boundary is shown as a black line in Figure 36(a,b). One can see that it is located away from the real boundary as in the considered system dampers dissipate part of the energy supplied by the excitation torques. This dissipation causes the reduction of the actual angular velocity of the pendula below their nominal velocity  $\dot{\varphi}_{Ni} = p_{0i}/p_{1i}$ .

Generally, designing a system supporting the pendula, the weight of the beam  $m_b$  and the stiffness coefficient  $k_x$  should be chosen in such a way that the resonance frequency of the system is smaller than the angular velocity of the pendula to obtain antiphase synchronization

or significantly higher than the angular velocity of pendula to achieve complete synchronization. Unfortunately, the angular velocity of the pendula can be determined only by numerical integration of equations of motion of a particular system (1,2).

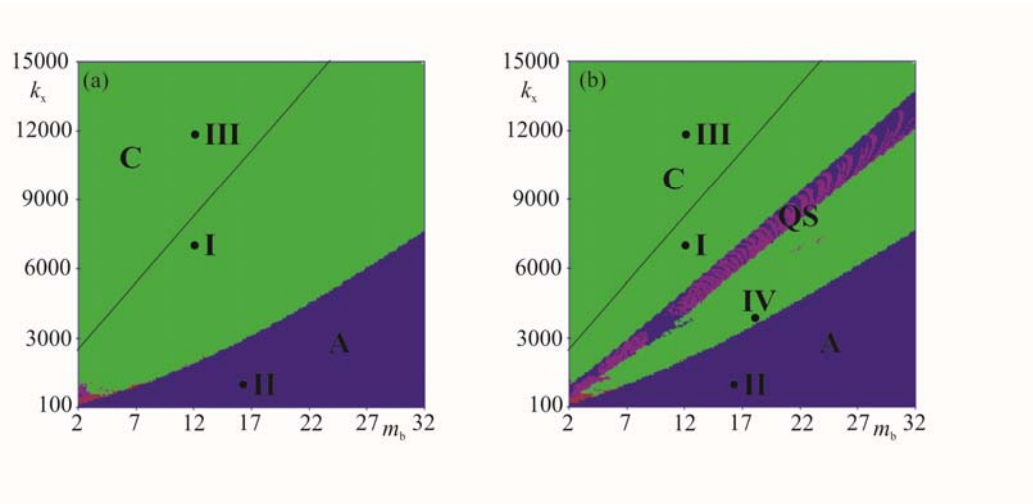


Figure 36. The regions of the parameters  $k_x - m_b$  space of complete (C) (green), antiphase (A) (navy blue), quasiperiodic (QS) (violet) synchronizations for the system of two identical and identically driven pendula rotating in the same direction:  $p_{01}=5.0, p_{11}=0.2, p_{02}=5.0, p_{12}=0.2$ , (a)  $\varphi_{10}=0, \varphi_{20}=0.5\pi, \dot{\varphi}_{10} = \dot{\varphi}_{20} = 25, x_0 = \dot{x}_0 = 0$ , (b)  $\varphi_{10}=0, \varphi_{20}=0.5\pi, \dot{\varphi}_{10} = 25, \dot{\varphi}_{20} = -25, x_0 = \dot{x}_0 = 0$ .

Now let us investigate the effect of sudden excitation switch off in one of the synchronized pendula, i.e., system (1,2) of two identical and identically driven pendula is in the synchronized state and the excitation of pendulum 2 is suddenly switched off. The results of our calculations are shown in Figure 37(a,b) and Figure 38(a-c). Then for given values of  $k_x$  and  $m_b$  the pendula are in the synchronized state described in Figure 36(a,b) when the excitation of pendulum 2 is switched off. After the initial transient pendula reach the state described in Figure 37(a,b). In the green and navy blue regions respectively initial complete and antiphase synchronization is replaced by the phase synchronization with various phase shifts between pendula. In the red region there is no synchronization and pendulum 2 stops. In small violet and blue regions we observed respectively quasiperiodic and multiperiodic synchronization. In Figure 38(a) we show the time series of pendula's angular velocities  $\dot{\varphi}_1, \dot{\varphi}_2$  for  $k_x=7000.0, m_b=12.0$  (point I in Figure 36(a) and 37(a)). Initially complete synchronization (C) is replaced by the phase synchronization with the phase shift between pendula equal to  $0.4\pi$ . The time series for  $k_x=1000.0$  and  $m_b=16.0$  (point II) is shown in Figure 38(b). In this case initially antiphase synchronization (A) is replaced by the phase synchronization with the phase shift between pendula equal to  $0.7\pi$ . In both cases pendulum 1 transfers sufficient amount of energy to keep pendulum 2 rotating. The phase shifts between pendula different from original 0 and  $\pi$  can be taken as indicators of the excitation switch off. In region (N) indicated in red color the synchronization is lost. Pendulum 2 slows down and finally stops. The time series of pendula's angular velocities  $\dot{\varphi}_1, \dot{\varphi}_2$  are shown in Figure 38(c) ( $k_x=12000.0, m_b=12.0$  - point III). Pendulum 2 performs oscillations caused by the oscillations of the beam –  $x$  and angular velocity of pendulum 2 oscillates around zero. In Figure 37(a,b) one can see small regions (violet) when quasiperiodic synchronization and the

synchronization during which pendulum 2 rotates in different direction than the excited pendulum 1 occur.

The time series showing the transient behavior of pendula's angular velocities  $\dot{\varphi}_1, \dot{\varphi}_2$ , the difference of pendula's displacement  $\varphi_2 - \varphi_1$  and beam's displacement  $x$  (magnified 100 times) are shown in Figure 39(a,b). At  $N=50$  the excitation of pendulum 2 is switched off. In the case of Figure 39(a) ( $k_x=7000, m_b=12$ ) after the short interval of the lack of synchronization the pendula became synchronized again but the phase shift between the pendula is larger than zero (phase synchronization with the phase shift equal to  $0.4\pi$ ). In the second case ( $k_x=12000, m_b=12$ ), when the excitation of pendulum 2 is switched off it stops to rotate. Pendulum 2 starts to oscillate as the result of the beam's oscillations  $x$  (see the fluctuations of the angular velocity  $\dot{\varphi}_2$ ). The difference of the angular displacements of the pendula  $\varphi_2 - \varphi_1$  grows to infinity.

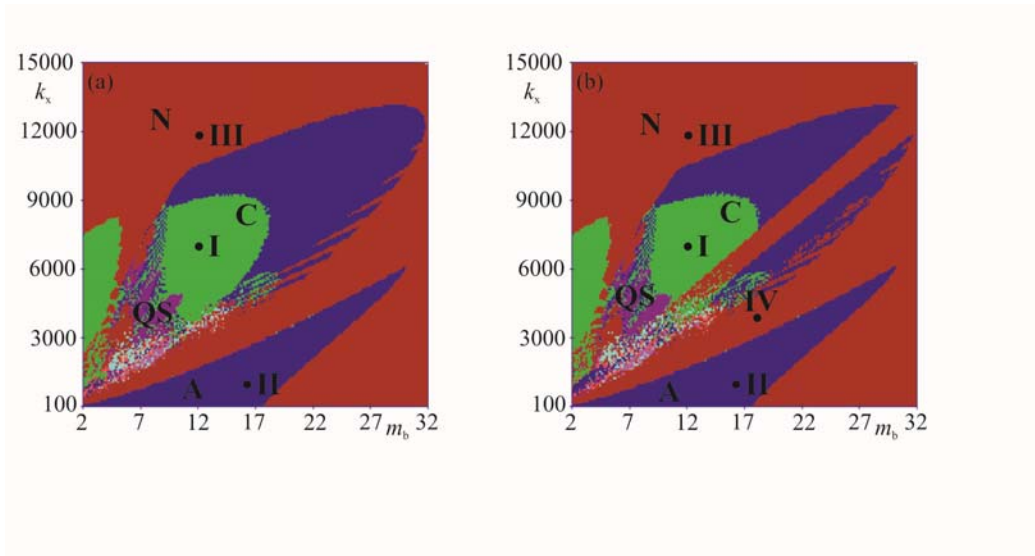


Figure 37. Synchronous states of the system of two identical pendula (the excitation of pendulum 2 is switched off after time  $60N$ ):  $p_{01}=5.0, p_{11}=0.2, p_{02}=0, p_{12}=0$  (the regions in parameters  $k_x - m_b$  space of synchronous pendula's rotation are shown in green, navy blue and violet and the region in which pendulum 2 stops in red colors). (a)  $\varphi_{10}=0, \varphi_{20}=0.5\pi, \dot{\varphi}_{10} = \dot{\varphi}_{20} = 25, x_0 = \dot{x}_0 = 0$ , (b)  $\varphi_{10}=0, \varphi_{20}=0.5\pi, \dot{\varphi}_{10} = 25, \dot{\varphi}_{20} = -25, x_0 = \dot{x}_0 = 0$ .

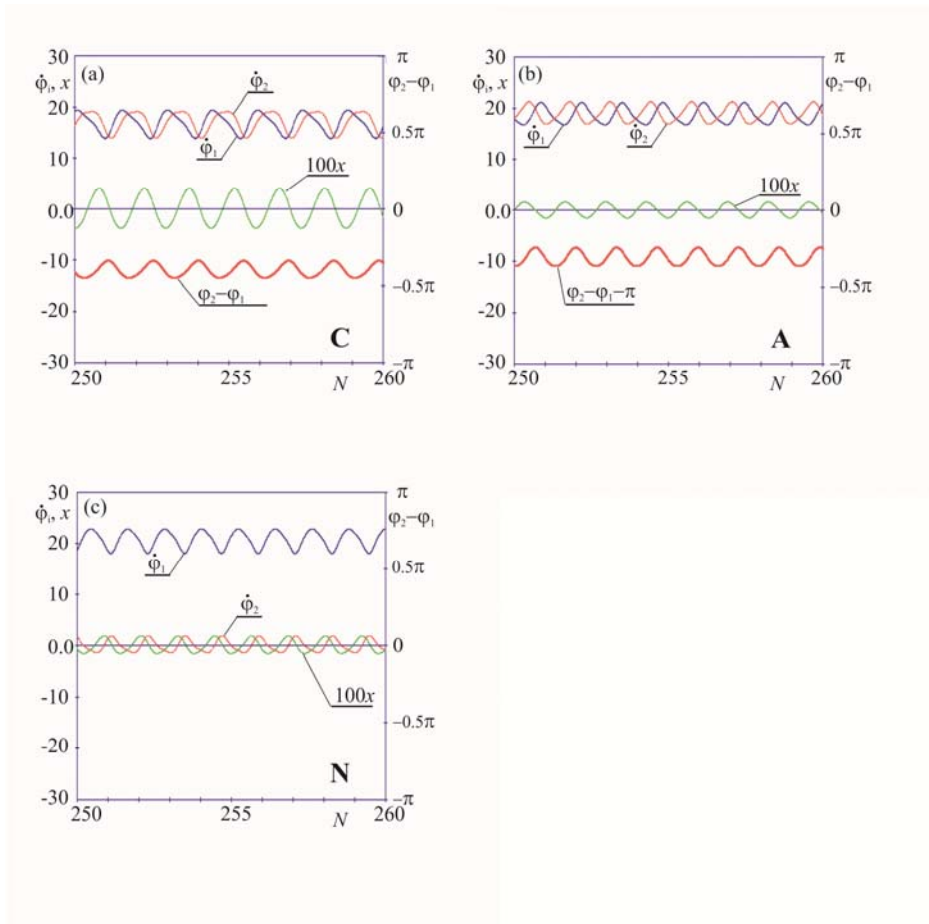


Figure 38. Time series of pendula's displacements  $\varphi_1, \varphi_2$ , angular velocities  $\dot{\varphi}_1, \dot{\varphi}_2$  and beam's displacement  $x$  (magnified 100 times):  $p_{01}=5.0, p_{11}=0.2, p_{02}=0, p_{12}=0, \varphi_{10}=0, \varphi_{20}=0.5\pi, \dot{\varphi}_{10} = \dot{\varphi}_{20} = 25, x_0 = \dot{x}_0 = 0$ , (the excitation of pendulum 2 is switched off after the time  $60N$ ), (a) phase synchronization with phase shifts between pendula equal to  $\pi/4$  (initially complete synchronization)  $k_x=7000.0, m_b=12.0$ , (b) phase synchronization with phase shifts between pendula equal to  $\pi/2$  (initially antiphase synchronization)  $k_x=1000.0, m_b=16.0$ , (c) pendulum 2 stops  $k_x=12000.0, m_b=12.0$ .

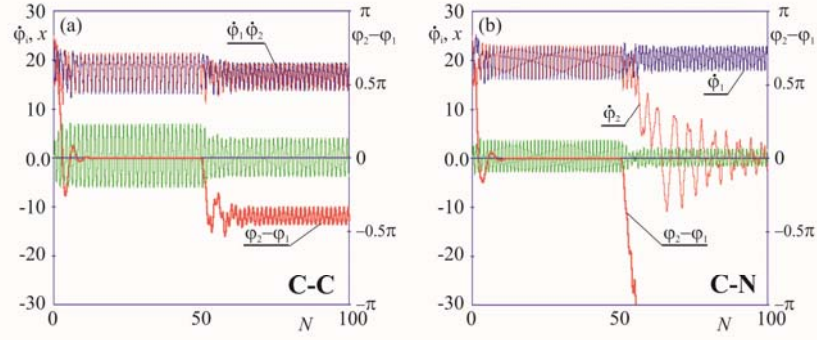


Figure 39. Time series showing the transient behavior of pendula's angular velocities  $\dot{\varphi}_1, \dot{\varphi}_2$ , the difference of pendula's displacement  $\varphi_2 - \varphi_1$  and beam's displacement  $x$  (magnified 100 times) in the case when the excitation of pendulum 2 is switched off at  $N=50$ :  $p_{01}=5.0$ ,  $p_{11}=0.2, p_{02}=5.0, p_{12}=0.2, p_{21}=p_{22}=0, \varphi_{10} = 0, \varphi_{20} = \frac{\pi}{2}, \dot{\varphi}_{10} = 0, \dot{\varphi}_{20} = 25, x_0 = \dot{x}_0 = 0$ , (a)  $k_x=7000.0, m_b=12.0$ , (b)  $k_x=12000.0, m_b=12.0$ .

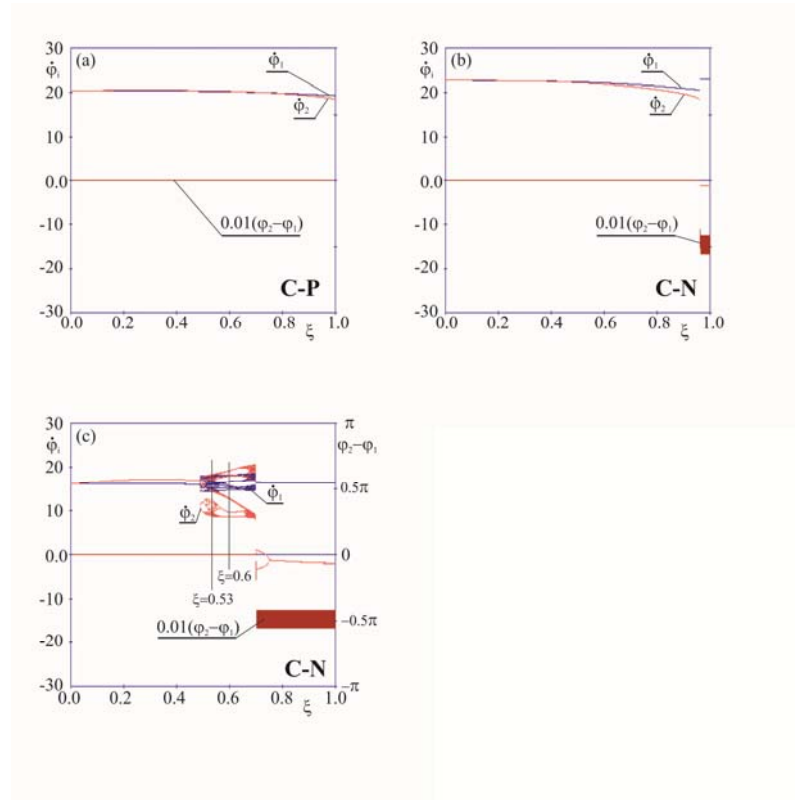


Figure 40. Bifurcation diagrams of pendula's angular velocities  $\dot{\phi}_1, \dot{\phi}_2$  and the difference of pendula's displacement  $\varphi_2 - \varphi_1$  versus parameter  $\xi$ , excitation of pendulum 2 gradually decays to zero, i.e.,  $(1-\xi)(p_{02} - \dot{\varphi}_2 p_{12})$ , (a)  $k_x=7000.0, m_b=12.0, \varphi_{10} = 0, \varphi_{20} = \frac{\pi}{2}, \dot{\varphi}_{10} = 0, \dot{\varphi}_{20} = 25, x_0 = \dot{x}_0 = 0$ , (b)  $k_x=12000.0, m_b=12.0, \varphi_{10} = 0, \varphi_{20} = \frac{\pi}{2}, \dot{\varphi}_{10} = 0, \dot{\varphi}_{20} = 25, x_0 = \dot{x}_0 = 0$ , (c)  $k_x=3700.0, m_b=18.0, \varphi_{10} = 0, \varphi_{20} = \frac{\pi}{2}, \dot{\varphi}_{10} = 0, \dot{\varphi}_{20} = 25, x_0 = \dot{x}_0 = 0$ .

Now let us consider the case when the excitation of pendulum 2 gradually decays to zero. The excitation decay can be described as  $(1-\xi)(p_{02} - \dot{\varphi}_2 p_{12})$ , where  $\xi$  ( $\xi \in [0,1]$ ) is a control parameter. The bifurcation diagrams shown in Figure 40(a,b) present the values of the pendula's angular velocities  $\dot{\phi}_1, \dot{\phi}_2$  (at the moments when pendulum 1 moves through the lower equilibrium position) and the difference of pendula's displacement  $\varphi_2 - \varphi_1$  versus parameter  $\xi$ . In the case of Figure 40(a) ( $k_x=7000.0, m_b=12.0$ , both pendula are in the state of complete synchronization) synchronization is preserved up to the value  $\xi=0.85$ . The phase shift between pendula is visible for larger values of  $\xi$  (complete synchronization is replaced by phase synchronization. In the whole interval of  $\xi$  pendulum 1 transfers enough energy to pendulum 2 to ensure the pendula's synchronization. The difference of the pendula's displacements  $\varphi_2 - \varphi_1$  is so small that it is not visible (in the scale of Figure 40(a)). Figure 40(b) presents bifurcation diagram for  $k_x=12000.0$  and  $m_b=12.0$ . In this case the phase synchronization is observed for  $\xi < 0.95$ . At this point pendulum 2 stops to rotate (pendulum 1 is unable to transfer enough energy to keep it rotating) and one observes the increase of the difference  $\varphi_2 - \varphi_1$ . The case of  $k_x=3700$  and  $m_b=18$  (point **IV** in Figure 36(b) and Figure 37(b) located close to the area of the coexistence of different synchronous configurations) is illustrated in Figure 40(c). In the interval  $0.0 < \xi < 0.49$  one observes periodic rotations of the



synchronized pendula (with the phase shift larger than zero). For larger values of  $\xi$  ( $0.49 < \xi < 0.70$ ) pendula perform periodic synchronous rotations with higher periods or quasiperiodic synchronous rotations. Further increase of  $\xi < 0.70$  stops pendulum 2.

*Example 2. Two pendula rotating in different directions*

Let us consider the same system as in Example 1 but assume that pendula rotate in different directions. We consider system (1-2) with the following parameter values:  $m_1=m_2=1.00$ ,  $l_1=l_2=0.25$ ,  $c_{\varphi_1}=c_{\varphi_2}=0.03$ . The excitation parameters of pendulum 1 are equal to  $p_{01}=5.0$ ,  $p_{11}=0.2$ . In the initial state it has been assumed that  $p_{02}=-5.0$ ,  $p_{12}=0.2$ , i.e., pendulum 1 rotates counterclockwise and pendulum 2 rotates clockwise. Later the parameters of pendulum 2:  $p_{02}$  and  $p_{12}$  are taken as control parameters.

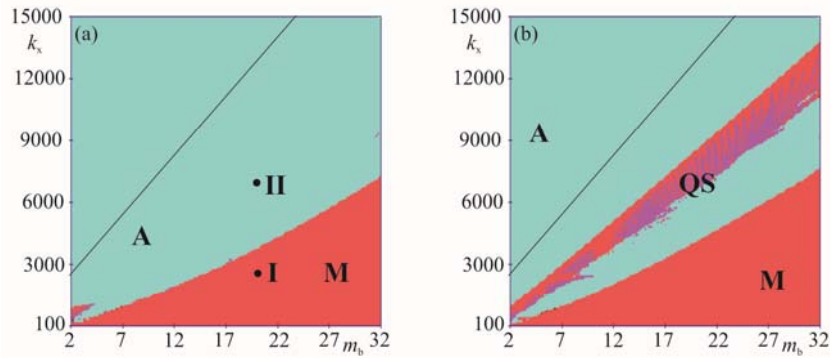


Figure 41. The regions the parameters space  $k_x - m_b$  of mirror  $M$  (light red), antiphase  $A$  (blue), quasiperiodic  $Q$  (violet) synchronizations for the system of two identical and identically driven pendula rotating in different directions:  $p_{01}=5.0$ ,  $p_{11}=0.2$ ,  $p_{02}=-5.0$ ,  $p_{12}=0.2$ , (a)  $\varphi_{10}=0$ ,  $\varphi_{20}=0.5\pi$ ,  $\dot{\varphi}_{10} = \dot{\varphi}_{20} = 25$ ,  $x_0 = \dot{x}_0 = 0$ , (b)  $\varphi_{10}=0$ ,  $\varphi_{20}=0.5\pi$ ,  $\dot{\varphi}_{10} = 25$ ,  $\dot{\varphi}_{20} = -25$ ,  $x_0 = \dot{x}_0 = 0$ .

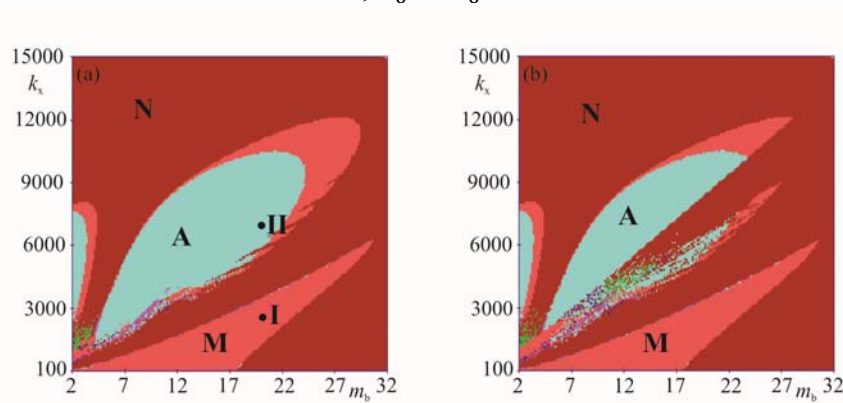


Figure 42. Synchronous states of the system of two identical pendula rotating in different directions (the excitation of pendulum 2 is switched off after the time  $60N$ ):  $p_{01}=5.0$ ,  $p_{11}=0.2$ ,  $p_{02}=0$ ,  $p_{12}=0$  (the regions in the parameters  $k_x - m_b$  space of synchronous pendula's rotation are shown in light red, blue and violet and the region in which pendulum 2 stops in red colors). (a)  $\varphi_{10}=0$ ,  $\varphi_{20}=0.5\pi$ ,  $\dot{\varphi}_{10} = \dot{\varphi}_{20} = 25$ ,  $x_0 = \dot{x}_0 = 0$ , (b)  $\varphi_{10}=0$ ,  $\varphi_{20}=0.5\pi$ ,  $\dot{\varphi}_{10} = 25$ ,  $\dot{\varphi}_{20} = -25$ ,  $x_0 = \dot{x}_0 = 0$ .



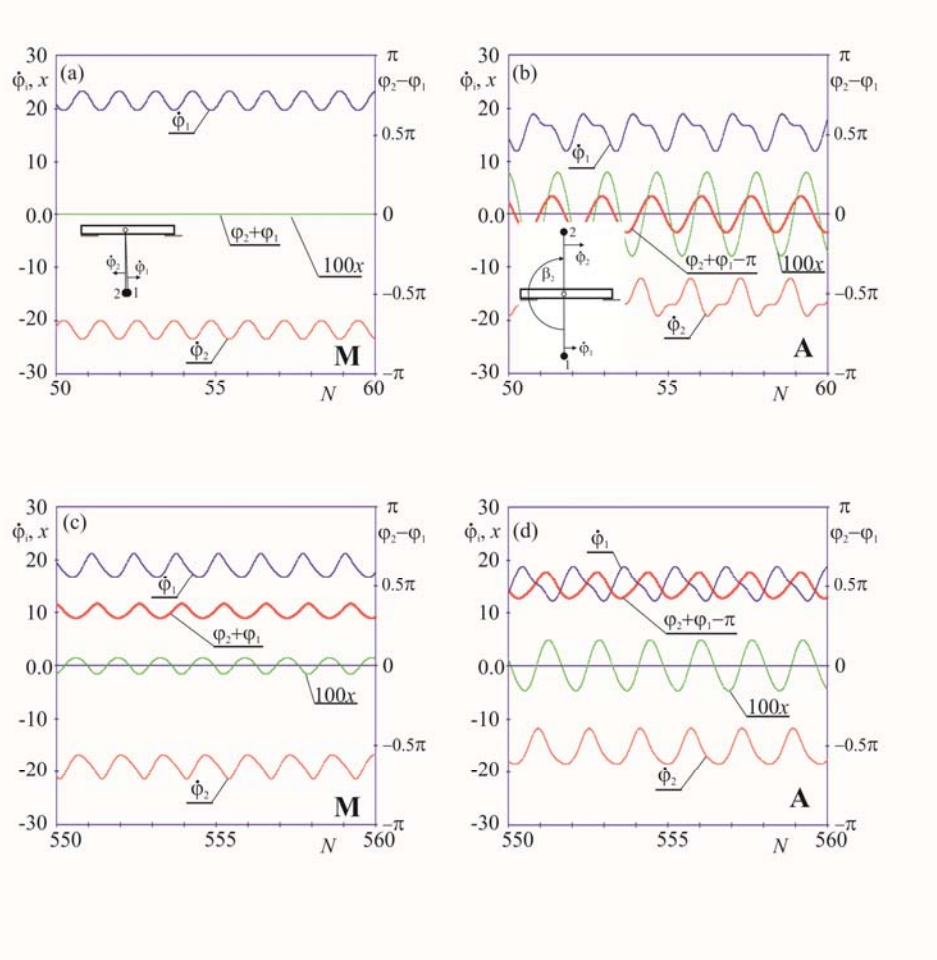


Figure 43. Time series of pendula's displacements  $\varphi_1, \varphi_2$ , angular velocities  $\dot{\varphi}_1, \dot{\varphi}_2$  and beam's displacement  $x$  (magnified 100 times) for the system of two pendula rotating in different directions;  $\varphi_{10}=0, \varphi_{20}=0.5\pi, \dot{\varphi}_{10} = \dot{\varphi}_{20} = 25, x_0 = \dot{x}_0 = 0$ , (a) mirror synchronization, both pendula excited:  $k_x=2000.0, m_b=20.0, p_{01}=5.0$ , (b) antiphase synchronization, both pendula excited:  $k_x=2000.0, m_b=20.0, p_{01}=5.0, p_{11}=0.2, p_{02}=-5.0, p_{12}=0.2$ , (c) initially mirror synchronization, at  $N=60$  the excitation of pendulum 2 switched off:  $k_x=2000.0, m_b=20.0, p_{01}=5.0, p_{11}=0.2, p_{02}=0.0, p_{12}=0.0$ , (d) initially antiphase synchronization, at  $n=60$  the excitation of pendulum 2 is switched off :  $k_x=2000.0, m_b=20.0, p_{01}=5.0, p_{11}=0.2, p_{02}=0.0, p_{12}=0.0$ .

To investigate the effect of sudden excitation switch off in one of the synchronized pendula we assume that system (1,2) of two identical and identically driven pendula is in the synchronized state and the excitation of pendulum 2 is suddenly switched off. The results of our calculations are shown in Figure 41(a,b), 42(a,b) and 43(a-d). For given values of  $k_x$  and  $m_b$  the pendula are in the synchronized state described in Figure 41(a,b) when the excitation of pendulum 2 is switched off. The calculations have been performed for  $p_{01}=5.0, p_{11}=0.2, p_{02}=-5.0, p_{12}=0.2$  and initial conditions  $\varphi_{10}=0, \varphi_{20}=0.5\pi, \dot{\varphi}_{10} = 25, \dot{\varphi}_{20} = -25, x_0 = \dot{x}_0 = 0$ , i.e., pendulum 2 initially rotate in different directions (Figure 41(b)). The regions of mirror *M*, antiphase *A*, quasiperiodic (*QS*) synchronizations are indicated respectively in light red, blue and violet colors. Notice the navy blue – violet band in the vicinity of the diagonal in Figure 41(b). In this region the antiphase synchronization (see Figure 41(a)) coexists with either mirror or quasiperiodic synchronization. After the sudden breakdown of pendulum 2 excitation

synchronization is not lost in the regions indicated in light red, blue (phase synchronization) and violet (quasiperiodic synchronization) colors shown in Figure 42(a,b). In the light red and blue regions respectively mirror and antiphase synchronization is replaced by the phase synchronization with various phase shifts between pendula. In region ( $N$ ) indicated in red color the synchronization is lost. Pendulum 3 slows down and finally stops. In Figure 43(a,c) we show the time series of pendula's angular velocities  $\dot{\varphi}_1, \dot{\varphi}_2$  for  $k_x=2000.0, m_b=20.0$  (point **I** in Figure 41(a)). In the case of Figure 43(a) both pendula are excited and reach the state of mirror synchronization ( $M$ ) is replaced by the phase synchronization with the phase shift between pendula equal to  $\pi/4$  as shown in Figure 43(c). The time series for  $k_x=7000.0$  i  $m_b=20.0$  (point **II**) is shown in Figure 43(b,d). In this case initially antiphase synchronization ( $A$ ) (Figure 43(b)) is replaced by the phase synchronization with the phase shift between pendula equal to  $\pi/2$  as shown in Figure 43(d). In both cases pendulum 1 transfers sufficient amount of energy to keep pendulum 2 rotating. The phase shifts between pendula different from original 0 and  $\pi$  can be taken as indicators of the excitation switch off. In region ( $N$ ) indicated in red color the synchronization is lost. Pendulum 2 slows down and finally stops.

### *Example 3. Three pendula rotating in the same direction*

In this section we reconsider system (1,2) consisting of three identical pendula rotating in the same direction. The presented results have been obtained from the numerical integration of equations of motion (1,2). In this example we consider the system (1-2) with the following parameter values:  $m_1=m_2=m_3=1.00, l_1=l_2=l_3=0.25, c_{\varphi_1}=c_{\varphi_2}=c_{\varphi_3}=0.03$ . We consider different values of the mass of the beam  $m_b$  and the stiffness coefficient  $k_x$ . The damping coefficient  $c_x$  has been selected in such a way as to be equivalent to the arbitrarily selected logarithmic decrement of damping  $\Delta=\ln(1.5)$  (the decrement characteristic for the linear oscillator with mass equal to the total mass of the system ( $m_b+nm$ ) mounted to the spring with the stiffness coefficient  $k_x$ ). The excitation parameters of pendulum 1 are equal to  $p_{01}=p_{02}=5.0, p_{11}=p_{12}=0.2$ . The excitation parameters of pendulum 3 are initially the same but after  $N=50$  the excitation is switched off, i.e.,  $p_{03}=0, p_{13}=0.2$ .

To investigate the effect of sudden excitation switch off in one of the synchronized pendula we assume that system (1,2) of three identical and identically driven pendula is in the synchronized state and the excitation of pendulum 3 is suddenly switched off. The results of our calculations are shown in Figure 44(a,b), and 45(a-b). Figure 44(a) shows the dependence of the synchronous configuration on the parameters  $k_x$  and  $m_b$ . One observes complete (green region), Yankee (navy blue region) and quasiperiodic (violet region) synchronous states (all pendula are excited). Additionally the synchronization is not observed for  $k_x$  and  $m_b$  from the red region. Then for given values of  $k_x$  and  $m_b$  the pendula are in the synchronized state described in Figure 44(a) when the excitation of pendulum 3 is switched off. After the sudden switch off of pendulum 3 excitation synchronization is not lost in the regions indicated in Figure 44(b) in green, navy blue (phase synchronization), blue (synchronous state in which pendula 1 and 2 create cluster which is in antiphase to nonexcited pendulum 3) and violet (quasiperiodic synchronization) colors. In the green and navy blue regions respectively complete and Yankee synchronization is replaced by the phase synchronization with various phase shifts between pendula. In region ( $N$ ) indicated in red color the synchronization is lost. Pendulum 3 slows down and finally stops.

The time series showing the transient behavior of pendula's angular velocities  $\dot{\varphi}_1, \dot{\varphi}_2, \dot{\varphi}_3$ , the differences of pendula's displacements  $\varphi_2 - \varphi_1, \varphi_3 - \varphi_1$  and beam's displacement  $x$  (magnified 100 times) are shown in Figure 45(a,b). At  $N=50$  the excitation of

pendulum 3 is switched off. In the case of Figure 45(a) ( $k_x=12000$ ,  $m_b=26$ , point **I** in Figure 44(a)) after the short interval of the lack of synchronization the pendula became synchronized again but the phase shift between the pendula is larger than zero (phase synchronization with the phase shift equal to  $0.3\pi$ ). In the second case ( $k_x=2000$ ,  $m_b=26$ , point **II**) shown in Figure 45(b), when the excitation of pendulum 3 is switched off it stops to rotate. Pendulum 3 starts to oscillate as the result of the beam's oscillations  $x$  (see the fluctuations of the angular velocity  $\dot{\varphi}_3$ ). The difference of angular displacements of the pendula  $\varphi_3 - \varphi_1$  grows to infinity.

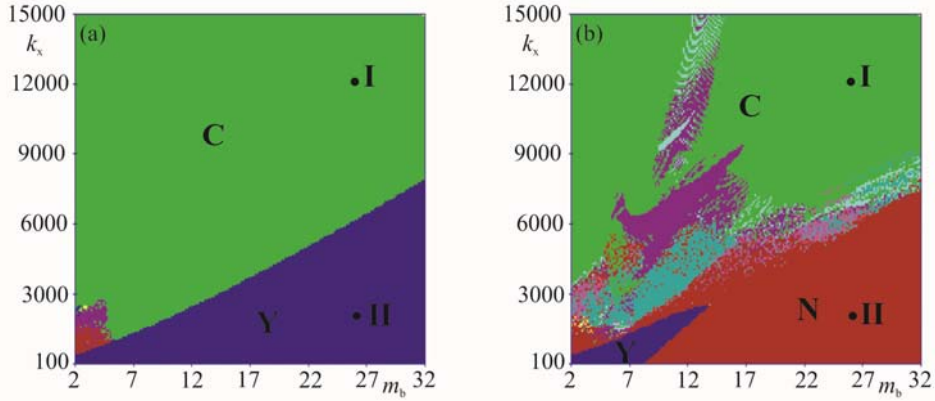


Figure 44. Synchronous states in  $k_x - m_b$  parameter space of three pendula rotating in the same direction:  $p_{01}=5.0$ ,  $p_{11}=0.2$ ,  $p_{02}=5.0$ ,  $p_{12}=0.2$ ,  $p_{03}=p_{13}=0$ ,  $\varphi_{10} = 0$ ,  $\varphi_{20} = \frac{\pi}{2}$ ,  $\varphi_{30} = \pi$ ,  $\dot{\varphi}_{10} = 0$ ,  $\dot{\varphi}_{20} = \dot{\varphi}_3 = 25$ ,  $x_0 = \dot{x}_0 = 0$ , (a) all pendula excited, (b) pendulum 3 switched off at  $N=50$ .

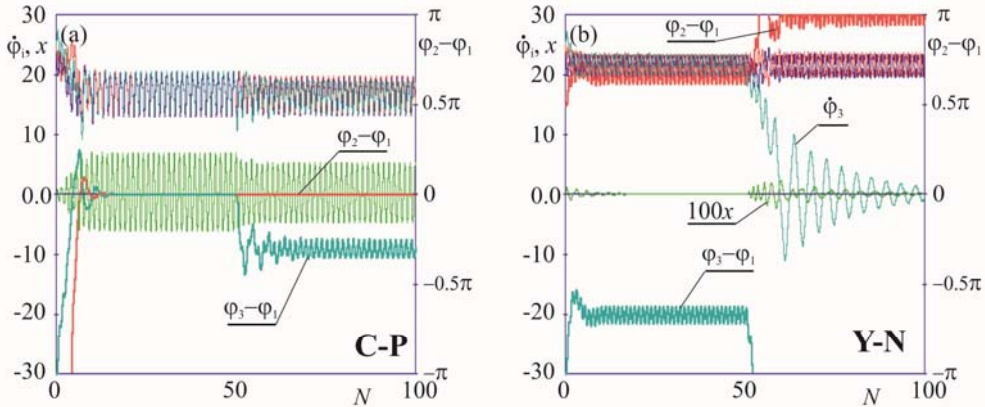


Figure 45. Time series showing the transient behavior of pendula's angular velocities  $\dot{\varphi}_1$ ,  $\dot{\varphi}_2$ ,  $\dot{\varphi}_3$ , the difference of pendula's displacement  $\varphi_2 - \varphi_1$ ,  $\varphi_3 - \varphi_1$  and beam's displacement  $x$  (magnified 100 times) in the case when the excitation of pendulum 3 is switched off at  $N=50$ :  $p_{01}=5.0$ ,  $p_{11}=0.2$ ,  $p_{02}=5.0$ ,  $p_{12}=0.2$ ,  $p_{03}=p_{13}=0$ ,  $\varphi_{10} = 0$ ,  $\varphi_{20} = \frac{\pi}{2}$ ,  $\varphi_{30} = \pi$ ,  $\dot{\varphi}_{10} = 0$ ,  $\dot{\varphi}_{20} = \dot{\varphi}_3 = 25$ ,  $x_0 = \dot{x}_0 = 0$ , (a)  $k_x=12000.0$ ,  $m_b=26.0$  (**I**), (b)  $k_x=2000.0$ ,  $m_b=26.0$  (**II**).

*Example 4. Two pendula with different masses rotating in the same direction*

In this example we consider the case of two pendula with different masses rotating in the same direction. Pendulum 1 has mass  $(1+\eta)m$  and pendulum 2 mass  $(1-\eta)m$ , where  $\eta$  is constant. Damping coefficients  $c_\varphi$  and excitation torques  $p_{0i} - p_{1i}\dot{\varphi}_i$  are proportional to the pendula's masses. In this case equations of motion can be rewritten in the following form:

$$\begin{aligned} (1+\eta)(ml^2\ddot{\varphi}_1 + ml\dot{x}\cos\varphi_1 + c_\varphi\dot{\varphi}_1 + mgl\sin\varphi_1) &= (1+\eta)(p_{01} - p_{11}\dot{\varphi}_1), \\ (1-\eta)(ml^2\ddot{\varphi}_2 + ml\dot{x}\cos\varphi_2 + c_\varphi\dot{\varphi}_2 + mgl\sin\varphi_2) &= (1-\eta)(p_{02} - p_{12}\dot{\varphi}_2), \end{aligned} \quad (35)$$

$$\begin{aligned} (m_b + nm)\ddot{x} + c_x\dot{x} + k_x x &= \\ = ml(1+\eta)(-\ddot{\varphi}_1\cos\varphi_1 + \dot{\varphi}_1^2\sin\varphi_1) + ml(1-\eta)(-\ddot{\varphi}_2\cos\varphi_2 + \dot{\varphi}_2^2\sin\varphi_2). \end{aligned} \quad (36)$$

In our numerical calculations we consider the following parameter's values:  $l=0.25$ ,  $m=1.0$ ,  $c_\varphi=0.03$ ,  $p_{01}=5.0$ ,  $p_{11}=0.2$ ,  $p_{02}=5.0$ ,  $p_{12}=0.2$ .

Figure 46(a,b) shows the dependence of the synchronous configuration on the parameters  $k_x$  and  $m_b$ . The calculations have been performed for initial conditions  $\varphi_{10} = 0$ ,  $\varphi_{20} = 0$ ,  $\dot{\varphi}_{10} = 25$ ,  $\dot{\varphi}_{20} = 25$ ,  $x_0 = \dot{x}_0 = 0$ , (compare with Figure 36(a) and 37(a) calculated for  $\eta=0$ ). The regions of complete (C), antiphase (A), quasiperiodic (QS) synchronizations are indicated respectively in green, navy blue and violet colors. Figure 46(a) illustrates the case of  $\eta=0.9$  ( $m_1=1.9$ ,  $m_2=0.1$ ). After the initial time  $50N$  the excitation of pendulum 2 is switched off. For  $k_x$  and  $m_b$  in the green region the synchronization is preserved but the complete synchronization (phase shift between pendula equal to zero) is replaced by phase synchronization (phase shift larger than zero). For the wide range  $k_x$  and  $m_b$  parameters the rotation of both pendula is preserved. Contrary to this for  $\eta=-0.1$ , i.e.,  $m_1=0.9$  and  $m_2=1.1$  the set parameters for which both pendula rotate is very small as shown in Figure 46(b) (green region). Notice that in this case the excitation of the heavier pendulum has been switched off. With the further increase of pendulum 2 mass we observe the loss of synchronization and the unexcited pendulum stops. Figure 47(a,b) shows time series of the transient behavior of pendula's angular velocities  $\dot{\varphi}_1, \dot{\varphi}_2$ , the difference of pendula's displacement  $\varphi_2 - \varphi_1$  and beam's displacement  $x$  (magnified 100 times) in the case when the excitation of pendulum 2 is switched off. The case of  $\eta=0.9$  ( $m_1=1.9$ ,  $m_2=0.1$ ) and  $m_b=12.0$ ,  $k_x=7000$  (point I in Figure 46(a)) is illustrated in Figure 47(a). Both pendula are in the state of complete synchronization when at time  $20N$  the excitation of pendulum 2 is switched off. After the transient time the system reaches the state of phase synchronization with nonzero phase shift between pendula. Notice that this phase shift is smaller than in the case of identical pendula (Figure 39(a)). Figure 47(b) shows the case for  $\eta=-0.15$ , i.e.,  $m_1=0.85$  and  $m_2=1.15$ . At time  $20N$  the excitation of pendulum 2 is switched off. Synchronization and rotation of both pendula are preserved but the phase shift  $\varphi_2 - \varphi_1$  increases to the value larger than  $\pi/2$ . Further decrease of  $\eta$ , (down to  $\eta=-0.17$ , i.e.,  $m_1=0.83$  and  $m_2=1.17$ ) leads to the loss of synchronization and pendulum 2 stops.

*Example 5. Larger number of pendula*

In the state of complete synchronization the forces with which pendula act on the beam are algebraically added so this example can be generalized to the case of any number of pendula of total mass equal to  $2m$ . Consider the case of  $n$  pendula in the state of complete synchronization. The effect of the switch off of the excitation of  $p$  pendula is the same as the effect of switch off of the excitation of pendulum with mass  $2mp/n$  in the system of two

pendula (the second one with mass  $2m(n-p)/n$ ). As an example consider the system of 20 identical pendula rotating in the same direction with masses ( $m_{1-20}=0.1, m_b=12.0, k_x=7000$ ) shown in Figure 48(a-d). All pendula are in the state of complete synchronization when at time  $50N$  the excitation of one (Figure 48(a)), ten (Figure 48(b)), eleven (Figure 48(c)) and twelve (Figure 48(d)) pendula is switched off. Up to the case of 11 pendula the initial complete synchronization is replaced by the phase synchronization and all pendula rotate. The phase shift between the clusters of excited and unexcited pendula increases with the increase of the number of unexcited pendula. When the excitation of the 12-th pendulum is switched off the synchronization is lost and all unexcited pendula stop to rotate.

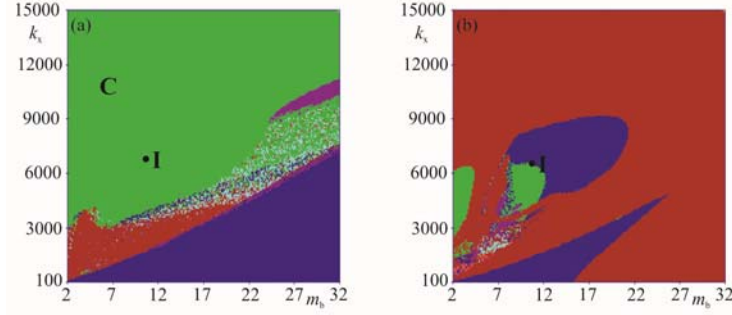


Figure 46. The regions of the parameters  $k_x - m_b$  space of complete ( $C$ ) (green), antiphase ( $A$ ) (navy blue), quasiperiodic ( $QS$ ) (violet) synchronizations for the system of two pendula with different masses rotating in the same direction;  $l=0.25, m=1.0, c_\varphi=0.03, p_{01}=5.0, p_{11}=0.2, p_{02}=5.0, p_{12}=0.2, \varphi_{10}=0, \varphi_{20}=0, \dot{\varphi}_{10}=25, \dot{\varphi}_{20}=25, x_0=\dot{x}_0=0$ , (a)  $\eta=0.9$ , i.e.,  $m_1=1.9$  and  $m_2=0.1$ , after the initial time equal to  $50N$ , excitation of pendulum 2 is switched off, (b)  $\eta=-0.1$ , i.e.,  $m_1=0.9$  and  $m_2=1.1$ , after the initial time equal to  $50N$ , excitation of pendulum 2 is switched off.

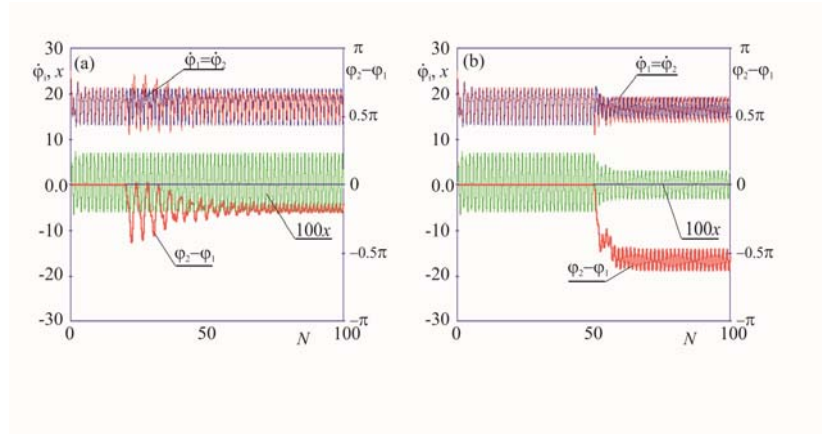


Figure 47. Time series showing the transient behavior of pendula's angular velocities  $\dot{\varphi}_1, \dot{\varphi}_2$ , the difference of pendula's displacement  $\varphi_2 - \varphi_1$  and beam's displacement  $x$  (magnified 100 times) in the case when the excitation of pendulum 2 is switched off:  $p_{01}=5.0, p_{11}=0.2, p_{02}=5.0, p_{12}=0.2, p_{21}=p_{22}=0, \varphi_{10}=0, \varphi_{20}=0, \dot{\varphi}_{10}=25, \dot{\varphi}_{20}=25, x_0=\dot{x}_0=0, k_x=7000.0, m_b=12.0$ , (a)  $\eta=0.9$  ( $m_1=1.9, m_2=0.1$ ) the excitation of pendulum 2 switched off at  $20N$ , (b)  $\eta=-0.15$  ( $m_1=0.85, m_2=1.15$ ) the excitation of pendulum 2 switched off at  $50N$ .

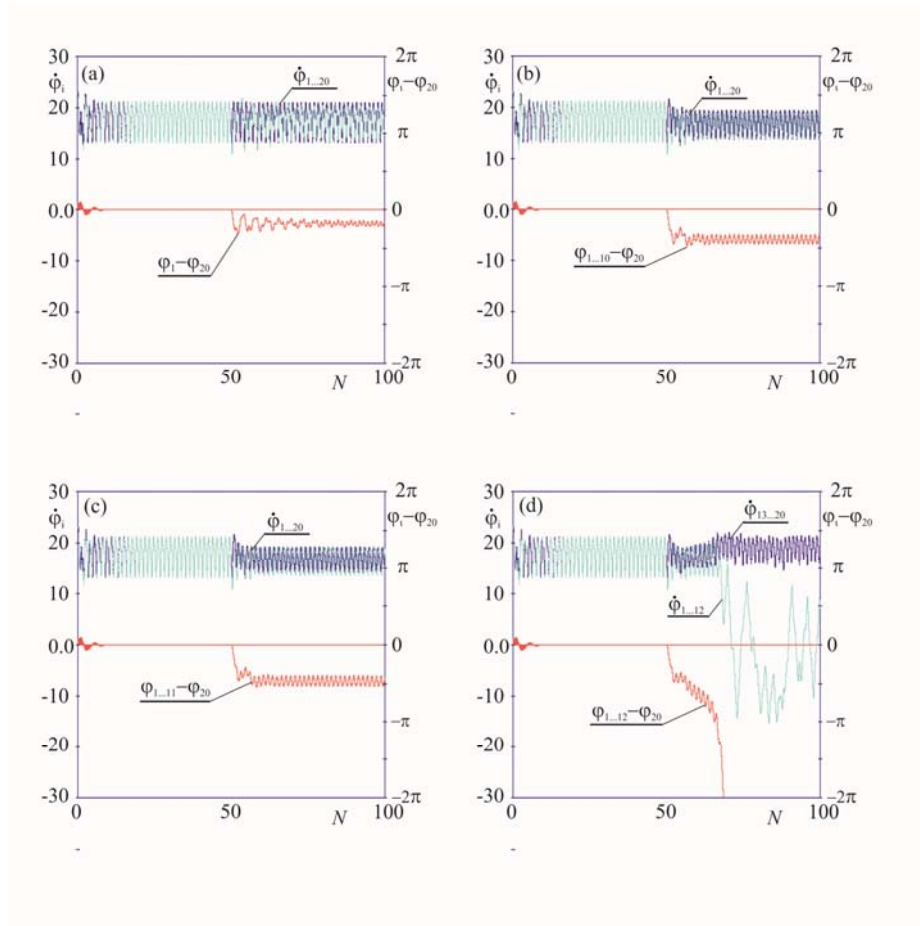


Figure 48. Time series showing the transient behavior of pendula's angular velocities  $\dot{\phi}_1, \dots, \dot{\phi}_{20}$ , the difference of pendula's displacement  $\phi_{1,\dots,19} - \phi_{20}$  and beam's displacement  $x$  (magnified 100 times) in the case when the excitation of a number of pendula is switched off for the system of 20 identical pendula with mass  $m=0.1$  rotating in the same direction,  $m_b = 12.0$ ,  $k_x = 7000$ ,  $\phi_{10,\dots,200} = 0$ ,  $\dot{\phi}_{10,\dots,200} = 25$ ,  $x_0 = \dot{x}_0 = 0$ . After time equal to 50N, excitation of some pendula is simultaneously switched off, (a) excitation of pendulum 1 is switched off, (b) excitation of ten pendula 1, ..., 10 is switched off, (c) excitation of eleven pendula 1, ..., 11 is switched off, (d) excitation of twelve pendula 1, ..., 12 is switched off.



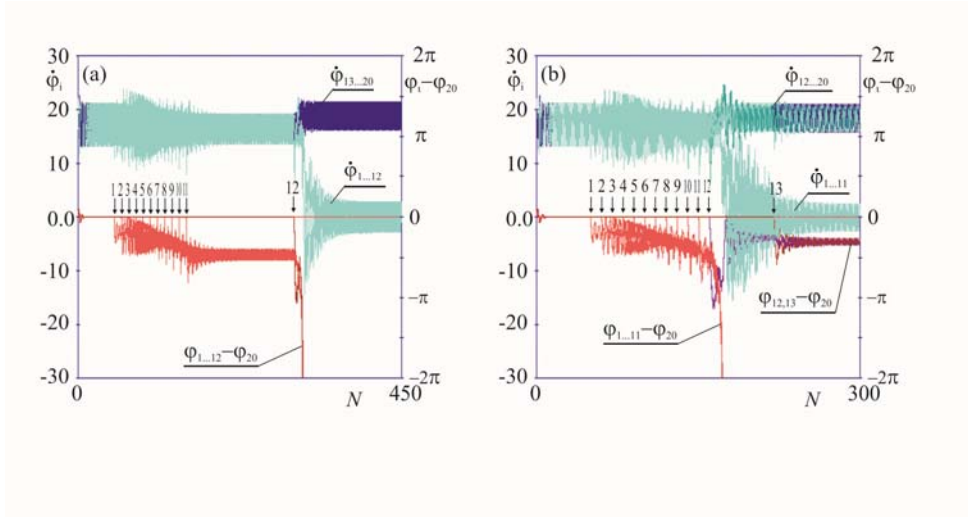


Figure 49. Time series showing the transient behavior of pendula's angular velocities  $\dot{\varphi}_1, \dots, \dot{\varphi}_{20}$ , the difference of pendula's displacement  $\varphi_{1,\dots,19} - \varphi_{20}$  in the case when the excitation of a number of pendula is switched off for the system of 20 identical pendula with mass  $m=0.1$  rotating in the same direction,  $m_b=12.0$ ,  $k_x=7000$ ,  $\varphi_{10,\dots,200} = 0$ ,  $\dot{\varphi}_{10,\dots,200} = 25$ ,  $x_0 = \dot{x}_0 = 0$ . At the moments indicated by the arrows the excitation of a number of pendula is switched off, (a) excitation of 11 pendula is switched off at  $N=50, 60, \dots, 150$ , excitation of the 12-th pendulum is switched off at  $N=300$ , (b) excitation of 12 pendula are switched off for  $N=50, 60, \dots, 150, 160$ , excitation of the 13-th pendulum is switched off for  $N=220$ .

In the considered examples a number of pendula losses excitation simultaneously, if the pendula's excitation is switched off one by the scenario can be different. In the case described in Figure 49(a,b) ( $m_{1-20}=0.1$ ,  $m_b=12.0$ ,  $k_x=7000$ ) the excitation is switched off at the moments indicated by arrows. In Figure 49(a) eleven pendula are losing excitations in the time intervals of  $10N$  starting at  $50N$ . The increase of the phase shift between the clusters of excited and unexcited pendula is visible. For  $N=300$  the excitation of the 12-th pendulum is switched off leading to the loss of synchronization (12 pendula stop to rotate). Different scenario is described in Figure 49(b). The 12-th pendulum loses excitation just after 11-th at  $N=160$ . Shortly after it 11 pendula (which lost excitation before) stop to rotate but the 12-th pendulum still rotates and is phase synchronized with the cluster of 8 excited pendula (the phase shift is close to  $\pi/4$ ). Later at  $N=220$  the 13-th pendulum loses excitation and two clusters of 7 excited and 2 unexcited are created.

The considered example shows that it is possible to estimate the critical number of pendula which excitation can be switched off and the rotation of all of them is preserved. In the case when the pendula's excitations are switched off non-simultaneously it is possible to observe the case in which unexcited pendula form two groups one of them stops to rotate and the second one rotates and is phase synchronized with the excited pendula.

## 6. Discussion and conclusions

In the system consisting of globally coupled pendula like the system of horizontally or vertically moving beam on which externally excited rotating pendula are mounted (see Figure 3(a,b)) one can observe both complete and phase synchronization of the pendula. Various configurations of phase synchronization are possible. In all cases of phase synchronization, the average phase shifts between the pendula are constant and characteristic for obtained configuration. As a result of constant acceleration and deceleration of the pendula due to the gravity, the instantaneous phase shifts fluctuate around these averages. Similarly to the case of oscillating pendula [17,18,37] we observe the creation of the clusters of completely synchronized pendula. Contrary to the oscillating case the rotating pendula are not grouped in three or five clusters only.

For some intervals of the system parameters we found the co-existence of different stable synchronized states. Such a coexistence has not been reported previously in the context of rotating pendula. This coexistence has not been identified in the previous studies [5], as the small parameter methods used there, do not allow it.

Our approximate analytical studies allow the derivation of the conditions for different types of synchronous states as well as the equation for estimation of the shifts between the phases of the synchronized pendula. This analysis allows to understand the synchronization mechanism based on the energy transfer between the pendula via the oscillating beam. Both results are in good agreement with numerical results.

In the system, in which pendula rotate in opposite directions, one can observe a number of different types of phase synchronization. During the synchronous motion the average (over the period of rotation) value of the sum of angular displacements of pendula rotating to the right and left is constant. The approximate analytical studies of synchronization moments, i.e., moments responsible for energy transfer between pendula, allow prediction of the mirror ( $M$ ), antiphase ( $A$ ) synchronization in the system of  $n=2$  pendula and tree ( $T$ ) and cluster antiphase ( $CA$ ) synchronization in the system of  $n=3$  pendula. These types of synchronization occur for both horizontal (without gravity) and vertical (in the gravitational field) planes of pendula rotation.

Numerical simulations confirm the existence of these types of synchronization. In the system with two pendula they additionally show that due to gravity, at sufficiently large values of the stiffness coefficient of stiffness  $k_x$ , one can observe two modifications of ( $A$ ) type synchronization, namely the first-quarter ( $1Q$ ) and the third-quarter ( $3Q$ ) synchronization. In the system with three pendula we show that the analytically predicted tree ( $T$ ) and cluster antiphase ( $CA$ ) types of synchronization occur independently of the consideration of gravity. For pendula rotation in the gravitational field one can also observe, for sufficiently large values of the stiffness coefficient  $k_x$ , two modifications of ( $T$ ) type, i.e., yankee ( $Y23$ ) and yankee ( $Y32$ ) synchronization and two modifications ( $CA$ ) types: ( $CL$ ) and ( $CR$ ) synchronization.

The types of synchronization which have been observed for the systems with two and three pendula are summarized in Table 3-6.

The types of synchronous configurations identified for the system of two and three pendula can be observed in the systems with larger number of pendula. Contrary to the case of oscillating pendulums [21,22] the rotating pendula are not grouped in three or five clusters only. The lack of this restriction causes that in the system (1,2) depending on initial condition one can observe a great variety of different synchronization configurations. The number of configurations grows with a number of pendulums  $n$ .



The system with identical pendula which rotate with the same (as to the absolute values) angular velocities located on the beam  $m_b$  which can oscillate horizontally (i.e.,  $k_x < \infty$ ) always reaches the state of synchronization. In the case of the non-movable beam  $m_b$  ( $k_x = \infty$ ) when the pendula cannot interact as their velocities have the same absolute values and constant phase differences between pendula are constant and defined by the initial conditions. When the oscillations of the beam  $m_b$  allow the interaction between pendula the process of synchronization is initiated and the phase differences between pendula's rotations tend to some characteristic values, e.g.:  $0, \pi, 2\pi/3$ , etc. (in the case of pendula rotating in the horizontal plane) or oscillate around these values (in the case of pendula rotating in the vertical plane). The lack of synchronization, i.e., a state in which such  $\varphi_2 - \varphi_1$  is not constant or aperiodic (when pendula rotate in horizontal plane) is observed in certain ranges of parameters in the system of pendula with different masses or different excitation torques which rotate with different angular velocities.

It can be shown that the initial synchronous state extends the lifetime of rotational behavior of the coupled pendula in the case when the excitation of one or a few pendula is suddenly (breakdown of energy supply) or gradually (as the effect of aging and fatigue) switched off. We give evidence that for the properly chosen coupling (in our system parameters  $k_x$  and  $m_b$ ) the energy transfer from the excited pendula allows nonexcited pendula to rotate. The initial synchronous configuration is replaced by phase synchronization with different phase shifts between pendula and the rotational velocity of the synchronized pendula is decreased. These two factors can be considered as the indicator of the breakdown of excitation in one or a few pendula.

The synchronization states of the externally excited globally coupled pendula (like systems of Figure 3(a,b)) are robust as they can be observed on the wide intervals of the system parameters. They can be easily observed in experiments [85]. Contrary to this statement synchronous rotating states of the sets of parametrically excited pendula (Figure 3(c)) are stable in the narrow range of control parameters [35,69] and not easily obtained in experimental studies.

Type of synchroniza-tion	Symbol	Average rotational velocity of pendula		Average angle of rotation		Shown on Figure No.	Remarks
		1	2	1	2		
complete	C	$\dot{\varphi}$	$\dot{\varphi}$	$\varphi$	$\varphi$		
antiphase	AS	$\dot{\varphi}$	$\dot{\varphi}$	$\varphi$	$\varphi + \pi$	9(a,b)	(1)
quasiperiodic	QP	$\dot{\varphi}$	$\dot{\varphi}$	$\varphi$	$\varphi + \pi$	35(c,d)	(2)
multiperiodic	MP	$\dot{\varphi}$	$d\dot{\varphi}$	$\varphi$	$d\varphi + \pi$	30(a,c)	(3)

Remarks:

- (1) period 1 motion – period equal to the time of one rotation,
- (2) quasiperiodic motion of the system,
- (3)  $d$  is the rational number, i.e., if  $d=e/f$  in the time of  $f$  rotations of pendulum 1 pendulum 2 rotates  $e$  times.

Table 3. Types of synchronization of  $n=2$  pendula rotating in the same direction.

Type of synchronization	Symbol	Average rotational velocity of pendula			Average angle of rotation			Shown on Figure No.	Remarks
		1	2	3	1	2	3		
complete	C	$\dot{\varphi}$	$\dot{\varphi}$	$\dot{\varphi}$	$\varphi$	$\varphi$	$\varphi$	12(a,b)	
phase	A	$\dot{\varphi}$	$\dot{\varphi}$	$\dot{\varphi}$	$\varphi$	$\varphi + \frac{3}{2}\pi$	$\varphi + \frac{4}{3}\pi$	11(a,b)	
cluster-antiphase	2-1	$\dot{\varphi}$	$\dot{\varphi}$	$\dot{\varphi}$	$\varphi$	$\varphi + \pi$	$\varphi + \pi$	13(a,b)	(1)

Remarks: (1) Cluster may be formed also by pendula 1 and 3, or pendula 1 and 2 – depending on initial conditions.

Table 4. Types of synchronization of  $n=3$  pendula rotating in the same direction.

Type of synchronization	Symbol	Average rotational velocity of pendula		Average angle of rotation		Shown on Figure No.	Remarks
		1	2	1	2		
mirror	M	$\dot{\varphi}$	$-\dot{\varphi}$	$\varphi$	$-\varphi$	19(a,b)	(1)
antiphase	AO	$\dot{\varphi}$	$-\dot{\varphi}$	$\varphi$	$-\varphi - \pi$	19(c,d)	(2)
third-quarter	3Q	$\dot{\varphi}$	$-\dot{\varphi}$	$\varphi$	$-\varphi - \pi$	20(a)	(3)
first-quarter	1Q	$\dot{\varphi}$	$-\dot{\varphi}$	$\varphi$	$-\varphi - \pi$	20(b)	(4)

Remarks:

- (1) pendula are passing each other on the vertical plane,
- (2) pendula are passing each other on the horizontal plane,
- (3)  $\delta \in (\pi, 3/2\pi)$ ,
- (4)  $\delta \in (1/2\pi, \pi)$ .

Table 5. Types of synchronization of  $n=2$  pendula rotating in the opposite directions.

Type of synchronization	Symbol	Average rotational velocity of pendula			Average angle of rotation			Shown on Figure No.	Remarks
		1	2	3	1	2	3		
tree	T	$\dot{\varphi}$	$-\dot{\varphi}$	$-\dot{\varphi}$	$\varphi$	$-\varphi - \frac{1}{3}\pi$	$-\varphi + \frac{1}{3}\pi$	23(a)	
cluster-antiphase	CA	$\dot{\varphi}$	$-\dot{\varphi}$	$-\dot{\varphi}$	$\varphi$	$-\varphi - \pi$	$-\varphi - \pi$	23(b)	(1)
cluster-right	CR	$\dot{\varphi}$	$-\dot{\varphi}$	$-\dot{\varphi}$	$\varphi$	$-\varphi - \frac{3}{2}\pi$	$-\varphi - \frac{3}{2}\pi$	23(d)	1)
cluster-left	CL	$\dot{\varphi}$	$-\dot{\varphi}$	$-\dot{\varphi}$	$\varphi$	$-\varphi - \frac{1}{2}\pi$	$-\varphi - \frac{1}{2}\pi$		1)
yankee 3-2	Y32	$\dot{\varphi}$	$-\dot{\varphi}$	$-\dot{\varphi}$	$\varphi$	$-\varphi - \frac{1}{2}\pi$	$-\varphi + \frac{1}{2}\pi$	23(c)	1)
yankee 2-3	Y23	$\dot{\varphi}$	$-\dot{\varphi}$	$-\dot{\varphi}$	$\varphi$	$-\varphi + \frac{1}{2}\pi$	$-\varphi - \frac{1}{2}\pi$		1)

Remarks:

- (1) Exact values of phase shifting between pendula depends on the system parameters – see the example on Figure 24.

Table 6. Types of synchronization of  $n=3$  pendula (pendulum 1 rotates in opposite direction to pendula 2 and 3).

**Acknowledgment:** This work has been supported by the Foundation for Polish Science, Team Programme -- Project No TEAM/2010/5/5.

## References

1. G.L. Baker, J.A. Blackburn, *The Pendulum : A Case Study in Physics*, OUP, Oxford: 2005.
2. J.M. Balthazar, J.L. Palacios Felix, R.M.L.R.F. Brasil,. Some comments on the numerical simulation of self-synchronization of four non-ideal exciters. *Applied Mathematics and Computation*, 164 (2005) 615–625.
3. C. M. Bender, D.D. Holm, W.H. Hook, Complex trajectories of a simple pendulum, *J. Phys. A: Math. Theor.*, 40 (2007) F81–F89.
4. M. Bennett, M.F. Schatz, H. Rockwood, K. Wiesenfeld, Huygens's clocks, *Proc. R. Soc. Lond. A* 458 (2002) 563-579.
5. I.I. Blekhman, *Synchronization in Science and Technology*, ASME Press, New York: 1988.
6. S. Boccaletti, J. Kurths, G. Osipov, D.L. Valladares, C.S. Zhou, The synchronization of chaotic systems, *Phys. Rep.* 366 (2002) 1-101.
7. Sz. Boda, Z. Neda, B. Tyukodi, A. Tunyagi, The rythm of coupled metronomes, *EPJB*, 86 (2013) 263.
8. J.J.H. Brouwers, Asymptotic solutions for Mathieu instability under random parametric excitation and nonlinear damping. *Physica D*, 240 (2011) 990-1000.
9. P. Brzeski, A. Karmazyn, P. Perlikowski, Synchronization of two forced double-well Duffing oscillators with attached pendulums, *Journal of Theoretical and Applied Mechanics* 51(3), (2013) 603-613.
10. P. Brzeski, P. Perlikowski, S. Yanchuk and T. Kapitaniak, The dynamics of the pendulum suspended on the forced Duffing oscillator", *Journal of Sound and Vibration*, 331 (2012) 5347-5357.
11. J. Buck, E. Buck, Mechanism of synchronous flashing of fireflies, *Science*, 159 (1968) 1319-1327.
12. D. Capecchi, S.R. Bishop, Periodic and non-periodic responses of a parametrically excited pendulum, Report 3/1990 of the Dipartimento di Ingegneria delle Strutture, delle Acque e del Terreno, Universita' dell'Aquila, Italy.
13. D. Capecchi, S.R. Bishop, Periodic oscillations and attracting basins for a parametrically excited pendulum, *Dynamics and Stability of Systems*, 9 (1994) 123-143.
14. M. Clerc, P. Coulet, E. Tirapegu, Lorenz Bifurcation: Instabilities in Quasireversible Systems, *Phys. Rev. Lett*, 88 (1999) 3820-3823.
15. M.J. Clifford, S.R. Bishop, Rotating periodic orbits of the parametrically excited pendulum, *Physics Letters A*, 201 (1995) 191–196.
16. K. Czolczynski, *Rotordynamics of Gas-Lubricated Journal Bearing Systems*, Springer, New York: 1999.
17. K. Czolczyński, P. Perlikowski, A. Stefański, T. Kapitaniak, Clustering of Huygens' Clocks, *Progress of Theoretical Physics*, 122 (2009) 1027-1033.
18. K. Czolczyński, P. Perlikowski, A. Stefański, T. Kapitaniak, Clustering and Synchronization of Huygens' Clocks". *Physica A*, 388 (2009) 5013-5023.
19. K. Czolczynski, P. Perlikowski, A. Stefanski and T. Kapitaniak, Synchronization of the self-excited pendula suspended on the vertically displacing beam,

- Communications in Nonlinear Science and Numerical Simulation 18(2) (2013) 386-400.
20. K. Czolczynski, P. Perlikowski, A. Stefanski and T. Kapitaniak, Synchronization of slowly rotating pendulums, *International Journal of Bifurcation and Chaos*, 22 (2012) 1250128.
  21. K. Czolczynski, P. Perlikowski, A. Stefanski and T. Kapitaniak, Synchronization of pendula rotating in different directions, *Communications in Nonlinear Science and Numerical Simulation*, 17 (2011) 3658–3672.
  22. K. Czolczynski, P. Perlikowski, A. Stefanski and T. Kapitaniak: "Why two clocks synchronize: Energy balance of the synchronized clocks", *Chaos: An Interdisciplinary Journal of Nonlinear Science* 21 (2011) 023129.
  23. K. Czolczynski, P. Perlikowski, A. Stefanski and T. Kapitaniak, Clustering of non-identical clocks, *Progress of Theoretical Physics*, 125 (2011) 1-18.
  24. R. Dilao, Antiphase and in-phase synchronization of nonlinear oscillators: The Huygens's clocks system, *Chaos* 19 (2009) 023118.
  25. B. Eckhardt, E. Ott, S. H. Strogatz, D. Abrams, A. McRobie, Modeling walker synchronization on the Millennium Bridge, *Phys. Rev. E* 75 (2007) 021110.
  26. F.A. El-Barki, A.I. Ismail, M.O. Shaker, T.S. Amer, On the motion of the pendulum on an ellipse, *ZAMM*, 79 (1999) 65-72.
  27. A. Fillipov, B. Hu, B. Li, A. Zeltser, Energy transport between two attractors connected by a Fermi-Pasta-Ulam chain, *J. Phys. A: Math. Gen.*, 31 (1998) 7719.
  28. A.L. Fradkov, B. Andrievsky, Synchronization and phase relations in the motion of two-pendulum system, *Int. J. Non-linear Mech.*, 42 (2007) 895-901.
  29. W. Garira, S.R. Bishop, Rotating solutions of the parametrically excited pendulum, *Journal of Sound and Vibration* 263 (2003) 233-239.
  30. Z.-M. Ge, T.-N. Lin, Regular and chaotic dynamic analysis and control of chaos of an elliptical pendulum on a vibrating basement, *Journal of Sound and Vibration*, 230 (2000) 1045-1068.
  31. A.N. Grib, P. Seidel, J. Scherbel, Synchronization of overdamped Josephson junctions shunted by a superconducting resonator, *Phys. Rev. B* 65 (2002) 4508.1-4508.10.
  32. B. Horton, B. Rotational motion of pendula systems for wave energy extraction, PhD Thesis, Aberdeen University: 2008.
  33. C. Huygens, C., Letter to de Sluse, In: *Oeuvres Complètes de Christian Huygens* (letters; no. 133 of 24 February 1665, no. 1335 of 26 February 1665, no. 1345 of 6 March 1665), *Société Hollandaise Des Sciences*, Martinus Nijhor, La Haye: 1665.
  34. C. Huygens, *Horoloqium Oscilatorium*, Apud F. Muquet, Parisiis: 1673; (English translation: *The pendulum clock*, Iowa State University Press, Ames: 1985.
  35. M. Kapitaniak, P. Perlikowski and T. Kapitaniak: "Synchronous motion of two vertically excited planar elastic pendula", *Communications in Nonlinear Science and Numerical Simulation* 18(8) (2013) 2088-2096.
  36. M. Kapitaniak, P. Brzeski, K. Czolczynski, P. Perlikowski, A. Stefanski and T. Kapitaniak, Synchronization thresholds of coupled self-excited nonidentical pendula suspended on the vertically displacing beam, *Progress of Theoretical Physics* 128 (2012) 1141-1173.
  37. M. Kapitaniak, K. Czolczynski, P. Perlikowski, A. Stefanski and T. Kapitaniak: Synchronization of clocks, *Physics Reports*, 517 (2012) 1-67.
  38. T. Kapitaniak, K. Czolczynski, P. Perlikowski and A. Stefanski, Energy balance of two synchronized self-excited pendulums with different masses, *Journal of Theoretical and Applied Mechanics*, 50 (2012) 729-741.

39. B.P. Koch, R.W. Leven, Subharmonic and homoclinic bifurcations in a parametrically forced pendulum, *Physica D*, 16 (1985) 1-13.
40. P. Kołuda, P. Perlikowski, K. Czołczyński, T. Kapitaniak, Synchronization configurations of two coupled double pendula, *Communications in Nonlinear Science and Numerical Simulation*, 19 (2014) 977-990.
41. M. Kumon, R. Washizaki, J. Sato, R.K.I. Mizumoto, Z. Iwai, Controlled synchronization of two 1-DOF coupled oscillators, *Proceedings of the 15th IFAC World Congress, Barcelona: 2002*.
42. C.W. Lee, *Vibration Analysis of Rotors*, Kluwer, New York: 1993.
43. S. Lenci, G. Rega, Competing dynamic solutions in a parametrically excited pendulum: attractor robustness and basin integrity, *ASME J. Comp. Nonlin. Dyn.*, 3 (2008), 41010 (1-9).
44. S. Lenci, E. Pavlovskaja, G. Rega, M. Wiercigroch, Rotating solutions and stability of parametric pendulum by perturbation method", *Journal of Sound and Vibration*, 310 (2008) 243-259.
45. S. Lenci, M. Brocchini, C. Lorenzoni, Experimental rotations of a pendulum on water waves, *ASME J. Comp. Nonlin. Dyn.*, 7 (2011) 011007.
46. R.W. Leven, B.P. Koch, Chaotic behaviour of a parametrically excited damped pendulum, *Phys. Lett. A*, 86 (1981) 71-74.
47. R.J. Lythgoe, Some observations on the rotating pendulum, *Nature*, 141 (1938) 474.
48. B.P. Mann, M.A. Koplów, Symmetry breaking bifurcations of a parametrically excited pendulum, *Nonlinear Dynamics*, 46 (2006) 427-437.
49. E.A. Martens, S. Thutupalli, A. Fourrière, O. Hallatschek Chimera states in mechanical oscillator networks, *PNAS* (2013), <http://dx.doi:10.1073/pnas.1302880110>
50. M.R. Matthews, C.F. Gauld, A. Stinner, (eds), *The Pendulum: Scientific, Historical, Philosophical and Educational Perspectives*, Springer, New York: 2005.
51. A. A. Nanha Djanan, B.R. Nana Nbenjo, P. Wofo, Self-synchronization of two motors on a rectangular plate and reduction of vibration, *Journal of Vibration and Control*, (2013) doi:10.1177/1077546313506925
52. A.H. Nayfeh, D.T. Mook, *Nonlinear oscillations*, Wiley, New York: 1979.
53. Z. Neda, E. Ravasz, Y. Brechet, T. Vicsek, A.-L. Barabasi, The sound of many hands clapping, *Nature*, 403 (2000) 849-850
54. J. Pantaleone, Synchronization of metronomes, *Am. J. Phys.*, 70 (2002) 992-1000.
55. A.S. de Paula, M.A. Savi, M. Wiercigroch, E. Pavlovskaja, Bifurcation control of a parametric pendulum, *International Journal of Bifurcation and Chaos*, 22 (2012) 1250111-1-14.
56. E. Pavlovskaja, B. Horton, M. Wiercigroch, S. Lenci, G. Rega, Approximate Rotational Solutions of pendulum under combined vertical and horizontal excitation, *International Journal of Bifurcation and Chaos*, 22 (2012) 1250100.
57. L.M. Pecora, T.L. Carroll, G.A. Johnson, D.J. Mar, J.F. Heagy, Fundamentals of synchronization in chaotic systems, concepts, and applications, *Chaos* 7 (1997) 520-543.
58. J. Pena Ramirez, R.H.B. Fey, H. Nijmeijer, Synchronization of weakly nonlinear oscillators with Huygens' coupling, *Chaos* 23 (2013) 033118.
59. P. Perlikowski, M. Kapitaniak, K. Czołczyński, A. Stefanski and T. Kapitaniak: Chaos in coupled clocks, *International Journal Bifurcation and Chaos* 22 (2012) 1250288.
60. A. Pikovsky, M. Rosenblum, J. Kurths, *Synchronization: An Universal Concept in Nonlinear Sciences*, Cambridge University Press, Cambridge: 2001
61. A. Pogromsky, V.N. Belykh, H. Nijmeijer, Controlled synchronization of pendula, *Proceedings of the 42nd IEEE Conference on Design and Control: 2003*, 4381-4385.

62. A. Prasad, Universal occurrence of mixed-synchronization in counter-rotating nonlinear coupled oscillators, *Chaos, Solitons and Fractals*, 43 (2010) 42-46.
63. M.G. Rosenblum, A.S. Pikovsky, J. Kurths, Phase synchronization of chaotic oscillators. *Physical Review Letters*. 76 (1996) 1804-1807.
64. M.G. Rosenblum, A.S. Pikovsky, J. Kurths, From phase to lag synchronization in coupled oscillators. *Physical Review Letters*. 78 (1997) 4193-4196.
65. C. Qing-Jie, H. Ning, T. Rui-Lan, A Rotating Pendulum Linked by an Oblique Spring, *Chinese Phys. Lett.* 28 (2011) 060502.
66. M. Senator, Synchronization of two coupled escapement-driven pendulum clocks, *Journal Sound and Vibration*, 291 (2006) 566-603.
67. S.-B. Shim, M. Imboden, P. Mohanty, Synchronized oscillation in coupled nanomechanical oscillators, *Science*, 316 (2007) 95-99.
68. S. H. Strogatz, D. M. Abrams, A. McRobie, B. Eckhardt, and E. Ott, *Nature*, 438 (2005) 43-44.
69. J. Strzalko, J. Grabski, J. Wojewoda, M. Wiercigroch, T. Kapitaniak, Synchronous rotation of the set of double pendula: Experimental observations, *Chaos* **22** (2012) 047503.
70. D. Sudor, S.R. Bishop, Inverted dynamics of a tilted pendulum, *European Journal of Mechanics A: Solids*, 18 (1999) 517-526.
71. W. Szemplinska-Stupnicka, E. Tyrkiel, A. Zubrzycki, The global bifurcations that lead to transient tumbling chaos in a parametrically driven pendulum”, *International Journal of Bifurcation and Chaos*, 10 (2000), 2161-2175.
72. W. Szemplinska-Stupnicka, E. Tyrkiel, The oscillation-rotation attractors in the forced pendulum and their peculiar properties, *International Journal of Bifurcation and Chaos* 12 (2002) 159-168.
73. J.M.T. Thompson, M. Wiercigroch, J. Sieber, B. Horton, Dynamics of the nearly parametric pendulum. *International Journal of Non-Linear Mechanics*, 46 (2011) 436-442.
74. H. Ulrichs, A. Mann, U. Parlitz, Synchronization and chaotic dynamics of coupled mechanical metronomes, *Chaos*, 19 (2009) 043120.
75. J.M. Vance, Y. Fouad, F.Y. Zeidan, B. Murphy, *Machinery Vibration and Rotordynamics*, Wiley, London: 2010.
76. K. Wiesenfeld, D. Borrero-Echeverry, Huygens (and others) revisited, *Chaos*, **21** (2011) 047515.
77. Y. Wu, N. Wang, L. Li, J. Xiao, Anti-phase synchronization of two coupled mechanical metronomes, *Chaos*, **22** (2012) 023146.
78. X. Xu, M. Wiercigroch, M.P. Cartmell, Rotating orbits of a parametrically-excited pendulum, *Chaos, Solitons and Fractals*, 23 (2005) 1537-1548.
79. X. Xu, Nonlinear dynamics of parametric pendulum for wave energy extraction, PhD Thesis, Aberdeen University: 2005.
80. X. Xu, M. Wiercigroch, Approximate analytical solutions for oscillatory and rotational motion of a parametric pendulum, *Nonlinear Dynamics* 47 (2007) 311-320.
81. X. Xu, E. Pavlovskaya, M. Wiercigroch, F. Romeo, S. Lenci, Dynamic interactions between parametric pendulum and electro-dynamical shaker, *ZAMM*, 87 (2007) 172-186.
82. H. Yabuno, M. Miura, N. Aoshima, Bifurcation in an inverted pendulum with tilted high frequency excitation: analytical and experimental investigations on the symmetry-breaking of the bifurcation, *Journal of Sound and Vibration*, 273 (2004) 479-513.

83. D. Yurchenko, P. Alevras, Stochastic dynamics of a parametrically base excited rotating, Pendulum, Procedia IUTAM 6 ( 2013 ) 160–168.
84. D. Yuchenko, A. Naess, P. Alevras, Pendulum's rotational motion governed by a stochastic Mathieu equation. Probabilistic Engineering Mechanics, 31 (2013) 12-18.
85. M. Lazarek, M. Nielaczny, Synchronization of slowly rotating pendula, M.Sc. Thesis, Technical University of Lodz: 2013.
86. S. H. Strogatz, Sync: The Emerging Science of Spontaneous Order , Penguin Science, London, 2004.
87. P. J. Menck, J. Heitzig, N. Marwan, J. Kurths, How basin stability complements the linear-stability paradigm, Nature Physics, 9 (2013) doi:10.1038/NPHYS2516.
88. E. Doedel, B. Oldeman, A. Champneys, F. Dercole, T. Fairgrieve, Y. Kuznetsov, R. Paffenroth, B. Sandstede, X. Wang, C. Zhang., AUTO-07P: Continuation and Bifurcation Software For Ordinary Differential Equations, Concordia University, Montreal, Canada, 2011.